INFORMATION TO USERS

This manuscript has been reproduced from the microfilm master. UMI films the text directly from the original or copy submitted. Thus, some thesis and dissertation copies are in typewriter face, while others may be from any type of computer printer.

The quality of this reproduction is dependent upon the quality of the copy submitted. Broken or indistinct print, colored or poor quality illustrations and photographs, print bleedthrough, substandard margins, and improper alignment can adversely affect reproduction.

In the unlikely event that the author did not send UMI a complete manuscript and there are missing pages, these will be noted. Also, if unauthorized copyright material had to be removed, a note will indicate the deletion.

Oversize materials (e.g., maps, drawings, charts) are reproduced by sectioning the original, beginning at the upper left-hand corner and continuing from left to right in equal sections with small overlaps. Each original is also photographed in one exposure and is included in reduced form at the back of the book.

Photographs included in the original manuscript have been reproduced xerographically in this copy. Higher quality 6" x 9" black and white photographic prints are available for any photographs or illustrations appearing in this copy for an additional charge. Contact UMI directly to order.

UMI

A Bell & Howell Information Company
300 North Zeeb Road, Ann Arbor MI 48106-1346 USA
313/761-4700 800/521-0600

Anisotropic Rotations of Perylene in Anisotropic Media

by

Salvatore H. Atzeni

A dissertation submitted to the Graduate Faculty in Chemistry
in partial fulfillment of the requirements for the degree of

Doctor of Philosophy

The City University of New York

1998

Approval Page

This manuscript has been read and accepted for the Graduate Faculty in Chemistry in satisfaction of the dissertation requirement for the degree of Doctor of Philosophy.

9/9/98
Date

Prof. Lesley Davenport
Brooklyn College

9/10/98
Date

Prof. G. Koeppl, Executive Officer
The Graduate School and University Center

Prof. W. E. L. Grossman
Hunter College

Prof. O. Popovych
Brooklyn College

Prof. I. Cohen
Brooklyn College

Prof. J. B. A. Ross
The Mount Sinai School of Medicine

THE CITY UNIVERSITY OF NEW YORK

Abstract

Anisotropic Rotations of Perylene in Anisotropic Media

by

Salvatore H. Atzeni

Adviser: Professor Lesley Davenport

The anisotropic rotations of perylene labeled small unilamellar vesicles prepared from symmetric chain 1,2-ditetradecanoyl-sn-glycero-3-phosphocholine (DMPC) and asymmetric chain 1-stearoyl-2-caproyl-sn-glycero-3-phosphorylcholine (C18:C10-PC) phospholipids have been studied using time-resolved emission anisotropy (TREA) measurements, as functions of temperature and excitation wavelength. Global analysis of the data was used, linking appropriate parameters according to photophysical and model constraints. Experimental temperatures included values below and above the phase transition of each phospholipid.

Perylene rotates anisotropically in isotropic solvents, and its rotational motions can be described using two rotational correlation times and two preexponential terms. Global analysis of TREA measurements of perylene in isotropic solvents recover constant values for preexponentials that are consistent with the photophysics of the molecule.

The phospholipid bilayers studied here present hindered, anisotropic environments, and the rotational motions of perylene become more complex, indicating possible lipid packing heterogeneity as well as heterogeneous distribution of perylene within the phospholipid bilayers. We eliminated the possibility of heterogeneous distribution of

perylene by excluding the volume between the bilayer leaflets, using an asymmetric chain phospholipid that is known to interdigitate below the phase transition. With this approach, perylene may only be aligned along the acyl chains of the bilayer.

Global analysis of the TREA of perylene in phospholipid bilayers using conventional models do not properly describe the decay of the molecule: the recovered preexponentials do not sum to the limiting anisotropy (r_0) at each temperature; and magnitudes of recovered preexponentials is lower than those obtained using isotropic solvents. Since the magnitude of hindrance changes with the phospholipid state, a temperature dependent expression is required to describe the rotational behavior in a way that does not violate the photophysics of the molecule.

A new mathematical model, which accounts for the changes in the preexponential terms with temperature, has been developed and applied to the two phospholipid bilayer systems described above. The new model is tested by comparing the results of global data analysis with two conventional models. The goodness of fit is similar between models, but the new temperature dependent model represents a better description of the physical nature of phospholipid bilayers.

Acknowledgments

I would like to express thanks to my adviser, Prof. Lesley Davenport, for her guidance and insight throughout my graduate school experience. Her support and encouragement over the years will always be remembered. Thanks also to the members of my committee, Profs. Cohen, Grossman, Popovych and Ross, who kept me on track towards successful completion and asked the right questions at the right times to improve the quality of this work. Dr. Piotr Targowski and Dr. Michael Straher also deserve special mention, each providing their own special support over the years.

I thank the Chemistry Department of Brooklyn College and the Merck Foundation for their generous financial support, the Physics Department (especially Prof. Lesser) for assistance with fast timing electronics, and the Brooklyn College Machine Shop, who turned my mechanical drawings into a real instrument.

Last, but certainly not least, I wish to extend deepest thanks to my parents and family, who have shaped my future beginning from a time that I cannot even remember, and brought me to this point. Without your unwavering support and motivation, this moment would never have been possible.

Table of Contents

List of Tables.

List of Figures.

Section I. - Introduction.

I.a. Rotation and Diffusion of Molecules in Solvents.

The Brownian rotational motions of molecules in solvent can be described in terms of the diffusion coefficients along the three principal diffusion axes of the molecule. Depending on the molecular symmetry, one or more of these diffusion coefficients may differ. The simplest example is a spherically symmetric molecule in a pure isotropic solvent such as water or alcohol. Here, the three diffusion coefficients are equal, and the Stokes-Einstein equation provides the relationship between the viscosity of the solvent, the volume of the molecule, and the friction coefficient:

$$f = 6\pi\eta a \qquad (1)$$

where f is the frictional coefficient, η is the viscosity, and a is the radius of the spherical particle. The frictional coefficient is difficult to determine directly, even if the shape of the particle is known. It is easier to measure the diffusion coefficient D, which relates to the frictional coefficient using:

$$D = \frac{RT}{N_0 f} \qquad (2)$$

where R is the gas constant, T is the temperature and N_0 is Avogadro's number. Einstein derived this relationship between the diffusion coefficient and the frictional coefficient in 1905 [1]. Once the diffusion coefficient(s) are known, the viscosity of the solvent in which the molecule is diffusing may be determined.

I.b. Isotropic and anisotropic rotations of molecules in isotropic solvents.

A molecule may rotate in different ways, depending on its shape and symmetry. The simplest case of molecular rotation is an isotropic rotor, an example being a spherically shaped molecule rotating in an isotropic solvent such as an oil. The diffusion coefficients would be equal along all three diffusion axes, and only one rotational motion would be observed. If a molecule has a non-spherical shape, such as a rod, cylinder or disk, its diffusion coefficients would no longer be equal in the three diffusion axes. Depending on the symmetry and experimental conditions, the rotational motions of the molecule may be determined along each of the diffusion axes.

Using polarized fluorescence emission anisotropy measurements, it is possible to measure the diffusion coefficient(s) of fluorescent molecules rotating in a solvent system. The number and kinds of rotational motions that may be detected using fluorescence emission anisotropy measurements depend on the molecular symmetry (point group), and the relative orientation of absorption and emission dipoles in the molecular frame. Depending on the instrumentation used, it is possible to measure an average diffusion rate, or completely resolve the rotational motions into their discrete components.

An example of a fluorescent molecule having rodlike symmetry is *trans* 1,3,5-diphenylhexatriene (DPH). Disklike symmetry is common with polyaromatic hydrocarbons such as pyrene, perylene, and coronene. Molecules that have different diffusion coefficients along one or more of the diffusion axes are termed *anisotropic*.

Fluorescence spectroscopy is a useful tool for determining the rotational motions of molecules in solvents, both isotropic and anisotropic. The basic types of spectral

information that can be obtained using fluorescence spectroscopy are outlined in the next section.

I.c. Fluorescence - Definitions / Types of Measurements

The definitions of fluorescence and phosphorescence, are '...processes in which radiation is emitted by molecules or atoms that have been excited by the absorption of radiation.' [2]. Fluorescence and phosphorescence can be grouped into a larger category of 'luminescence', which has been defined as the emission of photons from electronically excited states [3]. The different classes of luminescence are divided by the nature of the ground and excited states of the molecule or atom, and depend on the relative spin orientation of the electrons involved in the transition. If electron spin is preserved in the excited state, an excited state singlet occurs, with both electrons being paired with opposite spin orientation. If electron spin is not preserved, the resulting excited state will have two electrons possessing the same spin quantum numbers, which will require the reversal of one electron spin to return to the ground state. This triplet state is the origin of phosphorescence emission, which results from a transition between states of different multiplicity. These transitions are quantum mechanically forbidden, and therefore they occur at a lower rate than the allowed fluorescence emission, which involves transitions between states of the same multiplicity.

Jablonski diagram

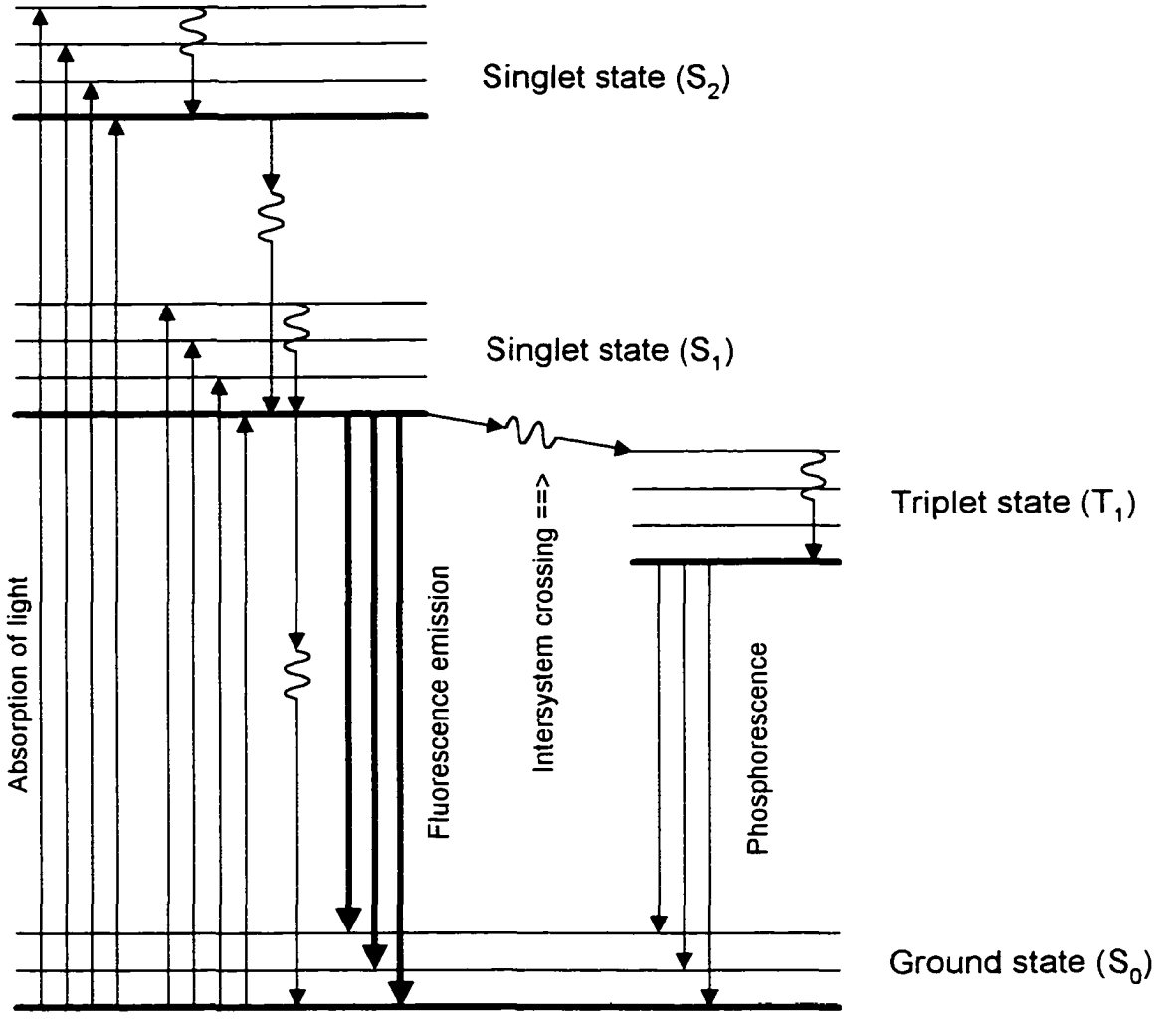

Figure 1. Jablonski diagram. The possible pathways for creation and depopulation of different electronic states are shown in this diagram. The heavy lines, from the lowest vibrational energy level of S_1, to different vibrational levels of the ground state S_0, are fluorescence emission. Broken lines indicate non-radiative transitions.

I.c.0. Steady state measurements.

The most common measurements of fluorescence are performed using a continuous-wave illumination source, usually a xenon arc lamp. An excitation spectrometer is used to select discrete excitation wavelengths, and usually supports scanning of the wavelength drive to allow automatic recording of excitation spectra. The fluorescence emission is usually detected at a right angle with respect to the excitation beam, minimizing the fraction of exciting light that reaches the emission detector. In some instrumental arrangements, collection geometries other then 90° viewing are used. A 'front-face' arrangement, using a collection angle of less than 90° from the excitation beam, is used when right angle viewing is inappropriate. Two examples when front-face viewing is advantageous include a) samples having a high absorbance are being measured; and b) solid samples, including glass substrates and powders or thin films. The emitted light passes through an emission spectrometer and is detected using a photomultiplier tube. This type of instrumentation provides the time-averaged (integrated) fluorescence signal as a function of wavelength. The most common types of steady state experiments include:

Excitation scans. In an excitation scan, the emission wavelength is held constant, and the excitation spectrometer is scanned over a range. Peaks occurring in the excitation scan give information about the excited state electronic and vibrational details, over the S_1 and higher absorption bands. Excitation, or absorption, usually occurs from the lowest energy level of the ground state, and the structure in the excitation spectrum can identify vibrational spacing within a transition band. An ideal excitation spectrum, properly corrected for instrument response and excitation lamp profiles, will match the absorption spectrum for that

molecule, since both absorption and fluorescence excitation involve the same electronic transitions.

Emission scans. Here, the excitation wavelength is held constant, and the emission spectrometer is scanned over a range of wavelengths. The shape and structure of the emission spectrum gives information about the ground-state electronic and vibrational details of the molecule, independent of the excitation wavelength. This is true because fluorescence emission normally occurs from the lowest vibrational level of the first singlet excited state S_1. Energy is usually lost as the molecule undergoes vibrational relaxation to this lowest vibrational level of S_1, and this energy loss results in the emission spectrum shifting to longer wavelengths. The wavelength shift is called the Stokes' shift.

Synchronous scans. In a synchronous scan, both excitation and emission spectrometers are varied during a scan, with a fixed offset between them. This offset may be a constant wavelength difference, i.e. 15 nm to longer wavelength, as in CWLS (constant wavelength luminescence scanning), or it may be a constant energy difference (i.e -200 cm^{-1}), as in CESLS (constant energy synchronous luminescence scanning). Both techniques are useful in resolution of complex mixtures that have large degrees of spectral overlap, and have been used successfully in identification of polyaromatic hydrocarbons in wastewater [4].

Polarization and anisotropy measurements. The absorption of light by a fluorophore is most probable when the electric vector of the excitation light beam is aligned with the transition moment of the molecule [5]. Placing polarizers in the excitation and emission paths of the instrument allows photoselection of an ensemble of molecules whose absorption

dipoles are aligned with the excitation beam electric vector. If all of the photoselected molecules remain stationary, then all of the fluorescence emission will be polarized in the direction of the emission dipole. Usually, the molecules undergo Brownian rotational diffusion, resulting in emission of fluorescence that is partially polarized. The measurement of the relative intensity of the vector components of the fluorescence emission, with fixed excitation polarization direction, can be used to estimate the rotational behavior of the fluorophore. When the molecule rotates rapidly, the fluorescence emission tends to randomize, with the vector components of the emission becoming equal.

The absorption and emission dipoles have a fixed orientation within a molecule. The angle between these dipoles, combined with certain photoselection criteria, defines the fundamental anisotropy r_0 for a molecule. The relationships between dipole angles and fundamental anisotropies will be described in more detail later in this Thesis.

Measurement of the steady-state anisotropy <r>, the ratio of the difference in the vertical and horizontal components of the fluorescence emission to the total intensity of emission, can provide information about the angular displacement of the molecule during the lifetime of the excited state. These measurements may be used to determine the apparent hydrodynamic volume of a rotating fluorophore, or the apparent viscosity of the solution in which it is rotating, by use of the Perrin equation:

$$\frac{<r>}{r_0} = \frac{1}{(1 + \frac{\tau}{\phi})} \qquad (3)$$

in which τ is the fluorescence lifetime and ϕ is the rotational correlation time.

The viscosity or apparent volume may be obtained from the rotational correlation time:

$$rotational\ correlation\ time = \phi = \frac{\eta V}{kT} \quad (4)$$

The diffusion coefficient for a sphere of equivalent volume can be measured using:

$$diffusion\ coefficient = D = \frac{1}{6\phi} \quad (5)$$

These equations represent the time-averaged (steady-state) observations.

I.c.1. Time-resolved Fluorescence Measurements

Usually, dynamic fluorescence measurements are measured using fixed excitation and emission wavelengths. These measurements are generally not spectral scans. Sets of lifetime measurements having different wavelengths of excitation or emission may be collected separately. The *temporal* characteristics, rather than the *spectral* characteristics, are the observables in the dynamic fluorescence experiment. Automation of the instrumentation makes complex series of experiments possible with minimum user supervision.

Fluorescence Lifetime Measurements. The fluorescence lifetime, τ_F, represents the average time that the molecule spends in the excited state. The fate of a molecule, specifically its transition from an excited state S_b back to a ground state S_a, may be radiative or non-radiative. If the only path for the return to the ground state is radiative, the lifetime

of this excited state would be the intrinsic lifetime [6]:

$$\tau_R = \frac{1}{A_{ba}} \quad (6)$$

where A_{ba} is the Einstein coefficient for spontaneous emission from electronic state *b* to *a*. This coefficient depends on several factors, including the dipole strength D_{ab} and the frequency of light:

$$A_{ba} = \left(\frac{32\pi^3\nu^3}{3c^3\hbar}\right) D_{ab} \quad (7)$$

The rate of return to the ground state *a* from the excited state *b* may be written as the differential equation:

$$\frac{dn_b}{dt} = -A_{ba} n_b \quad (8)$$

whose solution is:

$$n_b(t) = n_b(0)\, e^{-A_{ba} t} \quad (9)$$

In Equation 9, $n_b(0)$ represents the initial (boundary) condition of excited states at t=0. The solution leads to Equation 6, where τ_R is the radiative lifetime of the excited state S_b.

The radiative pathway is usually not the only deexcitation path, and the actual lifetime is reduced. A Jablonski diagram (Figure 1) shows possible pathways that create and

depopulate common electronic states. Since nonradiative pathways such as quenching (by collision with solvent or other molecules), internal conversion and intersystem crossing (singlet - triplet conversion, which is a spin-forbidden process) compete with the radiative decay pathway, the net fluorescence quantum yield Φ_F will decrease:

$$\Phi_F = \frac{k_F}{[k_F + k_{ic} + k_{isc} + k_q[Q]\ ]} \qquad (10)$$

The *k* terms are the rate constants for each of the competing pathways for depopulation of the excited state. In Equation 10, k_{ic} represents the rate of internal conversion, k_{isc} the rate of intersystem crossing, and k_q indicates the quenching rate constant. The symbol k_F is the fluorescence emission rate constant. Fluorescence emission (singlet-singlet) occurs on the nanosecond timescale, and phosphorescence emission (singlet-triplet) can range from microseconds to hours. The fluorescence lifetime of the excited state in the presence of the other possible decay pathways is given by

$$\tau_F = \frac{1}{[k_F + k_{ic} + k_{isc} + k_q[Q]\ ]} \qquad (11)$$

Combining these expressions gives:

$$\Phi_F = \frac{\tau_F}{\tau_R} \qquad (12)$$

A measurement of the fluorescence lifetime τ_F can provide a measure of the quantum yield,

since, in principle, the intrinsic lifetime τ_R can be calculated from an absorption spectrum. Fluorescence lifetime measurements can provide information about kinetics of excited state reactions, quenching, and energy transfer [7].

Time-resolved emission anisotropy measurements.

Steady-state polarization (or anisotropy) measurements give time-averaged values of the rotational motions of fluorophores. Such measurements yield a single rotational correlation time that represents the average diffusion coefficient of a sphere of equivalent volume (Equations 4 and 5). To obtain more detailed descriptions of the rotational motions, time-resolved emission anisotropy measurements are necessary.

As an example, the rotational motions of perylene may be separated into in-plane and out-of-plane motions at different temperatures, revealing specific information about changes in the individual rotational rates. As this Thesis deals almost entirely with these topics, further discussion of these points will be presented later.

I.c.2. Theory of Fluorescence Anisotropy.

Fluorescence anisotropy, r, is a measure of the mean alignment between the axis of excitation and emission. Once a probe molecule is excited, both electronic and molecular reorientations can rotate the emission axis away from the excitation axis direction. The fluorescence anisotropy is [8]

$$r(t) = 0.4 < P_2(\cos \alpha) > \qquad (13)$$

where P_2 is the second Legendre polynomial:

$$P_2(x) = \frac{(3x^2 - 1)}{2} \quad (14)$$

Using α for the angle between excitation and emission at time zero, two specific cases apply for perylene. If excitation and emission dipoles are collinear (α = 0°), the fundamental anisotropy r_f (the theoretically expected value for single-photon excitation) is:

$$r_f = 0.4 \frac{(3\cos^2\alpha - 1)}{2} = 0.4 \frac{(3(1)-1)}{2} = +0.4 \quad (15)$$

corresponding to the S_0->S_1 transition of perylene. When α = 90°:

$$r_f = 0.4 \frac{(3\cos^2\alpha - 1)}{2} = 0.4 \frac{(3(0)-1)}{2} = -0.2 \quad (16)$$

and this negative anisotropy corresponds to the S_0->S_2 transition of perylene.

Electronic reorganization occurs within 10^{-15} seconds and causes the observed r_f value to decrease. The anisotropy measured obtained when only electronic orientations have occurred, before any molecular orientations, is termed r_0. In practice, r_0 values can be measured by cold temperature (-50°C or lower) measurements in solvent, or embedding it in a glass. Table I lists the pertinent r_0 values for perylene, taken from the literature [9].

Table I. Limiting Anisotropies of Perylene.

Excitation Wavelength	Limiting Anisotropy, r_0
410 nm	+0.335
314 nm	+0.100
252 nm	-0.165

The general expression for the time decay of fluorescence emission anisotropy is:

$$r(t) = r_0 \sum_i \beta_i e^{\frac{-t}{\Phi_i}} \qquad (17)$$

where the β_i terms are simple functions of the angles between absorption and emission of light. In theory, the fluorescence anisotropy of a rigid body will have five exponential terms [10], but in practical cases, at most three will observed (of which 2 are independent). Figure 2 defines the angles used to describe the beta terms. The molecular symmetry axis is along the z axis.

Definition of Transition Dipole Angles in the Molecular Frame

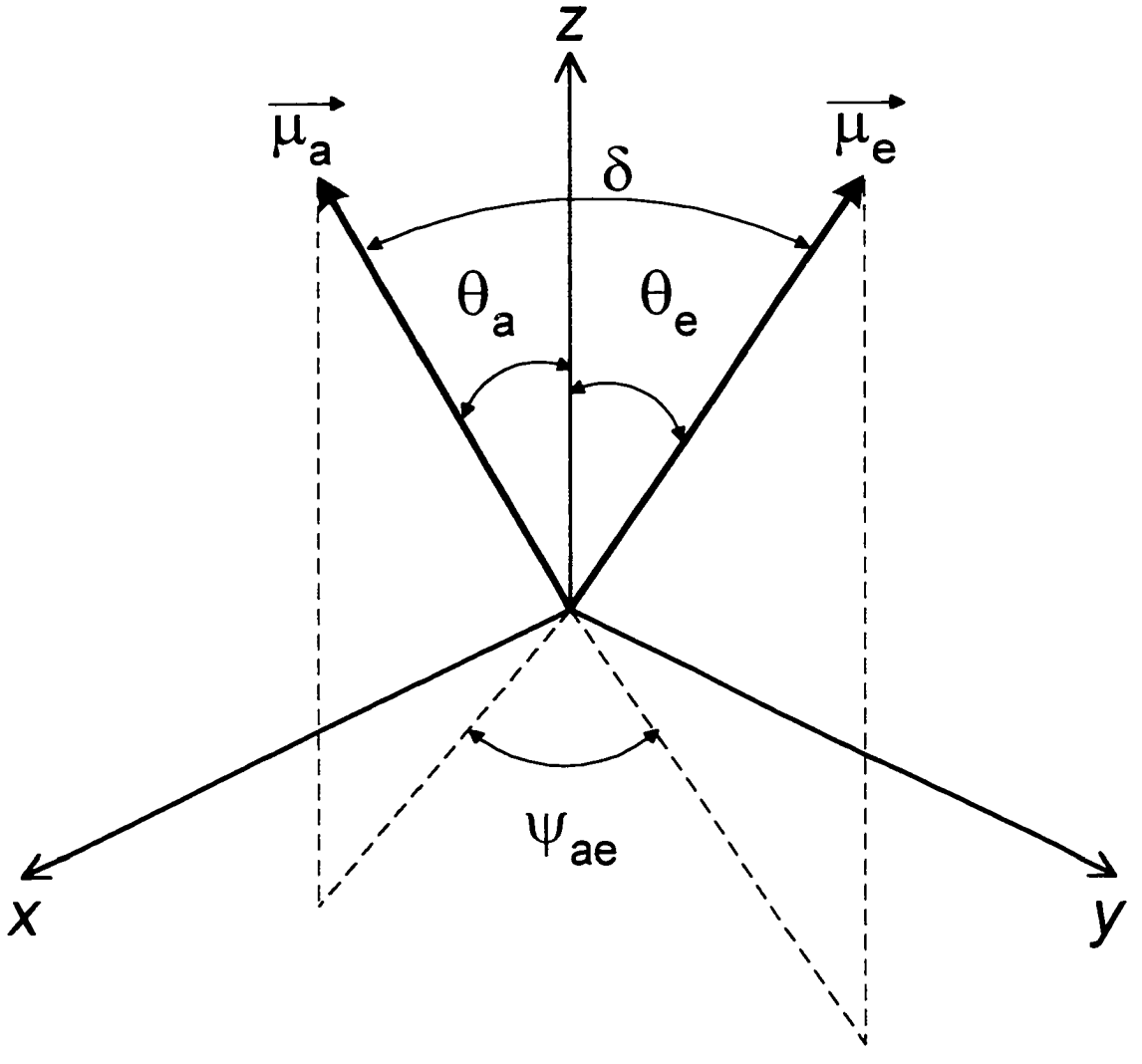

Figure 2. Definition of the angles about the molecular frame of perylene which define the preexponential (β) terms.

Referring to Figure 2, the expected magnitude range of each preexponential term is given by:

$$\beta_1 = 0.3 \sin^2 \theta_a \sin^2 \theta_e \cos 2\psi_{ae} \quad (18)$$

$$\beta_2 = 0.1 (3 \cos^2 \theta_a - 1)(3 \cos^2 \theta_e - 1) \quad (19)$$

$$\beta_3 = 1.2 \sin \theta_a \cos \theta_a \sin \theta_e \cos \theta_e \cos \theta_{ae} \quad (20)$$

When one of the transition dipoles is aligned with a principal diffusion axis, the β_3 term reduces to zero. This is true for perylene, due to its D_{2h} symmetry.

The rotational correlation times (ϕ_i) are functions of the temperature and viscosity of the environment around the probe molecule, independent of excitation wavelength. The rotational correlation times are combinations of the rotation rates $D_{\|}$ and $D_{\perp}$ [11]:

$$\phi_1 = \frac{1}{(2D_{\perp} + 4D_{\|})} \quad (21)$$

$$\phi_2 = \frac{1}{6D_{\perp}} \quad (22)$$

The third rotational correlation time (ϕ_3) is not observed in the fluorescence emission anisotropy of perylene:

$$\phi_3 = \frac{1}{(5 D_{\perp} + D_{\parallel})} \qquad (23)$$

Due to perylene's molecular symmetry, $\beta_3 = 0$ (Equation 21), and the contribution of ϕ_3 to the observed rotational motion is zero. $D_{\perp}$ is the rotational rate about an axis perpendicular to the symmetry axis, and $D_{\parallel}$ is the rotational rate about an axis parallel to the symmetry axis. For perylene, these represent out-of-plane and in-plane rotational rates, respectively. The rotational rates of perylene can be calculated from the rotational correlation times, by rearrangement of Equations 21 and 22.

I.c.3. Hindered Rotations and Probe Order Parameters.

Extensive theoretical work has been performed, in which the decay of fluorescence anisotropy of probes in macromolecules [12] and membranes [13] is derived from first principles, expanding to a theory of 'wobbling' between restrictive barriers to rotation [14]. When the rotational motions of the fluorophore are hindered, the time dependent emission anisotropy expression becomes:

$$r(t) = (r_0 - r_\infty) \sum_i \beta_i e^{\frac{-t}{\phi_i}} + r_\infty \qquad (24)$$

where r_∞ is the limiting anisotropy, meaning a nonzero anisotropy value existing at times long compared to the fluorescence lifetime of the probe. For perylene. the r_∞ represents a hindrance, or rotational barrier, of either or both rotational motions of the molecule. It is essentially the steady-state anisotropy in the case of extremely rapid rotational motion [15]. A nonzero value of r_∞ has also been interpreted as possible heterogeneity between environments of the probe in the lipid bilayer [16].

The ratio of limiting to zero-point anisotropies is the order parameter S (for the fluorescent *probe*), defined as [17]:

$$S^2 = \frac{r_\infty}{r_0} \tag{25}$$

Phospholipid matrices are anisotropic solvent environments. Below their phase transition, restrictions to rotational freedom of probe molecules would be expected. Then, depending on the degree of restriction:

$$-0.2 \leq r_\infty \leq +0.4 \tag{26}$$

in which the magnitude of r_∞ also depends on the excitation wavelength that was used. This implies that the range of order parameters that may be reported by a probe in a phospholipid environment is:

$$0 \leq S^2 \leq 1 \tag{27}$$

since squaring the ratio in Equation 25 always produces a positive result.

A probe located in a totally unrestricted solvent environment would have r_∞ equal to zero, resulting in an order parameter of zero. This is expected at high temperatures, above the phase transition:

$$S^2 \rightarrow 0 \ as \ r_\infty \rightarrow 0 \qquad (28)$$

A probe molecule in a completely immobile environment would have a probe order parameter of unity:

$$S^2 \rightarrow 1 \ as \ r_\infty \rightarrow r_0 \qquad (29)$$

I.d. Perylene: a disklike, anisotropic rotator.

Perylene is an example of an anisotropic rotator, having different rates of rotation in and out of the molecular plane. This is easily rationalized due to the disklike shape of the molecule. An 'out-of-plane', tumbling rotation requires a large displacement of solvent, compared with an 'in-plane', spinning motion. Using time-resolved fluorescence emission anisotropy measurements, resolving the different anisotropic motions of perylene in various solvent systems is possible. Two rotational motions are observable with perylene due to its D_{2h} symmetry and the arrangement of the molecular absorption and emission dipoles. Not all anisotropic rotations are revealed by fluorescence emission anisotropy measurements. For example, coronene, a disk-shaped molecule, is also an anisotropic rotator. However, its in-plane motion is not detected using fluorescence emission anisotropy measurements due

to its higher D_{6h} symmetry. For coronene, only the out-of-plane motion is revealed by the fluorescence emission anisotropy experiment.

I.e. Anisotropic Solvent Systems.

Anisotropic solvents cause preferred alignment of solute molecules. Examples of solvents that fall into this category are liquid crystals, lipid bilayers, membranes and stretched polymer films. The alignment may even be caused by a magnetic field, as was used by Johansson to study a liquid crystal prepared from potassium dodecanoate labeled with perylene [18].

Biological membranes are an example of an anisotropic solvent environment. Fluorophores will have a preferential alignment within a membrane or bilayer. A suspension of membranes containing embedded fluorophores is a special case of a macroscopically isotropic system, which is microscopically anisotropic [19]. The system is macroscopically isotropic, because all membrane orientations occur with equal probability. The fluorophores are in an anisotropic environment because they are under the influence of an orienting potential within each membrane. The macroscopically isotropic sample simplifies the mathematics regarding photoselection and polarized fluorescence emission. Since the orientation and angles between the absorption and emission dipoles μ_a and μ_e are known, tensor equations reduce to vector equations [20].

I.f. Phospholipids as Models of Cell Membranes.

Phospholipid bilayers may be used as models of biological cell membranes. It is

possible to prepare solutions of small unilamellar vesicles (SUVs), which are bilayers arranged in a spherical shape. This is different from a micelle, in which the cross-section does not consist of a bilayer. The interior volume of an SUV is hollow, and contains solvent. In a micelle, the solvent is excluded from the interior.

As models of real cell membranes, phospholipid bilayers can be used as a simplified system with which interactions involving the cell membrane may be studied as isolated systems. Natural cell membranes contain many elements besides phospholipids, such as proteins and other steroids. This model of a natural membrane is often referred to as the fluid mosaic model [21]. Using a pure phospholipid system as a model simplifies the bilayer structure, and allows the characterization of its properties without considering additional effects due to the complex nature of real cell membranes.

Properties of phospholipid bilayers that are of interest include phase transition temperature, packing of the molecules of which the bilayer is composed, effects of chain length, packing disruptions caused by small peptides or the introduction of cholesterol, and the potential for transport of material across the bilayer. Changes in the diffusion rates of the fluorophore signal changes in the microviscosity of the phospholipid bilayer, revealing structural changes in the arrangement of the phospholipid acyl chains.

I.g. Fluorescent labeling of phospholipid bilayers.

Most materials used for the preparation of phospholipid bilayers are not fluorescent. A fluorophore may be introduced into the system in two ways. Most often, a fluorophore is introduced during preparation of SUVs. The fluorophores are selected to be water

insoluble, so they partition in the hydrophobic region of the bilayers. The fluorophore probe should not perturb the membrane system under investigation. To minimize perturbations, probes with a high quantum yield are used at low mole fractions. Sometimes, the fluorophore is covalently bound at or near the end of one of the acyl chains of the phospholipid. The tagged phospholipid is mixed with untagged phospholipid so that the ratio of fluorophore to total phospholipid is low. This covalent binding is advantageous in that the location of the fluorophore within the bilayer structure is known. A potential disadvantage is that the fluorophore is not free to rotate in the same way as in the non-covalently labeled system. The molecular symmetry will be different, and certain diffusional motions may be restricted.

Use of rotational correlation times to investigate changes in probe environment.

Using time-resolved fluorescence emission anisotropy measurements, the rotational correlation time(s) of the probe may be determined, and used to quantitate changes in the probe's local environment. Changes in the rotational dynamics may be correlated with differences in acyl chain length, phospholipid membrane composition, and structural changes due to the addition of cholesterol or small proteins which locate themselves in the hydrophobic region of the phospholipid bilayer.

I.h. Perylene - Structure and Photophysics.

Perylene (Figure 3) is a planar polyaromatic hydrocarbon, measuring about 8Å in diameter. It is a member of the D_{2h} symmetry point group. The symmetry of the molecule

requires that all $^1\pi\pi^*$ transitions are polarized in the plane of the molecule [22]. This property becomes important when considering the rotational dynamics. Spectroscopically, perylene has the interesting property of two different absorption dipoles. Both lie in the plane of the molecule, as does the emission dipole. Excitation into the lowest singlet excited state ($S_0 \rightarrow S_1$) at 430 nm, is collinear with the emission dipole. The second absorption dipole ($S_0 \rightarrow S_2$) at 256 nm, is oriented 90 degrees from the emission dipole [5]. Fluorescence emission usually occurs from the $S_1 \rightarrow S_0$ energy levels [23], with the maximum emission near 448 nm for perylene. Steady state excitation and emission spectra of perylene dissolved in glycerol are presented in Figure 4.

Excitation at wavelengths between 410 nm and 256 nm varies the angle between the absorption and emission dipoles from approximately 0 to 90 degrees. Polarized excitation of perylene into different absorption bands, followed by detection of polarized emission, allows the determination of different combinations of in-plane and out-of-plane rotational rates. By exciting perylene at different wavelengths, more information is available than by using only a single excitation wavelength. At constant temperature, excitation into different absorption dipoles will not affect the measured rotational correlation times, since the rotational rate of the molecule is a function of the viscosity of the immediate environment of the molecule. Instead, a preexponential term associated with the rotational correlation time varies. The result is observation of the same parameter (the rotational correlation time at constant temperature) using two different and independent observations. The rotational correlation time is said to be *overdetermined*. Different preexponential values are expected for each excitation wavelength used, since these preexponential terms depend on the

excitation wavelength. The mathematical details of this strategy will be described in the experimental section.

Proper analysis of overdetermined parameters (rotational correlation times as well as preexponential terms) is made possible by the use of global analysis techniques [24]. Certain parameters may be linked between experiments, as determined by theoretical considerations. For example, the rotational correlation times may be linked along isotherms, measured using multiple excitation wavelengths. Preexponential terms may be overdetermined by using one excitation wavelength across several temperatures. Then, the preexponential terms would be constant, and the rotational correlation time(s) would vary. Several relationships between temperatures and excitation wavelengths may exist among a series of experiments. Combining these data results in an experimental surface results in a total information content that is much greater than any single experimental 'slice'. The data are fitted simultaneously using global analysis, yielding a unique solution over the entire surface.

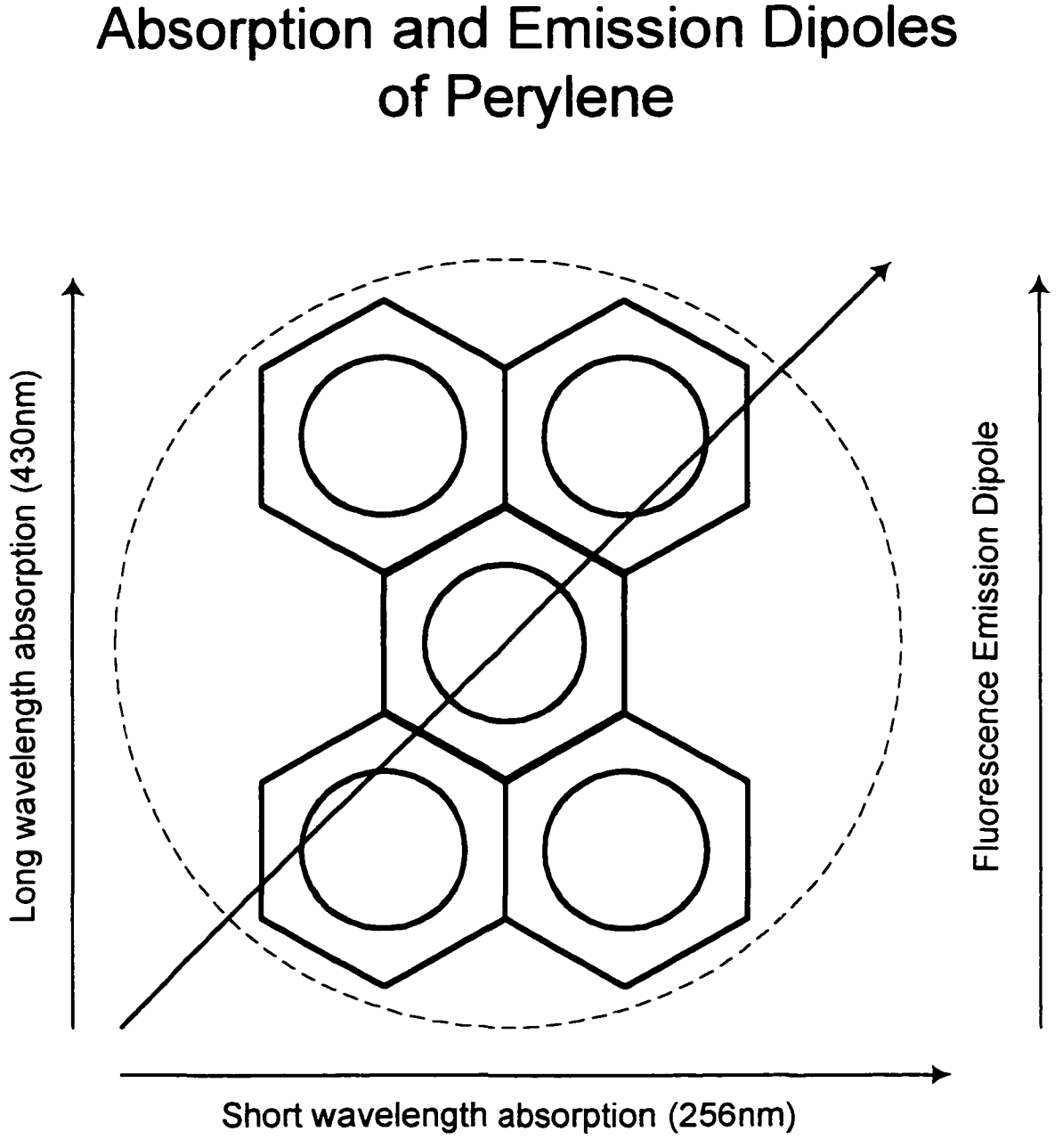

Figure 3. Absorption and emission dipole moments of perylene. There are two orthogonal absorption dipoles in the molecular plane. The emission dipole is also in the molecular plane, collinear with the long wavelength absorption dipole. Using the appropriate excitation wavelength results in an angle of approximately 0° or 90° between the respective excitation and emission dipole moments. The angle between the dipoles determines the magnitude of the fundamental anisotropy r_0, which is measured by immobilizing the fluorophore in a frozen solvent, such as propylene glycol at -65°C.

I.i. Isotropic solvent systems - Existing knowledge.

Previous work has focused on the anisotropic motions of perylene in isotropic solutions of propylene glycol [9], glycerol [11], glycerol/water mixtures [25] and paraffin [26]. Fluorescence emission anisotropy measurements were used to resolve the different rotational rates of perylene. The results were similar in all cases, showing a fast rotational rate as well as a slower rotation. Considering that the in-plane rotation displaces less solvent, the faster rotation was assigned to the in-plane rotation, and the slower rotational rate to the out-of-plane tumbling motion. The rotational rates increase with temperature, while the ratio between them remained nearly constant, reflecting changes in the viscosity of the solvent.

Excitation anisotropy spectrum of perylene in a phospholipid bilayer.

Figure 5 is a excitation anisotropy spectrum of perylene embedded in DMPC (dimyristoyl phosphatidylcholine) small unilamellar vesicles (SUVs). The excitation anisotropy spectrum shows the relationship between the steady-state anisotropy and the excitation wavelength. The superimposed dotted line shows the excitation spectrum of perylene. The relative maxima at 430 nm and 256 nm correspond to two absorption dipoles ($S_0 \neg S_1$ and $S_0 \neg S_2$, respectively) of perylene.

Steady-State Fluorescence Spectra of Perylene in Glycerol

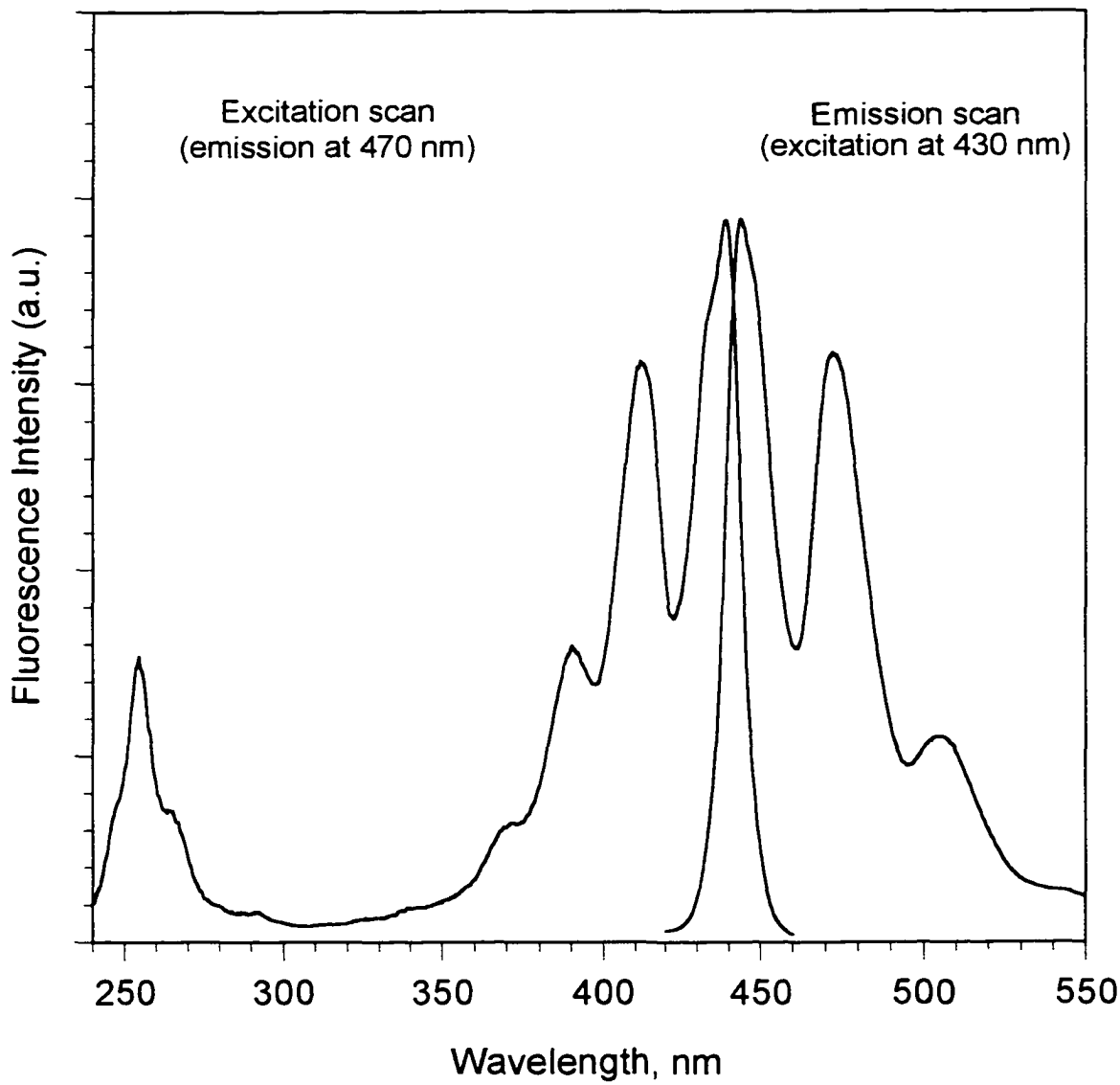

Figure 4. Steady state fluorescence spectra (uncorrected) of perylene in glycerol. The spectra were obtained using 2 nm bandpass on both excitation and emission monochromators, a wavelength step of 0.5 nm and an integration time of 0.5 second. The excitation spectrum shows the vibrational structure of the first singlet excited state (S_1) as well as the higher energy (S_2) absorption band.

Anisotropic systems - existing knowledge.

When fluorophores are dissolved in anisotropic media, it is possible for their rotational freedom to be hindered by the anisotropic solvent. When this happens, fluorescence emission anisotropy decay measurements will show a relatively long (compared to the fluorescence lifetime of the probe) rotational correlation time in addition to the one(s) that are observed in an isotropic solvent system. This additional term is symbolized by r_∞. Typically, values of rotational correlation times longer than five lifetimes of the probe would be considered hindered rotation. For phospholipid bilayers, this residual anisotropy term appears below the phospholipid phase transition temperature, when the bilayer is partially ordered. As the phospholipid bilayer melts, the structural order decreases, and the residual anisotropy term decreases or disappears completely. In addition to the main melt transition, a broad 'pretransition' has been observed for dimyristoyl- and dipalmitoyllechithin phospholipids [27]. This pretransition is caused by a structural transformation of the phospholipids from a one-dimensional lamellar to a two-dimensional monoclinic lattice.

Lakowicz and Knutson observed the hindered depolarizing motions of perylene in DMPC using oxygen quenching of fluorescence lifetimes, thereby obtaining lifetime-resolved anisotropies [9]. Using steady-state anisotropy measurements at different excitation wavelengths to probe the origin of the r_∞ values, Lakowicz and Knutson suggested that both in-plane and out-of-plane rotations were partially hindered. Since the polarization experiments were carried out in steady-state, it was not possible to resolve the out-of-plane or in-plane motions hindrances in a quantitative way.

Lakowicz, Cherek and Maliwal used frequency domain (phase and modulation)

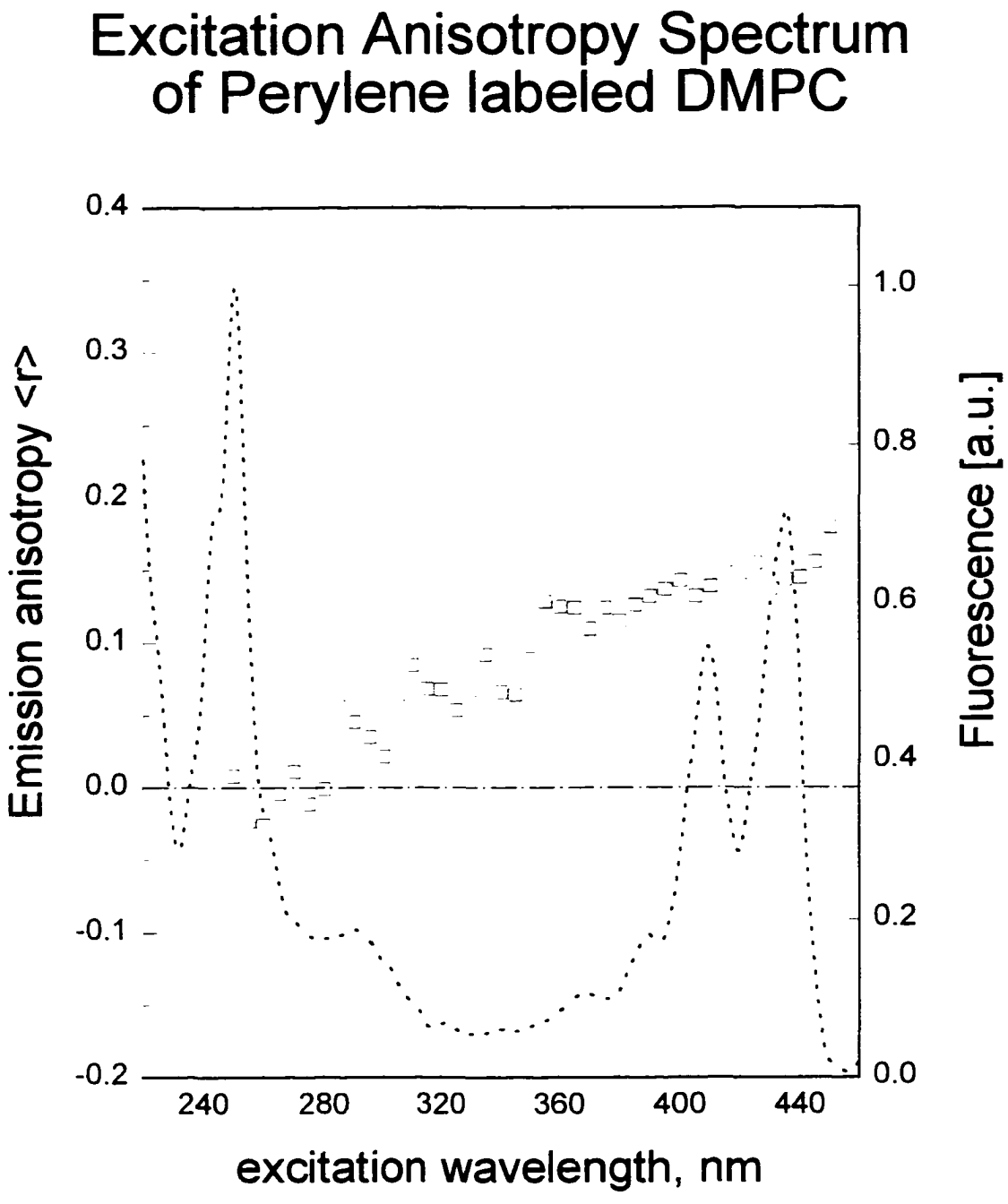

Figure 5. Excitation anisotropy spectrum of perylene in DMPC phospholipid bilayers, superimposed on the excitation spectrum.

methods to resolve the anisotropic rotations of perylene in DMPC [28]. At 5°C, three components were needed to adequately describe the anisotropy decay, fitting to rotational correlation times of 0.20 ns, 1.46 ns and 47 ns. They assigned the two shorter times to the rotational motions of perylene, and the long time to a hindrance (r_∞) term. However, only one temperature below the phase transition was examined for the perylene/DMPC system.

Chong, van der Meer and Thompson have investigated the effects of pressure and cholesterol on rotational motions of perylene in POPC multilamellar vesicles [15]. Expanding the work of Lakowicz and Knutson, they derived an expression relating the in-plane and out-of-plane motions to the steady state anisotropy and lifetimes. Chong recognized the advantage of using multiple excitation wavelengths, and measured r_0 and fluorescence lifetimes as functions of excitation wavelength (340-410 nm). From those data, an expression was derived to calculate the in-plane and out-of-plane rotational rates (R_{ip} and R_{op}). Their results indicated $R_{op} = 0.09 \pm 0.07$ GHz (11 ns rotational correlation time) and $R_{ip} = 0.25 \pm 0.08$ GHz (4.0 ns rotational correlation time) for perylene in POPC MLVs. The experiments were performed at 10°C, above the phase transition for POPC, representing an *isotropic* environment.

van Zandvoort, *et al.* [29], measured the emission anisotropy decay of perylene in POPC vesicles as functions of excitation wavelength and temperature (all above the phase transition), and used a global target analysis approach to recover sets of orientational distribution parameters. Their analysis supports a two-population model, in which two distinct rotational environments exist for perylene in the bilayer. This is consistent with the bilayer model in which perylene can be oriented along acyl chains of the phospholipid, or

in the volume between bilayer leaflets. van Zandvoort, *et al.* recovered parameters for the fundamental anisotropy which show marked reductions in magnitude from the results obtained using other analyses, and conclude that their results are ambiguous due to lack of the exact distribution of perylene in the phospholipid bilayer.

Brand, *et al.* [16] performed time-resolved emission anisotropy measurements of perylene in DMPC vesicles, using two excitation wavelengths, corresponding to the orthogonal dipoles in perylene. Using temperatures of 3°C, 10°C and 24°C, all below the phase transition temperature, they demonstrated that both in-plane and out-of-plane motions were restricted, but were cautious to note that the data could be interpreted in terms of 'microheterogeneity': different locations of perylene within the phospholipid bilayer. Brand, *et al.* have suggested the value of anisotropic rotors such as perylene in defining the anisotropic nature of lipid bilayers [16].

Wolber and Hudson used trans-parinaric acids to investigate acyl chain order in bilayers consisting of dipalmitoyl phosphatidylcholine (DPPC) and dielaidoylphosphatidylcholine (DEPC), and observed a nonzero asymptote (r_∞) of the decay of emission anisotropy [30]. Vincent, *et al.* used a series of 9-anthroyl-fatty acid compounds to probe membranes at varying depths within the bilayer [31]. Their results suggest that the out-of-plane motions of the probe are not hindered.

Models for the anisotropy decay of perylene in lipid bilayers suggest 'microheterogeneity' - multiple environments of the probe within the lipid matrix. Possible interpretations include:

a) Probe heterogeneity: Perylene is physically located in different areas of the

bilayer, either between the acyl chains, or between the bilayer leaflets.

b) Lipid packing heterogeneity: Perylene is distributed uniformly within the bilayer, but local regions of lipid are packed differently.

In reality, it is possible that both types of heterogeneity are present in a system.

I.j. Research goals.

Goal 1. - Instrumentation Design and Implementation

Design, construct and test a fluorescence lifetime system, capable of the specific requirements of this laboratory. Characterize and verify performance of the instrument, using known standards for both lifetime and anisotropy decay measurements. Once performance has been verified, the instrument will be used to perform time-resolved emission anisotropy measurements of the anisotropic rotations of perylene in anisotropic phospholipid bilayers.

Goal 2. - Anisotropic rotations of perylene in anisotropic media.

This research examines the rotational motions of perylene in various phospholipid bilayers, as examples of anisotropic solvent systems. The anisotropic solvent systems are represented by the hydrophobic regions of phospholipid bilayers. Perylene 'reports' the apparent viscosity of the environment immediately around itself. Since perylene is water-insoluble, it is not present in the bulk solvent (aqueous buffer) in which the phospholipid bilayers are suspended. The viscosity of the hydrophobic region of the bilayer is termed 'microviscosity', to distinguish it from the viscosity of the bulk solution, in this case aqueous

buffer .

The anisotropic rotations of perylene embedded in these anisotropic phospholipid bilayers will be used to obtain information about the structure, packing and 'microviscosity' of these systems. To this end, we have obtained a comprehensive set of time-resolved anisotropy decay measurements of perylene in various phospholipid matrices. Using multiple excitation wavelengths and temperatures, a complete experimental 'surface' is formed for the anisotropy decay of perylene in two phospholipids. Global data analysis techniques are used to solve these experimental surfaces, yielding unique solutions.

One aim of this research is to differentiate between probe distribution heterogeneity and lipid packing heterogeneity. The ability to resolve the heterogeneity question helps resolve the ambiguity of results, a problem recognized in a recent paper [29]. To differentiate between the possible cases, we used two different phospholipid systems. DMPC is a symmetric chain length phospholipid, which allows partitioning of perylene into two different regions, between the acyl chains and the volume between the bilayer leaflets. To eliminate the partitioning of perylene into the volume between the bilayer leaflets, we used an asymmetric chain phospholipid (C18):C(10)-PC, which interdigitates below its phase transition temperature. In this novel phospholipid, perylene is excluded from between the bilayer leaflets, and will only be located along the acyl chains. The rotational motions reported by this population of probes will correspond only to a homogeneous probe distribution. Figure 6 shows a cross-sectional schematic of bilayers prepared from symmetric and asymmetric chain phospholipid bilayers, with possible locations of perylene in each.

Ideally, the rotational rates of perylene in lipid bilayers should come from dynamic (time-resolved) data, but complete sets of data are not available in the literature [15]. At this time, there are no reported studies of perylene embedded in asymmetric lipid bilayers in the literature.

When perylene is used as a probe for phospholipid bilayer packing and dynamics, the solutions for isotropic solvents are no longer valid, due to the anisotropic nature of the microenvironment in which the perylene dye molecules partition into. Models used for isotropic solvent systems such as glycerol do not account for the existence of hindered motions of the probe when it is dissolved in an anisotropic environment. For phospholipid bilayers, the magnitude of the hindrance (r_∞) is temperature dependent. This temperature dependence must be accounted for in the mathematical fitting parameters (preexponentials) that describe the rotational motions.

We have derived an extended rotational model, which accounts for temperature dependent preexponential terms. This model can be applied to different phospholipid bilayer matrices, and reduces mathematically to the same expressions for unhindered, isotropic solvent systems, once the phospholipid has undergone a phase transition from the crystalline to liquid crystalline phase.

Phospholipid Bilayers and Probe Heterogeneity

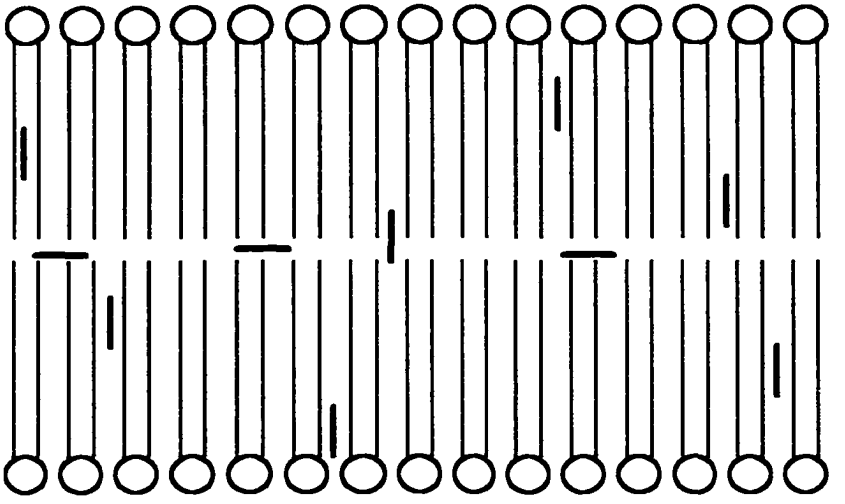

DMPC - A Symmetric Chain Phospholipid Bilayer

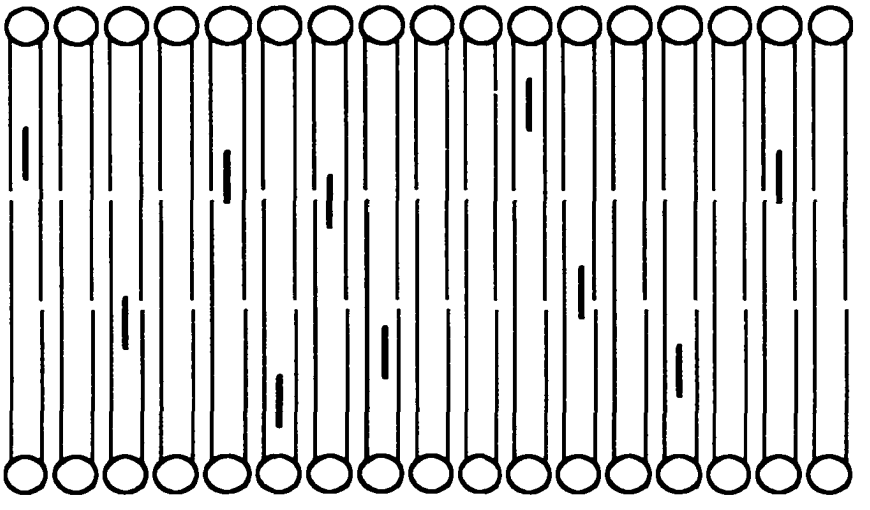

C(18):C(10) PC -
An Asymmetric Chain Phospholipid Bilayer

| = Perylene Molecule Aligned with Acyl Chains

— = Perylene Molecule Located Between Bilayer Leaflets

Figure 6. Diagram of a cross section of a bilayer, showing the possible locations of the perylene fluorescent probe. In the symmetric DMPC bilayer, there is the possibility of partitioning between the bilayer leaflets. In the novel asymmetric lipid, C(18):C(10)-PC, this region is excluded due to interdigitized lipid acyl chains.

Section II. - Construction of a Time-Resolved Fluorometer.

The first section of this Thesis details the construction of a time-resolved fluorometer, with the following capabilities:

* Multiple samples ;

* Polarization of excitation and emission light;

* Automated sample and polarizer angle selection;

* Automated emission wavelength selection;

* Automated temperature scanning;

* T-format design, using two detectors to allow simultaneous collection of emission from two faces of the sample cuvette simultaneously.

Several instrumental methods and techniques are available for the measurement of fluorescence lifetimes on the nanosecond timescale, commercially as well as in the research laboratory domain. The major techniques include:

a) Phase and modulation (frequency domain);

b) Pulse-sampling methods;

c) Time-correlated single photon counting (time-domain).

There are tradeoffs in all of these techniques, and there is no one best approach to the measurement of fluorescence lifetimes. Table II is an overview of advantages and disadvantages of three major techniques.

Table II. Overview of Methods for Fluorescence Lifetime Measurements

	TCSPC (Time Domain)	**Phase/Modulation (FD-Frequency Domain)**	**Stroboscopic (Time Domain)**
Main Advantages	Direct measurement. Extremely Sensitive. High precision and resolution of multicomponent decays.	Short ps lifetimes relatively easy to measure. Broadband source offers excitation wavelength tunability. Less expensive for a given performance level than TCSPC.	Inexpensive low rep-rate laser offers good sensitivity. Inexpensive to construct.
Main Disadvantages	True picosecond lifetimes require expensive source and detectors. Flashlamps and lasers lack broad tunability of wavelength.	Sensitivity is lower than TCSPC. Requires good signal level (photon flux) to obtain best s/n.	Resolution of multicomponent decays more problematic than TCSPC and FD.

The choice of the method used affects the instrument design process at an early stage. In terms of the actual hardware, the excitation source and signal detector show the greatest differences between the methods. Supporting electronics will also vary widely among the methods. Data analysis techniques will be different, depending on the mathematical form of the observed signal. Usually, a non-linear least squares search algorithm is used to fit the experimental data to proposed physical models.

Figures of merit for fluorescence lifetime systems include:

a) Experimental observables

b) Precision and accuracy

c) Complexity and cost

d) Special considerations and requirements, peculiar to each technique.

A matrix of figures of merit for the three main techniques is presented in Table III , below.

Table III.Main Hardware Differences for Lifetime Measurement Schemes.

	TCSPC (Time Domain)	**Phase/Modulation (FD-Frequency Domain)**	**Stroboscopic (Time Domain)**
Source	Flashlamp Pulsed Laser	CW Lamp CW Laser Pulsed Laser	Pulsed Laser
Detector	Fast PMT MCP / PMT	Fast PMT MCP / PMT	Fast PMT / Modified Dynode Chain
Observable	Time Difference between Excitation and Single Photon Emission	Phase Shift and Demodulation (Harmonic Response)	Intensity at Specific Time after Excitation Pulse
Precision	good-high	good-high	good-varies
Accuracy	high	high	good, varies with sample
Complexity	varies, generally complex	varies, often simple	varies, often simple
Cost	varies, depends on source. Cost can be high for true ps lifetimes	generally lower than TCSPC with ps resolution	generally lower than TCSPC and good FD systems
Speed	Generally fast, but varies, depends on signal level and source.	Varies, depends on available signal level, and therefore, the source.	Varies, can be relatively fast.

The light source and detector vary greatly among the various implementations of lifetime instrumentation. The source in frequency domain instrumentation is usually a continuous wave arc lamp (Xe or Xe(Hg)), or a CW laser. Pulsed laser sources may be used in certain implementations of frequency domain instrumentation, utilizing the harmonic content of the sharp laser pulse to extend the effective frequency range of the instrument.

II.a. Comparison of fluorescence lifetime measurement schemes.

II.a.1. TCSPC (Time-correlated single-photon counting).

The time-correlated single photon counting experiment is fundamentally simple. It is an interval timing method, where many START/STOP intervals are measured and stored in an accumulator, forming a histogram of the events.

The sample is excited by a brief pulse (2-3 ns with a flashlamp, much less, ca 60 ps, with pulsed laser) of light, and a photomultiplier tube monitors the sample emission. The time difference between these events is measured and recorded. The experimental conditions are adjusted so that the ratio of detected photons to excitation events is small, typically less than two percent. This low counting rate is necessary to prevent pulse pile-up distortion and assure a Poisson distribution of the data. Pulse pile-up is a phenomenon which biases the measured decay towards shorter times, due to multiphoton events being detected by the emission photomultiplier [32]. For the data analysis, a Poisson distribution is assumed. Without the assumption of Poisson counting statistics, the statistical weights used would be incorrect, leading to the recovery of incorrect parameters for the fluorescence decay.

Traditional spark gap flashlamps, used as excitation sources, are relatively inexpensive. Such lamps are offered with several commercial time domain instruments, including products from Edinburgh, IBH and PTI. The main disadvantages of spark gap flashlamps include pulse width limitations, low repetition rates and the relative lack of wavelength tunability. Mode locked laser arrangements are much more costly to implement, but, compared to flashlamps, offer narrow pulse widths at high intensity and high repetition rate. Laser based systems are more common in research labs who have constructed their own instrumentation to meet specific requirements. With either a laser or flashlamp, pulse profile, stability and pulse width are important. Time resolution as well as the successful analysis of TCSPC data rely on narrow, stable pulses over the time course of the entire experiment. For best results, time domain data must include correction for the distortion of signals by the instrument system. The excitation source, emission detector and electronic responses tend to distort the measured decay by convolving the true signal with the instrument response. The details of the experimental and mathematical treatment of these distortions are discussed in more detail in a later section.

II.a.2. Frequency domain (phase and modulation) method.

Frequency domain (FD) measurements are indirect, and measure the harmonic response of a sample to intensity modulated light at various frequencies. The data provided by early FD instruments was limited to simple decays, due to the limited number and range of frequencies available for modulation. More recent instrumentation uses continuously variable modulation frequencies. Modulation frequencies ranging from a few kilohertz to

300 MHZ or higher are used to span lifetime ranges from hundreds of nanoseconds to picoseconds, by selecting the appropriate frequency range. These frequencies are near the microwave region, and high precision and stability radiofrequency (RF) modules are required. The cross-correlation technique, a form of heterodyning, has made the frequency domain measurements easier to perform. By heterodyning, the analytical signal is encoded at a much lower frequency, typically near 25 Hz. Electronics that process low frequency signals are available at low cost. This cross correlation technique is the basis for several commercial frequency domain lifetime fluorometers.

Both FD and TCSPC data can be collected to the required degree of statistical precision. In the TCSPC method, the experimental run time is increased to collect a higher number of counts in the decay curve. The precision of frequency domain measurements improves with a greater number of independent measurements of the phase shift and demodulation at each modulation frequency. Both TCSPC and FD data require a reference compound to be measured during the data collection. The reference compound is used in different ways: Frequency domain systems use the reference lifetime to compensate for frequency response of the instrument system, time-domain systems use the reference compound to determine the instrument response function. TCSPC also requires an additional reference compound, to calculate the color shift (Qshift) parameter, necessary since the instrument response function is measured at a different wavelength than the fluorescence emission.

The overall cost of a TCSPC system can be lower than other methods, since only a few of the electronic modules must be capable of measuring fast time events. In other

methods, most, if not all, of the electronics must be able to encode very short (nanosecond time scale) time intervals in real time, and the added expense of these faster modules increases the total system cost.

In all instruments, the photon detector itself is usually a commercially available photomultiplier tube. Figures of merit common to all fluorometers include high gain, low dark noise characteristics, and good timing response over the wavelength range of interest. Various techniques for setting up the photomultiplier voltage divider are used to optimize the signal appropriate for each method. Often, the different methods are not interchangeable between systems, even though they might all use the same photomultiplier tube type. This is especially true of the side-window Hamamatsu R928 PMT, which has been used in all major lifetime designs, as well as in many steady-state instruments. In TCSPC, the tube is wired in a manner that provides excellent timing characteristics with high gain. In frequency domain systems, one of the dynodes in the photomultiplier chain is modulated at RF frequencies to accomplish heterodyning, which encodes the phase shift and modulation information of the sample from high frequency (RF) to low frequency (subaudio) domain. This makes measurements of small phase shifts possible with high precision, using lower cost electronics. In stroboscopic methods, the entire photomultiplier tube bias voltage is applied as a pulse, which propagates along a strip line connected to the dynodes. This enables gain in the tube for only the time window in which there is voltage present at a given dynode [33].

Table IV outlines a matrix of detector characteristics that are important for each technique.

Table IV. Detector Characteristics.

	TCSPC	Freq Domain	Stroboscopic
Signal Type	Pulse	heterodyne difference frequency	Pulse
voltage divider	tapered dynode	modified to modulate gain of intermediate stage dynode	dynode 'strip line'
bias voltage	high >2kV typ	moderate ~1kV	moderate ~1kV
gain	very high	high	high
dark signal	very low	low	
risetime	fastest	less critical, if differential measurements are used.	
Timing Response	very important	less important	

II.b. General Design Considerations.

Optical design requirements for any fluorometer system include high sensitivity and throughput, with minimum stray light. The core optical components, which direct the light through the instrument, will be similar in all fluorescence instruments. The simplest and least expensive optical path is usually lens based. Lens based designs suffer from chromatic aberrations, due to the varying index of refraction of the lens material with wavelength. This results in changes in focus as the wavelength is varied. Use of mirrors, both planar and curved (spherical, ellipsoidal and/or toroidal) to collimate and redirect light eliminates chromatic aberration effects, since the light is reflected rather than refracted.

Stray light rejection is important with weak emitters and polarization studies.

Scattered light may cause serious artifacts in measurements of fluorescence emission anisotropy, producing artificially high steady-state values for emission anisotropy. Rayleigh scattered light is completely polarized, and the measurement of a scattering material will provide an anisotropy value of 1.00. (This fact is useful for verifying the alignment of polarizers.) The range of anisotropy values allowed, with 90 degree viewing, is -0.2 to +0.4, and values outside this range may be caused by the incomplete removal of scattered light by the emission monochromator. In emission anisotropy *decay* experiments, scattered light may distort the measured preexponential values, giving rise to unrealistic values for the limiting anisotropy of the fluorophore under study.

Optimization of experimental conditions is important in the elimination of scattered light. When experimental conditions make scattered light rejection difficult, it may be possible to correct for this component mathematically, by adding a compensatory term during the data fitting process. Such situations may arise when:

a) the samples are highly scattering, turbid media, which scatter the excitation light (Rayleigh scatter). Rayleigh scatter can be reduced or eliminated by using appropriate experimental conditions. Usually, appropriate choices of emission wavelength and spectral bandpass help avoid detection of scatter. An optical filter, placed in the emission path, may also be used.

b) Raman scatter is present in the emission spectrum and cannot be avoided by choosing alternate wavelengths. Raman scatter mimics fluorescence, since it is shifted to a longer wavelength with respect to the excitation wavelength. If the Raman band superimposes the fluorescence emission range of interest, it cannot be removed by using a

filter. For the excitation wavelengths used in the experiments presented here, the Raman bands of water (the bulk solvent) would appear as shown in Table V:

Table V. Expected positions of water Raman interference.

Perylene Excitation Wavelength, nm	water Raman peak position, nm	Perylene Emission wavelength, nm
260nm	285nm	448nm
315nm	353nm	448nm
410nm	476nm	448nm

Both Rayleigh and Raman scattered light have a lifetime of zero, but differ in the wavelength of observation with respect to the excitation wavelength. For the experiments performed here, Raman scatter did not present a major problem, due to the excitation and emission wavelengths used, as well as the spectral bandpass of the monochromators in the emission path.

We have chosen the time-correlated single photon counting method for reasons of simplicity, sensitivity, directness and resolving power. Sensitivity and precision are important when considering the type of experiments required to resolve multicomponent intensity decays and multicomponent anisotropy decays expected in our samples. Calculation of the rotational correlation times involves the difference between two polarized emission decay curves. The number of counts in each curve must be high, so that the difference between them contains a sufficient number of counts to be statistically valid. With TCSPC, increasing the experimental run time results in higher precision due to signal averaging. There are practical upper limits to total experiment run time. Samples may photodegrade or decompose, and the excitation (flash lamp) source also becomes unstable,

requiring cleaning and realignment between experiments.

II.c. Implementation of the TCSPC method in this laboratory.

Figure 7 is a block diagram of the TRF (Time-Resolved Fluorometer) that was constructed in this laboratory. A timing event begins with the discharge of the IBH Coaxial Nanosecond System 5000 flashlamp. The flash is detected by a 1P28 photomultiplier tube coupled to the lamp with a fiber optic cable. The resulting anode pulse from this photomultiplier passes into an ORTEC 463 CFD (constant-fraction discriminator), which is used to START an ORTEC 566 TAC (time-to-amplitude converter).

The excitation light flash is collected by an f/2 achromatic focusing lens. Excitation wavelengths are selected with interference filters (Ealing Electro-Optics, bandpass 10 nm and 15 nm). Following wavelength selection, the excitation beam passes through a Da-Lite Polacoat UV sheet polarizer, to select a polarization orientation. The polarized light excites the sample under investigation. Light emitted from the sample is collected at right angles to the excitation beam, passes through a second Da-Lite Polacoat UV sheet polarizer, and is focused onto the entrance slit of an ISA H10 monochromator by a quartz lens. The image of the exit slit of the monochromator is focused onto a Philips XP2020Q quartz window photomultiplier tube, using a quartz lens. The anode pulse from this PMT is shaped by a TENNELEC TC455 CFD, and is applied to the STOP input of the TAC. The TAC converts the measured time difference between sample excitation and emission to an analog voltage proportional to the time difference between START and STOP signals. The analog output is routed to an ORTEC 918A multichannel analyzer through an ORTEC 476-8 multiplexer.

The MCA (multichannel analyzer) stores the data as a histogram of the number of photons versus the time of arrival of each photon. The multiplexer also routes signals from the second channel of the instrument into the MCA, avoiding duplication of an expensive module. This entire START/STOP cycle is repeated many times, until the required statistical precision has been obtained.

II.d. Details of the Instrumentation.

Figure 7 is a schematic diagram of the instrument, showing the layout of the system as a whole. Each major section will be described in more detail below.

Excitation Source.

The excitation source is a thyratron-gated low-pressure spark discharge lamp. It is a commercially available system (IBH Consultants, Ltd. 64 St. Vincent Crescent, Glasgow G3 8NG, Scotland, U.K.), using an all-metal design to maintain high stability pulses with low RF emission [34]. Figure 8 shows a cross sectional view of the IBH System/5000 Coaxial Flashlamp. Different filler gases may be used, depending on the desired spectral emission lines. Most commonly, nitrogen gas is used, but deuterium offers better UV intensity and narrower pulse widths. Argon and argon/hydrogen mixtures offer excitation wavelengths extending into the near infrared [35]. Excitation as far as 930 nm has been reached using this technique, using a red-extended (Philips XP2254B) photomultiplier tube for detection [36]. Operating conditions of the lamp vary, depending on filling gas and desired properties. Ideally, pulses produced by any source for TCSPC should be of narrow

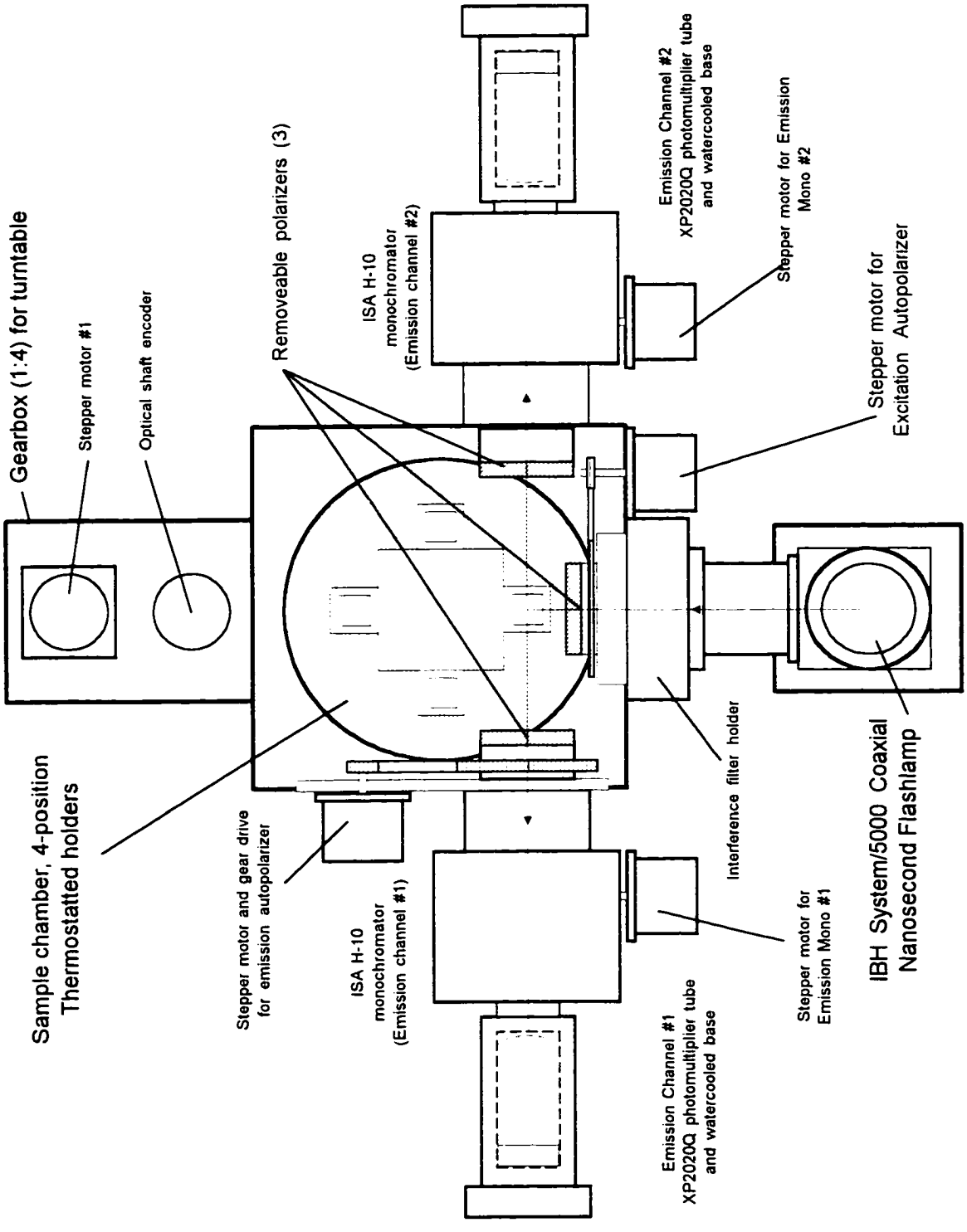

Figure 7. Layout of the TRF 'Time-Resolved Fluorometer' implemented in this Thesis. (This drawing is not to scale.)

width, reasonable intensity, with a high repetition rate, and stable over many hours [37]. In practice, it is not possible to satisfy all conditions simultaneously. It turns out that the narrowest pulses are not the most stable ones, and higher pulse repetition rates cause wider pulse profiles, as well as reduced intensity per flash. A compromise must be reached, depending on the particular needs of the experiment. For example, when measuring perylene at 250 nm / 448 nm, the intensity of the lamp is very low after passing through the interference filter and excitation polarizer. Attempting to increase the count rate by increasing the repetition rate was not successful, since the number of photons per flash decreases with higher repetition rates. By experimentation, a repetition rate of about 26 KHz was found to deliver stable, narrow pulses, with nearly maximum intensity. Additionally, lowered repetition rates result in the electrodes lasting longer between cleanings.

The most important factors governing lamp stability are summarized below [34-36]:

a) Applied potential to the electrodes.

b) Electrode spacing (gap).

c) Thyratron repetition rate, and heating current.

d) Pressure and quality of the lamp filler gas.

e) Arrangement and shape of the electrodes.

The applied electrode potential depends largely on the electrode gap. Optimum applied potential levels were initially determined by monitoring the stability indicators present on the front panel controls of the IBH Coaxial Flashlamp. These indicators correlate the thyratron trigger pulse with a detected flash. If a trigger pulse is issued, and no flash is detected, a 'Misfire' event is signaled. If a flash is detected (by the synchronizing

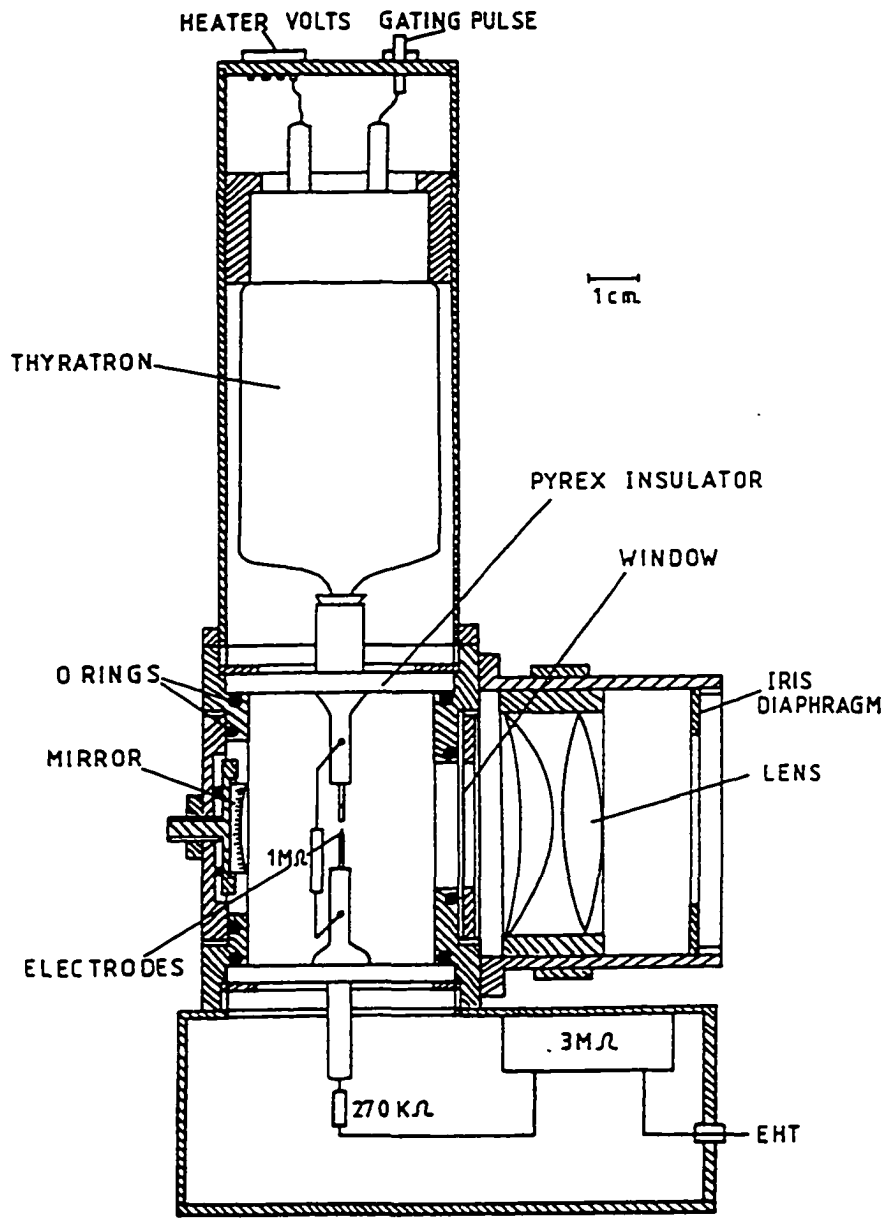

Figure 8. Cross-sectional view of the IBH System/5000 Coaxial Nanosecond Flashlamp used as the excitation source for the time-resolved fluorometer. (From reference 34).

photomultiplier via a fiber-optic coupling) without a trigger pulse, a 'Free-Run' condition is signaled. To refine the operating conditions, an oscilloscope was used to monitor a loop antenna device, fitted to the rear access port of the IBH System/5000 flashlamp. Using the oscilloscope, the electromagnetic pulse associated with each flash is easily monitored. Pulse distortion and jitter appear when the applied potential is too high. For nitrogen, applied potentials are always higher than those for deuterium, even though the optimum electrode gap is much smaller. The spark gap was set with an ordinary automotive feeler gauge after each lamp cleaning. The filler gas pressure is measured by a transducer, plumbed into the lamp inlet fitting, and can be read directly in bars on the IBH System/5000 controller. Typical operating conditions are listed in Table VI, below.

Table VI. Typical operating conditions: IBH System 5000 Flashlamp.

λ_{ex}	Filler Gas	Pressure (bar)	Electrode Gap	High Voltage	Pulse Rep Rate
430 nm	nitrogen	0.8-1.2	0.4-0.6 mm	5.5-7.0 kV	22-40 kHz
410 nm	nitrogen				
360 nm	nitrogen				
340 nm	nitrogen				
315 nm	nitrogen				
250 nm	hydrogen, deuterium	0.4-0.6	1.5-2.5 mm	5.0-6.5 kV	15-25 kHz

Filling gases were UHP Grade Nitrogen, obtained from Linde Specialty Gases, and Deuterium, C.P. from Matheson. Purity of the filler gas is very important for long-term stability of the flashlamp. Lower purity gases tend to foul the electrodes much earlier, and

cause lamp instability. The filler gases are handled by a small manifold equipped with separate valves to control the flow of each gas, and provide a vacuum pump inlet and atmospheric vent valve. With this manifold, the lamp can be isolated from the remainder of the gas handling system, so that gas cylinders may be exchanged, or the vacuum trap be cleaned without affecting a running experiment. A rotary vacuum pump, equipped with a liquid nitrogen cold trap, is used to evacuate the lamp housing. Trapping is required to ensure that no vacuum pump oil vapors enter the lamp, which causes electrode contamination and unstable operation. Evidence of such contamination includes greyish to black residues which coat the entire interior of the flashlamp housing. Removing this filmy deposit satisfactorily requires that the entire flashlamp be torn down, cleaned and reassembled. A superficial cleaning through the rear access port has not been found to be successful.

Sample Compartment.

The sample chamber and its associated gearbox were constructed by the Brooklyn College Machine Shop. It consists of a motor-driven turntable which supports four water-cooled cuvette holders. These holders are arranged 90 degrees apart on a 4.0 inch bolt circle. A stepper motor drives the turntable through a 1:4 underdrive gearbox. This multiplies the torque of the small stepper motor and allows for greater precision in the angular positioning of the turntable. Under software control, the samples are moved into the optical path in a cyclic fashion. Four Superior Electric SLO-SYN 200 pulse/rev stepper motors handle all motion control, controlled by MetraByte MSTEP5 cards and remote STA-STEP

translator electronics mounted in a Hewlett Packard Vectra 286 PC. Each MSTEP5/STA-STEP combination can drive two stepper motors.

Temperature Controller.

Automatic temperature control is implemented using a Lauda K-2/R refrigerated water bath, controlled by an OMEGA 6071A PID temperature controller. A ceramic RTD (resistance temperature detector, OMEGA part number 1 Pt 100 K 20 28) mounted directly in the sample holder, is used to monitor the sample temperature as close to the cuvette as possible. The signal from this RTD is used by the OMEGA controller to drive the heating coil of the water bath through an external triac. The OMEGA controller is linked to the HP Vectra 80286 acquisition computer using a standard RS-232 interface.

Autopolarizers.

The excitation port and left emission arm of the sample chamber are fitted with stepper-motor autopolarizers, controlled by the acquisition program. These are useful for the determination of the G-factor and the V / H anisotropy components using one sample only. The right emission arm of the instrument can use a fixed polarizer when T-format measurements are desired. In a T-format polarization measurement, the instrument allows simultaneous acquisition of vertical and horizontal components of polarized emission spectra, by viewing the same sample along both emission faces of the cuvette. Alternately, two emission spectra can be collected at different emission wavelengths or time regions simultaneously.

Emission Optics.

Both emission sides of the sample chamber have been fitted with identical quartz emission optics and motorized emission monochromators. While it is possible to use optical filters to select the emission wavelength, there are advantages to using a monochromator. Filters are not tunable, so performing an automated series of experiments at different emission wavelengths would not be possible. In addition, some optical filters introduce artifacts, since some fluorescence and/or phosphorescence background may be present.

Using monochromators eliminates these problems, at a cost of lower throughput. We chose the ISA H-10 monochromator (Instruments SA, Inc. Edison, New Jersey) on the basis of its small size, low cost and excellent stray light rejection. The ISA H-10 monochromator uses a concave holographic grating as both a focusing and dispersion element. It is equipped with fixed, drop-in slits to adjust the spectral bandpass. Using the fixed slits provided, we can select a spectral bandpass of 4nm, 8nm or 16nm, which is comparable to a good interference filter. There are also the additional benefits of tunability while remaining free of artifacts from the glass elements of optical filters. Some specifications of the H-10 are listed in Table VII.

The wavelength of each monochromator is independently adjustable. Automation of wavelength selection was accomplished using two Superior Electric SLO-SYN 200 pulse/rev stepper motors, coupled to each monochromator using a 1:1 belt/gear drive system. The stepper motors are controlled by MetraByte MSTEP5 cards and remote STA-STEP translator electronics, and operate under software control of an HP Vectra 286. Figure 9 shows the interconnections and interface. Two MSTEP-5 cards were installed in the HP

Table VII. ISA H-10 Monochromator Specifications

Optical design	Seya-Namioka
Number of Gratings	Single grating
Focal length	0.10 meter
Numerical aperture	f/3.5
Grating	concave holographic, ion-etched 32x32 mm 1200 grooves/mm
Linear dispersion	8.0 nm / mm
Blaze wavelength	450 nm
Slits	0.5 mm, 1.0 mm, 2.0 mm
Stray light	10^{-5} (8 SBPs from 632.8 laser line)

Vectra, each set to a different base I/O address. Each MSTEP5/STA-STEP combination can control two motors. Both monochromators are controlled by one of the MSTEP5 cards. The sample turntable is controlled by one half of the second MSTEP5 card. An adjustable excitation polarizer, controlled by a fourth stepper motor, occupies the second channel of the card. All four available controller channels are in use. Five stepper motors are utilized in total, as shown on the instrument block diagram. To allow easy 'cable swapping' of the motors, 9-pin Amphenol CPC quick-disconnect plug and jack assemblies were employed. Each of the stepper motors is wired alike, so they may be easily interchanged without risking errors in reconnecting six leads per motor. An error in reconnecting the motor windings will damage the motor controller as well as the stepper motor itself. The risk of damaging the computer hardware is less, because the translators use optoisolators to protect the main controller cards from short circuits in the load.

Detector Photomultipliers.

The emission photomultipliers used in TCSPC have certain requirements [40]. These include:

- high gain
- low dark noise
- low transit time spread
- useable photocathode sensitivity over wavelength range of interest

A commercially available tube that satisfies all of the above requirements is the Philips XP2020Q photomultiplier tube. These photomultipliers have high gain with low dark noise, as well as low transit time spread across the photocathode area. The XP2020Q tube has a quartz window, allowing work in the UV, a requirement for the short wavelength (250nm) studies of perylene. Additionally, the UV response is advantageous when protein experiments are required, where the excitation wavelength is typically near 295 nm for tryptophan studies.

The Philips PMT base is wired for operation with the photocathode at a high negative potential, and the anode at ground potential. This places the entire envelope of the tube at a high negative potential with respect to ground. Dark counts are higher in this grounded anode configuration, since the anode is DC coupled directly into the discriminator [38]. However, the risk of high voltage entering the discriminator is eliminated. We found it necessary to use a continuous flow of dry grade compressed air, passed through an additional column of dessicant, into the photomultiplier housings to reduce the dark counts to an acceptable level. At least one research group has reported similar observations in the

literature [39] and eventually eliminated the purge gas requirement by rewiring the voltage dividers to operate in the grounded photocathode configuration as a permanent solution.

The emission photomultiplier tube housings are equipped with cooling coils. They consist of 0.25 inch copper tubing wound around the forward section of each of the photomultiplier tube bases. The purpose of cooling the tube housings is to decrease the dark counts caused by thermionic emission [40]. The coils are maintained at 15°C using a refrigerated circulator (Fisher Scientific IsoTemp Refrigerated Circulator).

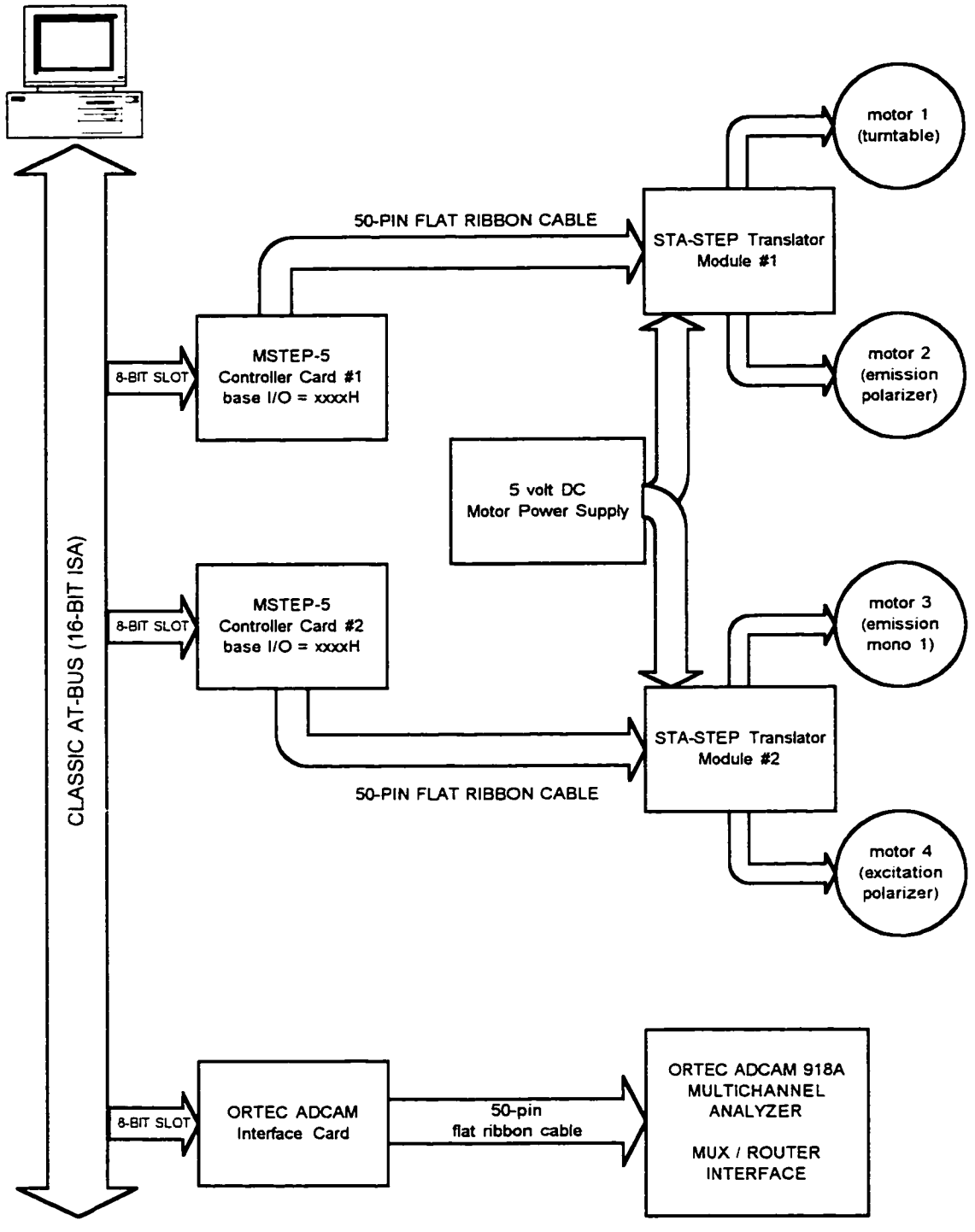

Figure 9. Interconnection of motion control hardware in the 'TRF' (Time-Resolved Fluorometer). Two MetraByte MSTEP-5 cards, in the host PC backplane, control two stepper motors each, for a total of four motion control channels. Each STA-STEP translator provides optoisolation to protect the host computer from higher currents required to drive the stepper motors. The multichannel analyzer also uses an 8-bit PC slot, and is shown for completeness of the computer interface elements.

II.e. Timing electronics used in the TCSPC system.

Figure 11 presents a diagram of the electronic interconnection of the timing system modules. Most of the modules are housed in a nuclear instrument bin (NIMBIN), which is itself mounted in a standard 19 inch rack. Having all electronics, including the lamp power supply, mounted in the same rack makes it easier to control grounding and reduces the potential for ground loops [41] and RF pickup. In addition, the chassis of all modules were interconnected by a continuous length of hollow braided wire, which was threaded with solid copper wire and soldered every 30 centimeters along its length. This technique provides a common DC and RF ground [42].

In TCSPC, the experimental observable is the difference in time between the excitation of the sample, and the emission of a photon from the sample. The excitation of the sample is coincident with the discharge of the flashlamp, which is monitored by a fiber optic cable and detected by the synchronizing photomultiplier. The emission of a photon from the sample is detected by the emission photomultiplier. The time difference between the excitation and emission of the sample is encoded as the time difference between the anode current pulses developed by these two photomultiplier tubes. To properly time this interval, the anode signals are shaped and converted into logic pulses, which are used to trigger the timing system.

Discriminators.

Pulse shaping is accomplished using a constant fraction discriminator (CFD). A CFD is best for timing measurements, since it triggers with lower time jitter than a leading-

edge discriminator [43]. Provided that the pulses have the same *risetime*, the CFD will properly time a series of pulses that have a range of amplitudes. This situation is precisely that of the pulses generated at the photomultiplier anode. A leading-edge discriminator is less precise for timing measurements, emitting an output pulse when the input signal exceeds a certain threshold. The output pulse is dependent on the amplitude of the photomultiplier signal, and this increases the timing error. We chose a commercially available CFD, the Tennelec 455, which has very low timing jitter. It adapts to various detector risetimes with a user-adjusted external delay line. Additional features of the Tennelec 455 include:

- it accepts four independent inputs simultaneously.
- User adjustable threshold, z/c (zero crossing) and output pulse width.
- CD Fraction: 20 percent, adjustable by changing a module.

The Tennelec 455 Quad CFD uses LEMO-style connectors, requiring use of RG-174 coaxial cable and BNC adapters for interconnection with the rest of the electronics.

Delay lines.

Delay lines are lengths of coaxial cable that delay the logic pulse. These delays are necessary to compensate for different propagation delays among the electronics, and allow proper synchronization of the pulses to the timing electronics. The delays must be variable, so that the decay curve can be 'shifted' in the multichannel analyzer memory to avoid regions of the TAC/MCA combination that are nonlinear. Pulses propagate in coaxial cable at 19 cm/nanosecond, varying with cable dielectric material and geometry. We have a commercial ORTEC Delay box which contains calibrated lengths of RG58 C/U coaxial

cable corresponding to 1,2,4,8 and 16 ns of delay. Additionally, we prepared a series of custom length RG-174C/U delay lines, and mounted them in a blank double width NIM module to provide RF shielding.

Time-to-amplitude converter (ORTEC 566 TAC).

The time-to-amplitude converter (Figure 10) is the heart of the system. The time difference between the excitation and emission of light from the sample is measured by the TAC. The TAC operates in a stopwatch fashion, with a START signal initiating a timing event, and a STOP signal terminating it. When the TAC receives a START signal, it initiates a ramp voltage function whose slope is variable, depending on the desired time region of interest. The ramp voltage rises linearly, until a STOP signal is received. The magnitude of the ramp voltage achieved is proportional to the time difference between the START and STOP signals. This analog voltage is presented at the TAC output, and a logic signal is also generated, to indicate that a valid conversion was completed. This VALID CONVERSIONS signal was used to count the actual number of START/STOP cycles measured per second. Figure 10 shows a diagram of the TAC module operation, as a 100 ns time difference is being converted. In the Figure, the slope of the TAC voltage ramp is 10.00V/200ns, or 50.00mV/ns. This corresponds to a full scale setting of the timing window of (200x1) nanoseconds.

Time to Amplitude Converter (TAC) Module Operation

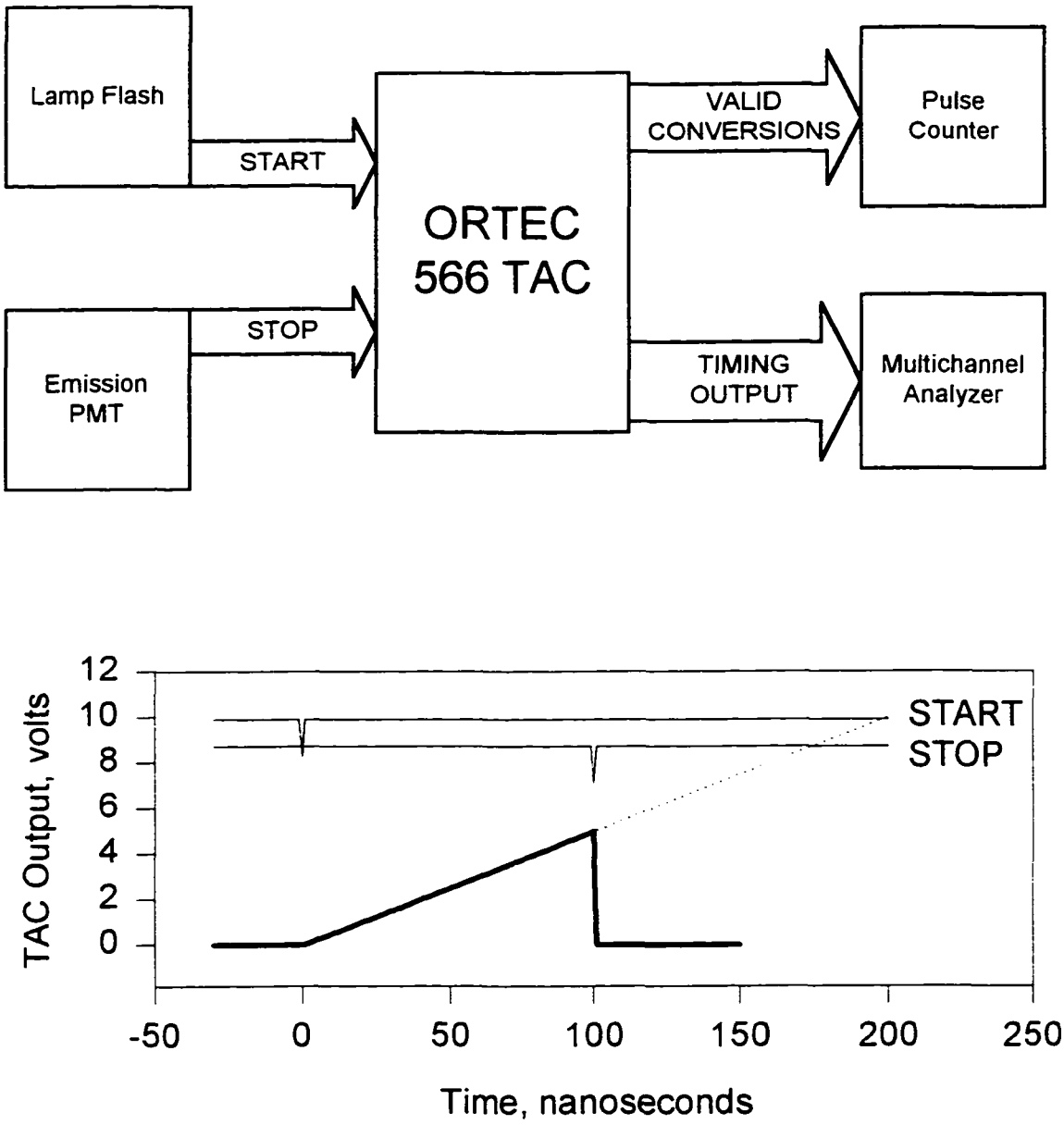

Figure 10. Diagram of TAC operation. The TAC accepts a START and STOP logic signal, and produces an output voltage that is proportional to the time difference between them. In this diagram, the TAC full scale is 10.0 volts at 200ns. The time difference shown here corresponds to 100 nanoseconds, producing a timing output pulse of 5.00 volts. The VALID CONVERSIONS signal line emits a pulse when such a START/STOP cycle has been completed.

Multiplexer (Ortec 476-8).

The instrument is capable of acquiring data from two detectors simultaneously. To process the timing information, two TACs are needed. The TAC outputs are fed into the multichannel analyzer through a multiplexer. The ORTEC 476-8 MUX is designed to work with the ORTEC 918A MCA, when the MCA is equipped with an optional internal board. Use of the MUX allows two TAC modules to share one MCA. Connectors for control and paging connect to the MCA logic board, routing the different signal channels into the appropriate regions of the MCA memory. Figure 11 shows the interconnection between the TACs, multiplexer, multichannel analyzer and the host computer.

Multichannel Analyzer (ORTEC 918A ADCAM MCA).

The TAC output is a square wave pulse, whose amplitude is proportional to the START/STOP time difference. The multichannel analyzer accepts the pulses from the TAC and stores them in an internal buffer. The pulses are digitized using an ADC (analog-to-digital converter), and then sorted according to their magnitude. Each time a pulse having a specific value occurs, the MCA increments a counter for that specific value by 1. Figure 13 shows the idea, using a series of pulses having amplitudes from 1 to 7 being sorted into MCA memory according to their frequency. In the Figure, the pulse amplitude value 2 has the highest frequency, and represents the peak value of the MCA data contents. The position of the curve in the MCA is easily shifted by adding a constant time delay to the system. As discussed above, delay lines are used to position the decay curve in the optimal region of the MCA.

Cables and connectors.

All interconnections of the electronics were accomplished in a manner consistent with good pulse handling and grounding techniques. It is especially important to be aware of situations that may cause impedance mismatches between modules. Such mismatches cause pulse reflections in the system [44], resulting in multiple triggering of timing units, leading to spurious peaks in the decay profiles. The basic signal types are either LINEAR (slow positive) signals, connected using 93 ohm RG-62 cable, or fast negative pulses, connected using 50 ohm RG-58 cable. Where appropriate, fast negative pulses were terminated using 50 ohm load impedances at the far end of the transmission cable.

II.f. Calibration of timescales and adjustment of the timing electronics

A critical adjustment of the timing system is the discriminator setting. A threshold that is too low allows excess noise pulses to be timed. A threshold that is set too high will bias the timing signals towards shorter times [45], introducing serious distortions in measured decay curves. To adjust the discriminator levels, instrument response (lamp) profiles were collected using a dilute solution of LUDOX in water. Each discriminator was trimmed separately, by adjusting to higher thresholds until a narrowing of the impulse response was noticed. A plot of the impulse response full width at half-maximum (FWHM) versus discriminator threshold showed a plateau region below the point of narrowing of the impulse response. The discriminators were set to approximately the center of each plateau region. Calibration of the time per channel of the TAC/MCA combination was accomplished as follows: An ORTEC 425 Nanosecond Delay Box was inserted into the

timing system. Fast pulses were generated by a HP 3311A signal generator driving a second ORTEC 463 CFD. Using the signal generator, the frequency of the pulses could be varied. The output of the CFD (fast negative logic pulses) was applied to the TAC inputs, replacing the lamp antenna and the PMT input signals. Delay was switched 'in', one nanosecond at a time, and the MCA was activated after each increment. As delay was added, the peak position of the MCA data was recorded. Plotting the added delay vs. peak channel number yields a calibration line. The slope, calculated using linear regression, gives the timing calibration in nanoseconds per channel. Once the TAC/MCA combination was calibrated, the custom length delay cables were calibrated against it.

Calibration of the longer time scales (500 ns and higher) using this method is really an approximation, since fewer MCA channels are spanned. The shorter time scales span over a wider range of channels, reflecting a true average timing calibration. As an example, the 100x1 ns time range on the TAC spanned from channel 205 to channel 505 in 32 time increments. In the 100x10 ns time range, the span was from channels 195-225, for 32 time increments of only 1 nanosecond each. To calibrate the longer timescales, we employed an ORTEC Time Calibrator (loaned by Dr. Massimo Sassaroli of the Mount Sinai School of Medicine).

Differential linearity of each time-to-amplitude converter was checked as follows: START signals were provided by the same pulse generator setup used for the timing calibrations. Random STOP signals were produced by allowing a low level of room light to enter the instrument, by slightly opening the sample chamber lid. These random photons pass through the emission monochromator and are detected by the photomultiplier tube. The

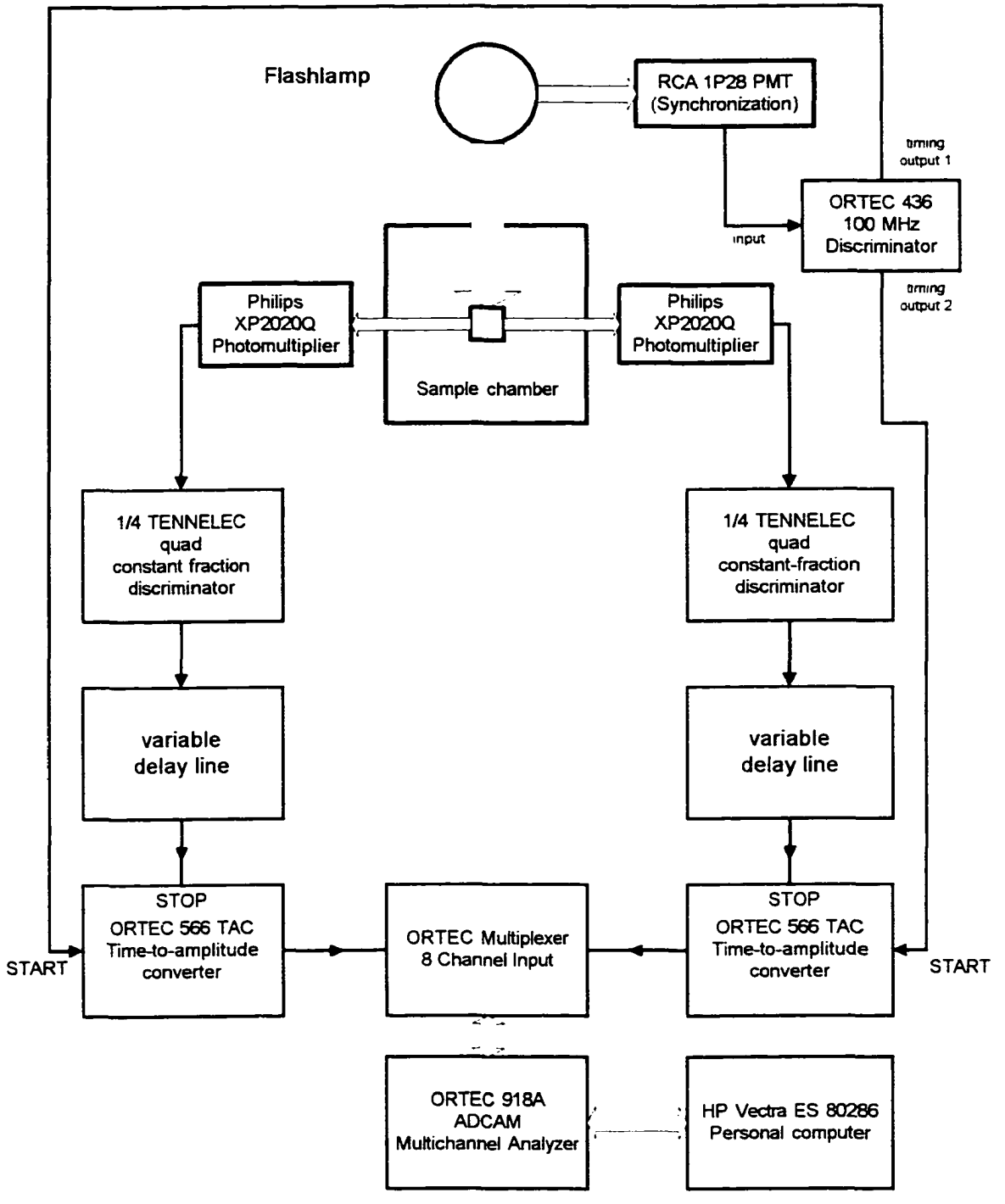

Figure 11. Electronic interconnection of the timing electronics for the time-resolved fluorometer. The system has duplicate detection channels, but shares one multichannel analyzer by using a multiplexer. This allows the simultaneous collection of two emission decay curves simultaneously. This is an advantage for time-resolved anisotropy decay studies, or for collection at two differing timescales to optimize the precision of the experiment.

Multiplexer and Multichannel Analyzer Interconnections

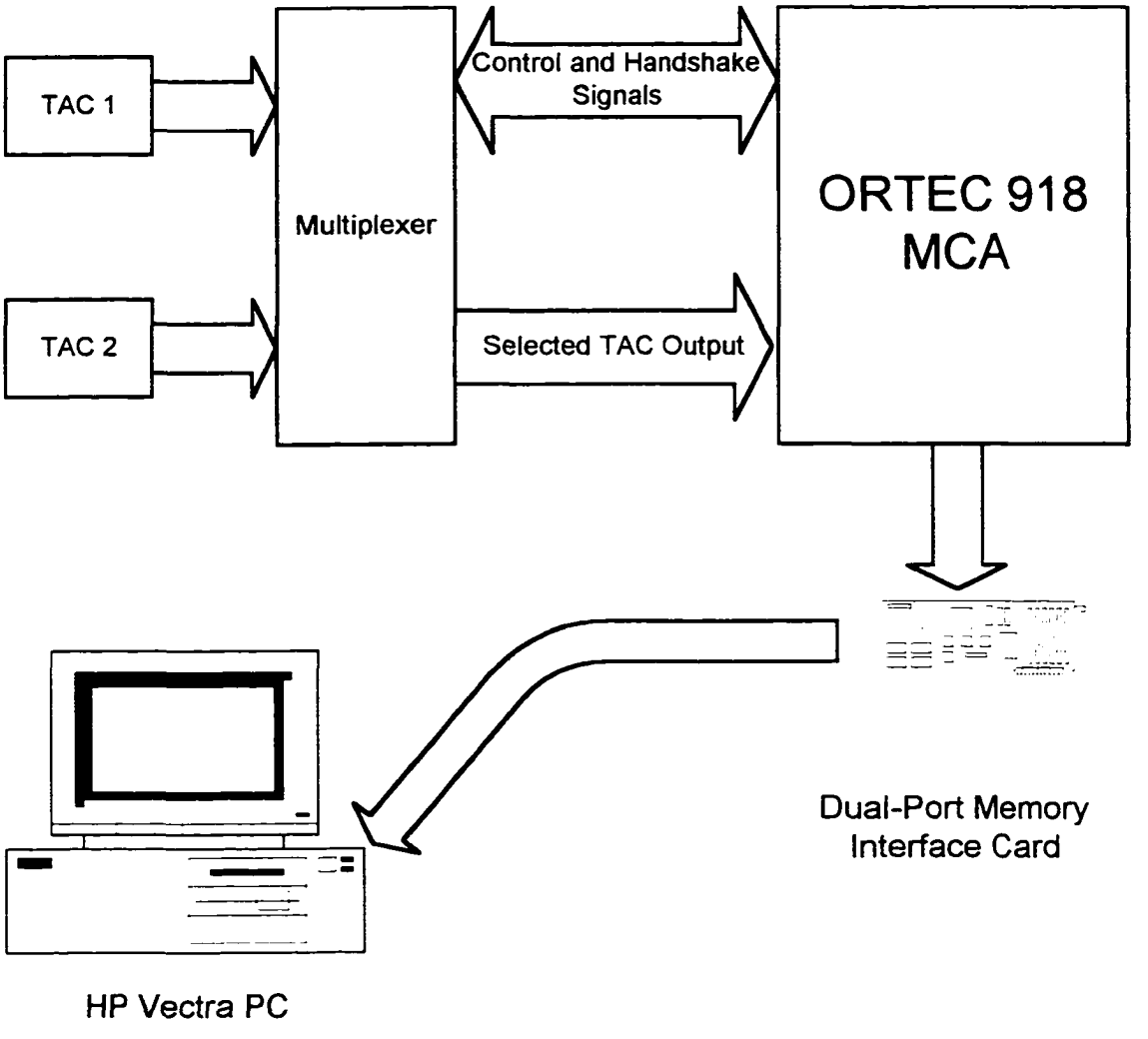

Figure 12. Multiplexer interconnections. The multiplexer allows two time-to-amplitude converters to share one multichannel analyzer (MCA).

Multichannel Analyzer (MCA) Module Operation

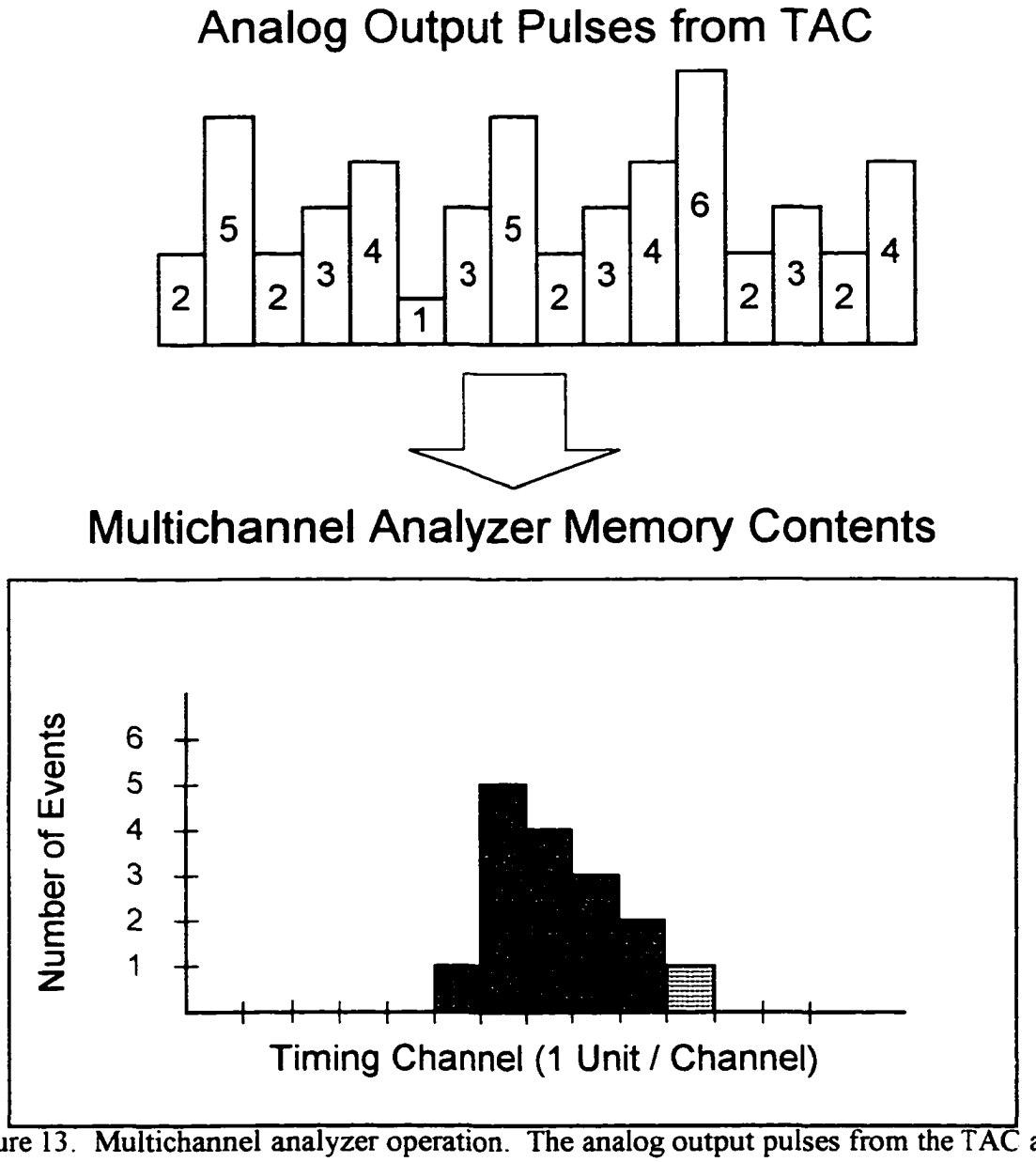

Figure 13. Multichannel analyzer operation. The analog output pulses from the TAC are sorted by amplitude, forming a histogram of the number of events that occurred with a specific amplitude. The analog signal amplitude is proportional to time, and the MCA memory will contain the number of photons that were emitted at a specific time difference. In the figure, the series of TAC output pulses in the upper diagram would form the histogram shown in the lower plot. In an actual experiment, the X-axis is divided into 1024 channels of time, with a typical channel width of 0.2 ns/channel.

multichannel analyzer was activated, and allowed to collect random START/STOP events for approximately 24 hours. An unbiased TAC should produce a spectrum that is flat and featureless over the timing region. We observed a small (approximately 2 percent) nonlinearity in the lower portion of the spectrum. This time region was avoided by arranging the delay lines so that the starting point in the MCA was above channel 300.

Background correction for dark counts was performed by calculating the average background counts in the first 50 channels of the MCA, and subtracting this average count channel by channel.

II.h. Software for data acquisition and instrument control.

The TCSPC Lifetime instrument is controlled entirely by an HP Vectra 286 computer. To reach the desired precision, a large number of counts (>2 x 10^4 in the peak channel of each curve) were required. Typically, each experimental point (temperature or emission wavelength) takes about 4 to 6 hours to collect. Automation was a necessity to avoid possible errors when switching between samples, wavelengths, temperatures and polarizer angles.

A new acquisition program (UAP, the 'Ultimate Acquisition Program') was developed to take advantage of the new capabilities of the instrument, including:

a)simultaneous 2-channel collection (T-Format);

b)multiple emission wavelength sets;

c)multiple temperature sets;

d)various polarization sets (allowing magic angle collection as well as V/H

collection on the same sample during the same experiment), and

e)extended number of timing channels in the MCA (from 512 to 2048.)

A global data area in the main procedure contains flags which indicate the status and current hardware configuration of the instrument. Examples of possible instrument configuration includes the optical path or paths being used for the particular experiment. In L-Format, only one of the two emission channels is in use, whereas in T-Format both emission channels are in use. Reverse-L uses only one emission detector, but it refers to the second emission channel of the instrument, along with its data acquisition channel and multichannel analyzer memory segment. Other parameters are needed to define multiple timing windows in use (for example, each TAC could be set to a different time window of observation). What are the positions of the autopolarizers for this experiment? Do the emission monochromators monitor different emission wavelengths at any given time? Such parameters are needed to control which segments of the MCA are used, how data will be routed and stored, as well as which monochromators and polarizer channels are active. Figures 17 through 19 show possible data collection scenarios, when L, Reverse-L or T format data collection is used.

The FORTRAN code of the UAP (Ultimate Acquisition Program) was developed over approximately a four month period in collaboration with Dr. Piotr Targowski. The data collection algorithm was based on FORTRAN code (&TWODK) supplied by Prof. L. Brand of the Johns Hopkins University. The major changes in the code involved motion control and multichannel analyzer control, since the hardware used by the Brand lab was significantly different from ours.

Software control of the motor control cards is accomplished by an assembly-language driver, provided by MetraByte in a BASIC callable form. Since this laboratory uses FORTRAN based code, it was necessary to modify the assembly language driver for use with Microsoft FORTRAN. Once the driver was modified, a high level subroutine call from FORTRAN was used to set up and move any of the four motors. The object code for these motion control commands was placed in a static object library entitled 'MOTLIB.LIB', and this library was specified during the program link phase to resolve references to modules needed for motion control.

Control of the ORTEC ADCAM MCA is done using mailbox I/O to specific hardware addresses in shared memory space. The use of mailbox I/O makes control and handshaking straightforward. Commands to the ADCAM MCA are placed in the 'mailbox'. The ADCAM MCA retrieves the commands, performs the task, and deposits a return message in the 'mailbox'. The code that requested the task reads the return message, which contains information on possible errors encountered by the ADCAM MCA for the task. These return messages are called 'percent response records', since they begin with the percent character, followed by a numerical code representing success or failure, and a checksum. As an example, the return message for a successful task is '%000 000 069'. The first six numerical fields '000 000' indicate 'unqualified success'. The FORTRAN calling program would interpret this as a successful task to the ADCAM MCA. If the numerical fields indicate errors, the FORTRAN calling routine will halt and display the error code, and the name of the module which called the ADCAM and received the error. In this way, the user can identify problems with hardware or higher level software design, and avoid

situations in which data are collected with uncertain hardware states. For example, if the ADCAM MCA is started, and the user software sends a request to start the ADCAM MCA again, an error will be reported in the mailbox with '%000 001', which is interpreted as 'Segment already stopped or started'. A library of FORTRAN routines was developed, which allows complete setup, control of data acquisition and data transfer, status and timing information and other multichannel analyzer tasks. By using these FORTRAN subroutines, the lower level processes of ADCAM MCA mailbox I/O are invisible to the user. These FORTRAN modules were combined in another object library (MCALIB.LIB) containing all of the ADCAM MCA control modules.

Code development was accomplished using the Microsoft FORTRAN 5.1 Compiler and the Microsoft Macro Assembler MASM 5.1 on an HP Vectra 386 personal computer, running under the MS-DOS operating system version 3.30.

II.g. Performance verification.

Before data collection, the light intensity, controlled by the lamp iris, is adjusted to maintain a count rate of less than two percent of the excitation lamp pulse rate. This condition is necessary to ensure that valid Poisson counting statistics are being applied. The performance of the system was verified in two experiment modes:

II.g.1. Fluorescence lifetime measurements.

The instrument's performance was tested by measuring standards, whose fluorescence lifetimes are well characterized in the literature [46]. The standard samples

chosen were anthracene in methanol (τ_F = 4.0 ns), 9-cyanoanthracene in methanol (τ_F = 11.8 ns) and POPOP in ethanol (τ_F = 1.32 ns). A sample with a short lifetime, known to be a single exponential decay, is preferred for testing. Polarizers were arranged at the 'magic angle' conditions to eliminate polarization artifacts in the measurements [47]. Systematic errors due to improper tuning of the instrument, or lamp instabi ity, are very pronounced in short lifetime measurements. Longer lifetime standards are easier, with less optimal conditions still yielding acceptable lifetime values and fits to the data. The three standards chosen are easily excited using either 340nm or 360nm excitation, available with nitrogen in the flashlamp. An interference filter, placed in the excitation light path, was used to isolate the desired spectral line from the flashlamp. Figure 14 is an example of a successful lifetime measurement of perylene in ethanol.

II.g.2. Emission anisotropy decay.

The measurement of the decay of fluorescence emission anisotropy requires that the instrumental system be well-tuned and stable over a longer period of time than for a lifetime measurement. Solutions of perylene in glycerol were used as standards, since the rotational behavior of perylene dissolved in glycerol has been well characterized in the literature. It is relatively easy to prepare, stable over many hours, and displays a single fluorescence lifetime and two rotational correlation times. In addition to being a lifetime standard, the perylene / glycerol system serves as a model system of anisotropic rotations of perylene in an isotropic solvent. Each anisotropy decay measurement requires that two polarized components of fluorescence emission be measured. Samples are excited with vertically

polarized light, and the emission polarizer is rotated from 0 to 90 degrees to measure both polarized fluorescence emission components. The polarized fluorescence emission data are stored in separate files for analysis. The instrument response (lamp) profile and a reference fluorophore decay curve (for determination of the Q-shift, discussed later) are also stored in separate files. Figure 15 shows the polarized decay curves of perylene in glycerol, using 410 nm excitation. The vertically polarized decay curve is greater in intensity than the horizontally polarized decay curve, resulting in a positive anisotropy over the lifetime of the excited state. At 10°C, the viscosity of the glycerol solvent is high, and the rotational motions of perylene are slowed down (but not *hindered*). This results in a relatively large difference between the vertical and horizontal decay curves.

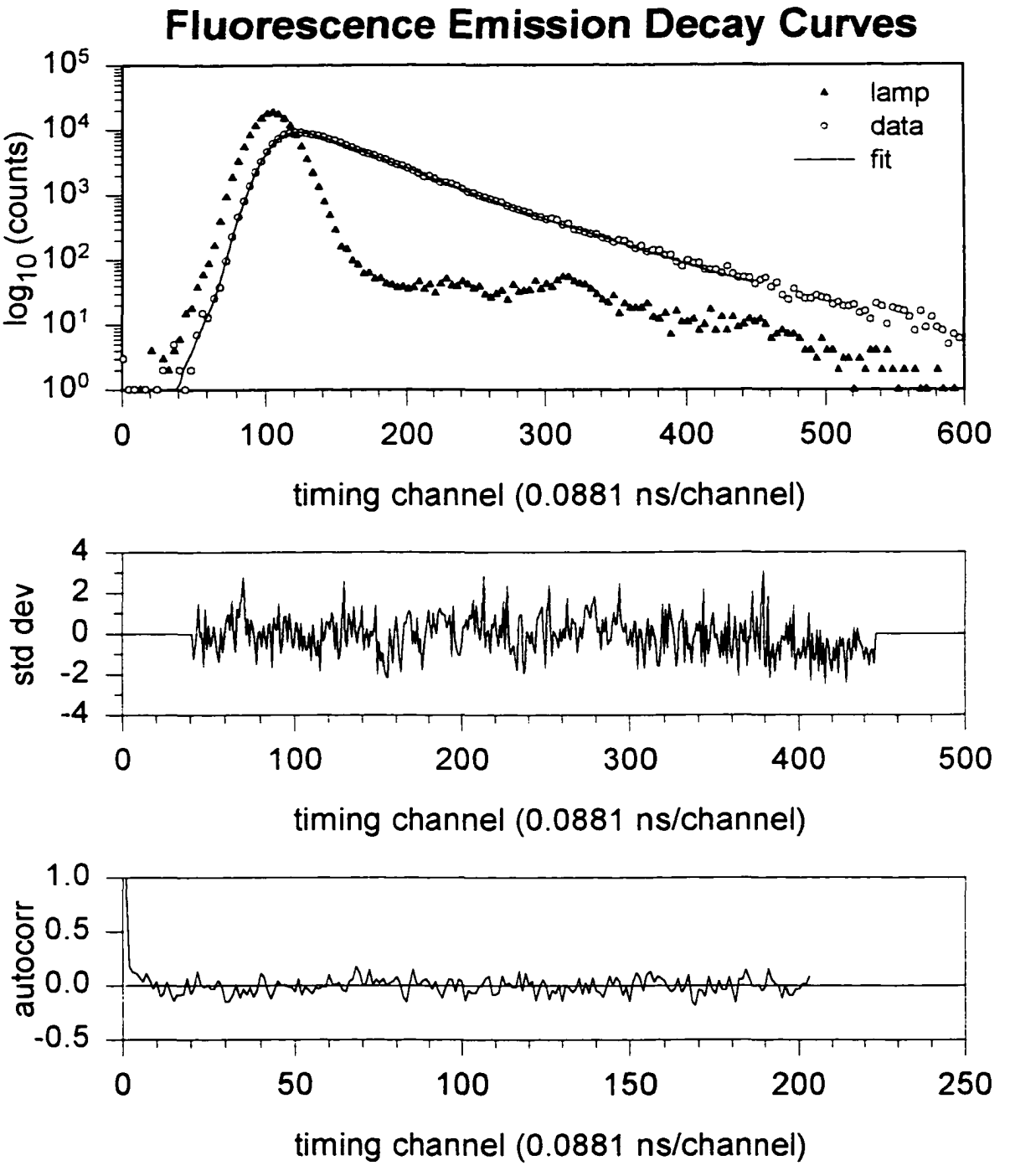

Figure 14. Decay curves for the determination of fluorescence lifetime of perylene in ethanol. Top graph: the excitation (lamp) profile and the fluorescence emission of perylene using magic angle polarizer positions (V/maV). Middle graph: Difference between the fitted function and the decay data. Lower graph: the autocorrelation of the weighted residuals, which should be randomly distributed about zero for a good fit. The recovered lifetime was 4.66 ns with a χ^2 value of 1.002.

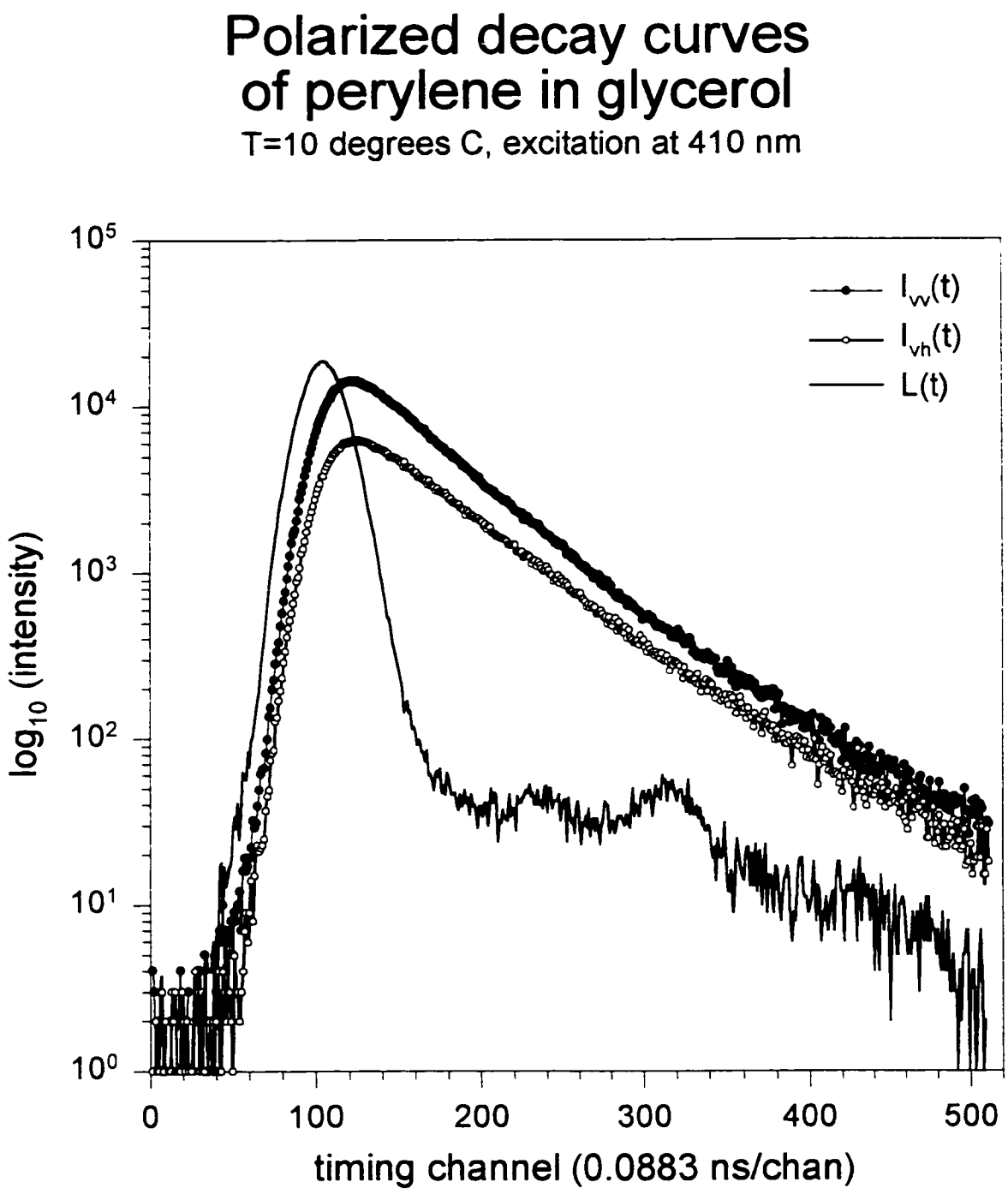

Figure 15. Measurement of fluorescence emission anisotropy decay of perylene using the positive anisotropy band (410 nm excitation). In this example, the V polarized curve is always greater in intensity than the H polarized curve, resulting in a positive anisotropy over the lifetime of the excited state. For completeness, the lamp (instrument response) decay curve is also shown.

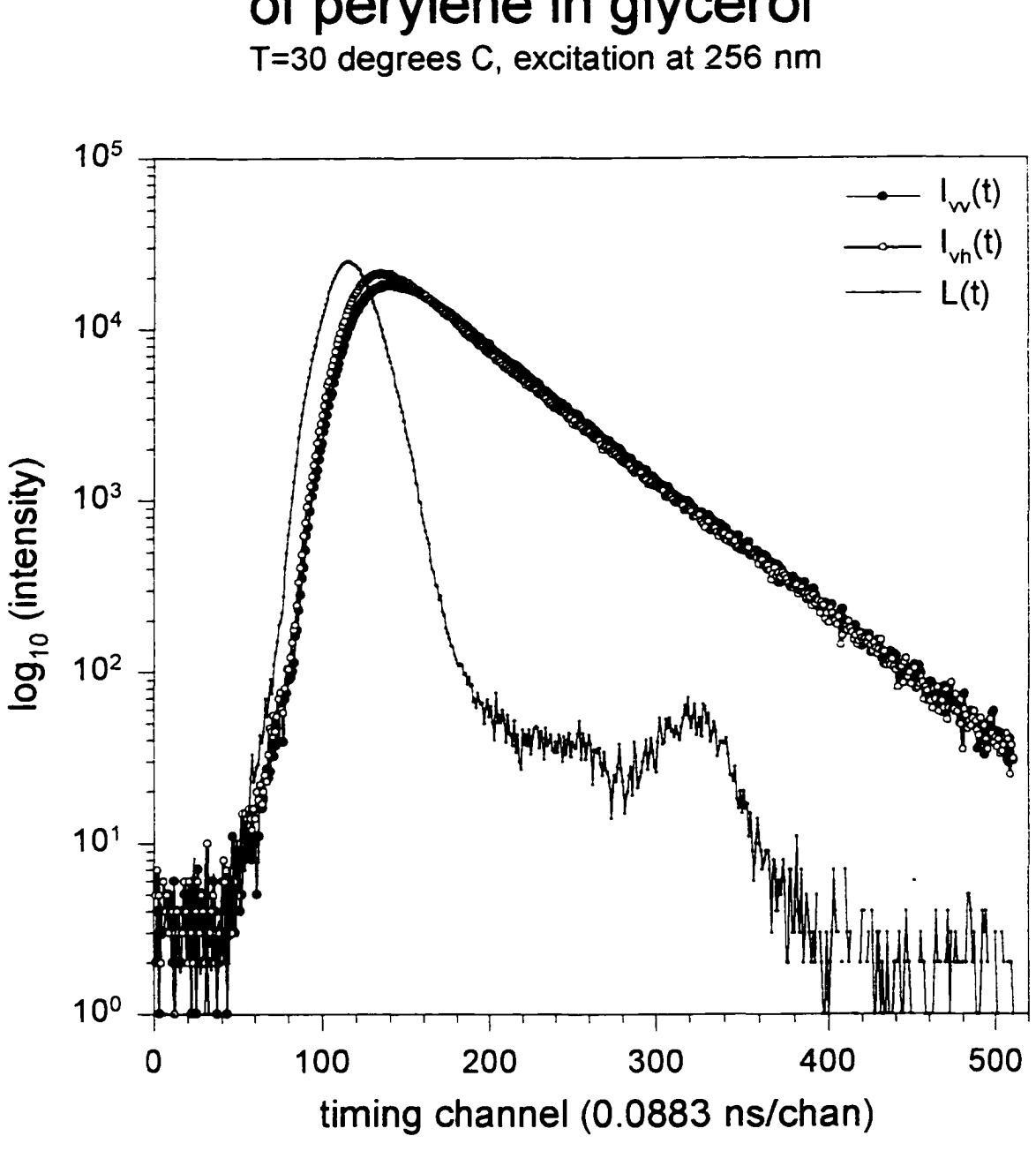

Figure 16. Measurement of fluorescence emission anisotropy decay of perylene using the negative anisotropy band (256 nm excitation). In this example, the H polarized curve is initially greater in intensity than the V polarized curve. The emission anisotropy decay is initially negative, and becomes positive before decaying towards zero. At 30°C, the viscosity of the glycerol solvent is low. The magnitude of the difference between the V(t) and H(t) curves is low, making recovery of the rotational parameters more difficult. For completeness, the lamp (instrument response) decay curve is also shown.

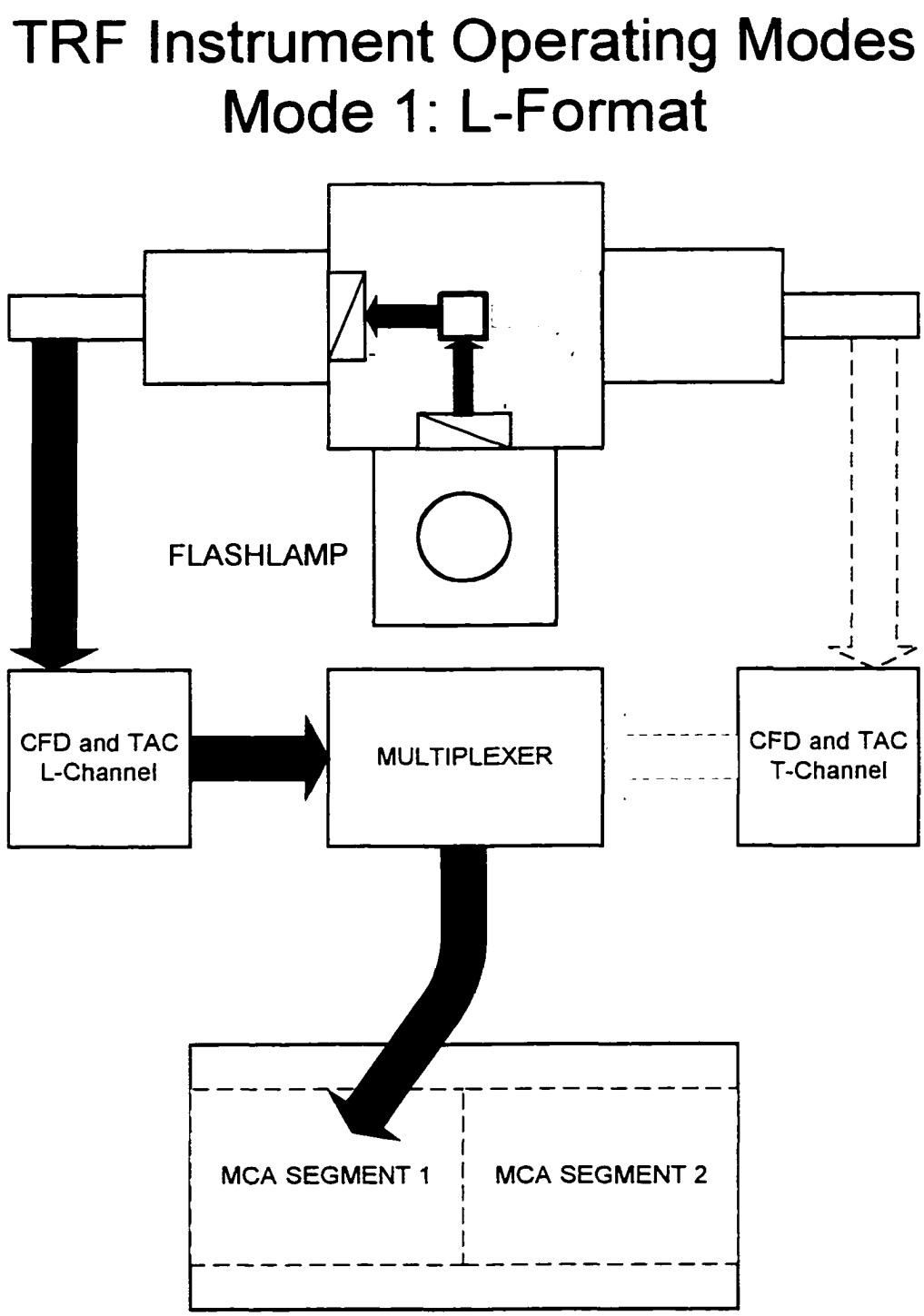

Figure 17. Signal routing in L-Format. In the L-Format scheme, one timing channel is used, and data are routed into one multichannel analyzer segment.

TRF Instrument Operating Modes
Mode 2: Reverse L-Format

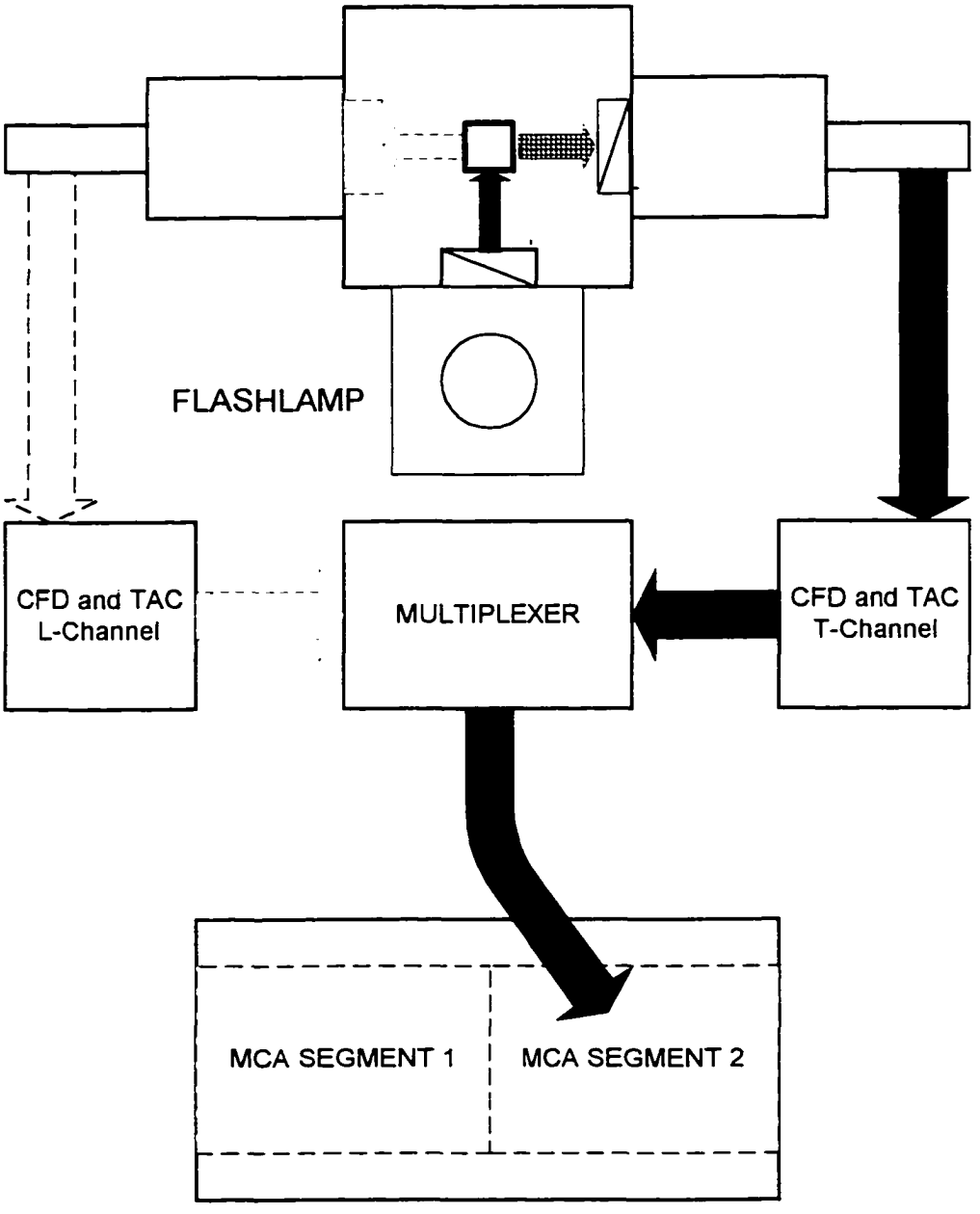

Figure 18. Signal routing in Reverse-L format. Here, only one timing channel is used, but the data originates from the second emission arm of the instrument. A different TAC is used, allowing a different timing window to be observed without changing the instrument configuration.

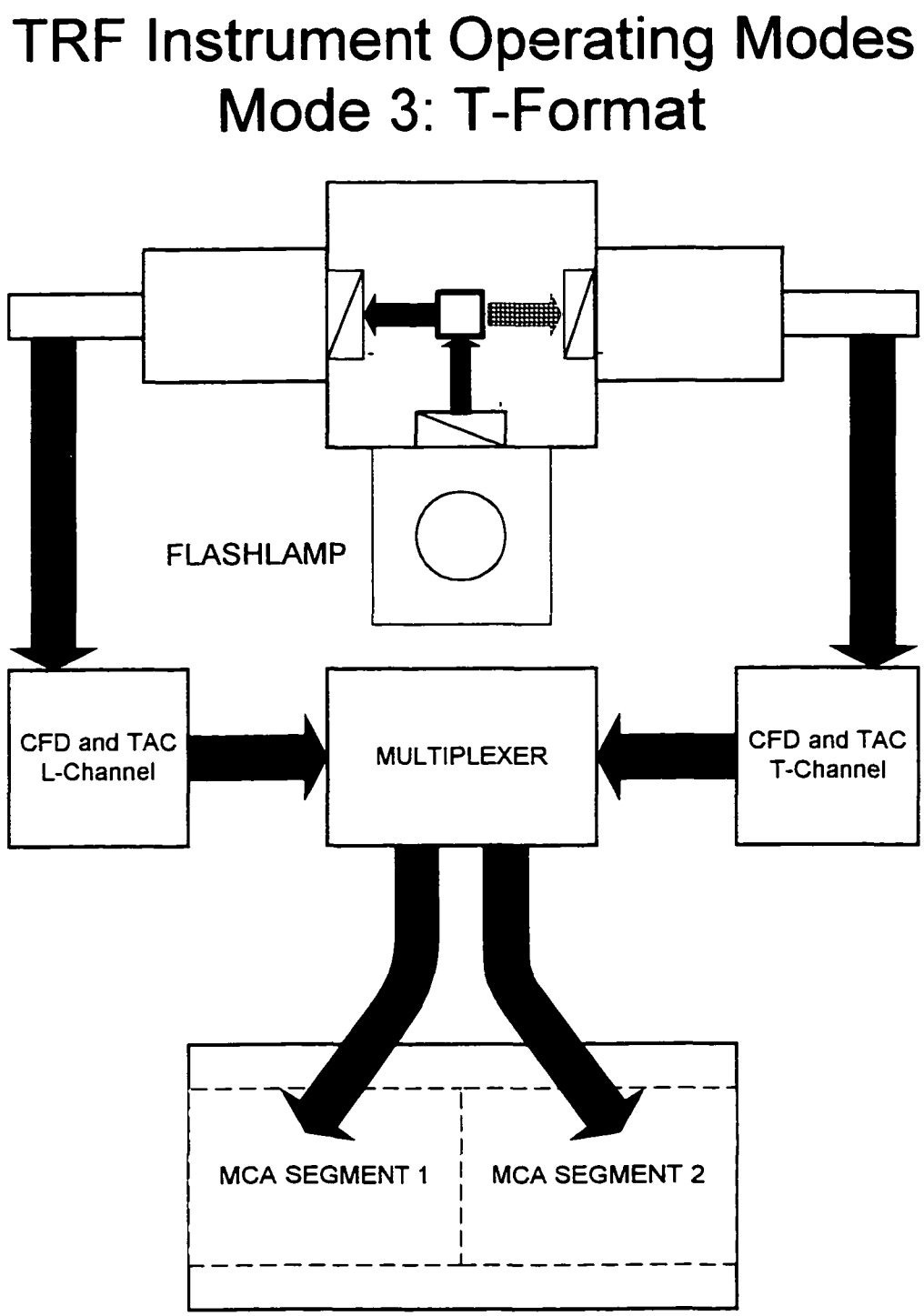

Figure 19. T-Format operation. In T-Format operation, both emission channels acquire data simultaneously. The timing windows, polarizer positions, and wavelengths may be different between both channels. The MCA stores each TAC data in a separate segment.

Section III. - Data Analysis of Lifetime and Emission Anisotropy Decay Data.

For measurements of the fluorescence lifetime of a sample, the instrument collects a histogram of the measured time differences between the excitation of a sample and the detection of an emitted photon. The multichannel analyzer contains the intensity vs. time curve for the sample. This decay curve contains the information needed to calculate the fluorescence lifetime of the sample, but it also includes the response of the instrument itself. The results of the experiment are not immediately apparent from the data, i.e. the instrument does not simply display a value indicating the lifetime of the sample. Rather, the data must be fitted to mathematical models, and the results of this fitting process are tested using statistical criteria. These statistical parameters will be described below.

Before discussing the curve fitting process, the systematic errors and assumptions of the experiment need to be considered. These include:

a) distortion of the true decay curve by the instrument response.

b) Poisson statistics are assumed for the single photon counting experiment.

c) true single-photon counting conditions are being observed.

d) instrumental bias, timing system linearity and calibration.

The first problem, distortion by the instrument response, cannot be removed by changing the experimental conditions. A mathematical correction for this distortion is possible, subject to certain assumptions about the data and conditions of the experiment. The assumption of Poisson statistics is easy to validate during an experiment, by regulating the count rate of emitted photons compared to the number of possible excitation events. The

last two major issues are purely instrumental. Proper setup and adjustment of the lifetime instrument will eliminate these potential errors.

The response of the instrument distorts the measured decay curve for two reasons:

a) the excitation lamp flash has a finite duration; and

b) the detector and electronics have their own finite response time.

If the lamp flash was infinitely narrow (a delta pulse) AND the detector/electronics had infinitely fast response, the measured decay curve would equal the true decay curve. The nature of the distortion is not a simple blank subtraction. It is a convolution of the instrument response function with the sample decay function. The true decay function can be extracted from the measured decay curve, if the instrument response function is known. The decay curves are distorted by convolution with the excitation pulse profile as well as the instrument response, which consists of the detection system and the timing electronics. Even if the excitation pulse width approaches a delta pulse, the response of the photomultiplier and electronics tends to broaden and distort the detected pulse.

The entire instrument response function, which takes into account the excitation pulse profile, as well as the detector and electronic response, is measured by collecting the decay curve of a scattering solution of glycogen or LUDOX (colloidal silica, DuPont) using the excitation wavelength for the particular experiment being performed. Silica may fluoresce when excited near 300 nm [48], so glycogen is preferred in this wavelength region. Using the scattering compound as an additional sample in the instrument, the instrument response function is collected at the same time as the unknown sample. This instrument response function or 'lamp profile' is used to recover the true decay from the measured data.

It is possible to use a standard compound of known lifetime, from which the instrument response function can be calculated, and then applied to the unknown sample. The technique is known as reference deconvolution [49]. In frequency domain instruments, the practice of using a fluorophore having a single exponential lifetime as a reference, instead of a scattering reference, is very common.

III.a. Convolution.

The mathematical definition of convolution [50] is the folding and shifting of a signal. For two continuous time signals x(t) and v(t), the convolution of x(t) and v(t) is defined by:

$$(x \otimes v)(t) = \int_{-\infty}^{\infty} x(\lambda)v(t-\lambda)d\lambda \qquad (30)$$

In general, signals which can be defined as follows:

$$(x \otimes v)(t) = 0, \; t<0 \qquad (31)$$

$$(x \otimes v)(t) = x(\lambda)v(t - \lambda)d\lambda, \; t \geq 0. \qquad (32)$$

with the integrals satisfying the conditions:

$$\int_0^t |x(\lambda)|\,d\lambda < \infty \quad , \textit{for all } t > 0. \tag{33}$$

$$\int_0^t |v(\lambda)|\,d\lambda < \infty \quad , \textit{for all } t > 0. \tag{34}$$

can be convolved. Our experimental decay curves meet these criteria. It is interesting to notice the convolution of a signal with a delta pulse is the identity element of the convolution operation:

$$(x \otimes \delta)(t) = x(t) \qquad \textit{Identity Element of Convolution} \tag{35}$$

The identity element of convolution shows that, given an infinitely narrow excitation pulse width AND an infinitely fast detector response, the measured decay would be equivalent to the true sample decay.

Having the measured decay curve and the instrument response functions in hand, in the form of two decay curves, makes the extraction of the true decay parameters possible. There are two possible approaches:

a) 'deconvolve' the measured decay curve, separating it into the true decay and the measured instrument response function; then fit the 'true' function in terms of lifetimes;

b) form a mathematical expression of the true decay, convolve it with the measured instrument response function, and compare it to the actual measured decay curve.

The first approach, using a deconvolution method, is more complicated. The deconvolution method uses Fourier analysis. In Fourier space, the convolution integral of two signals becomes a product of two functions.

It is computationally easier, and faster, to 'reconvolve' a trial function with the measured lamp profile. The lamp profile and the decay data are stored in arrays, and it is easy to form the convolution sum in a point-by-point fashion across the entire array of data. The array of numbers formed in this way is termed the fit. The fit is compared, point-by-point, with the actual measured decay curve, and deviations between the fit and the data are used to calculate the goodness of fit between them. A perfect match would show no deviation across the entire array of data. Depending on the degree of deviation between the fit and the data, new trial functions are calculated, reconvolved with the lamp profile, and compared to the decay curve. This procedure is repeated until either a convergence occurs, or the fit fails. The criteria for successful convergence or failure are described below.

III.b. Poisson Statistics and Count Rates.

For a Poisson distribution of the data, the fraction of emitted photons F_D

$$F_D = \frac{N_D}{N_E} = \frac{number\ of\ detected\ photons}{number\ of\ possible\ events} \qquad (36)$$

must be kept low. The exact value of this ratio depends on the degree of error that can be tolerated. Numerical calculations of the magnitude of the error [51] have predicted a value of 0.05 as an upper count rate limit. To prevent distortion of the data by pulse pileup, a

lower fraction is generally better. A fraction of less than 0.02 (2 percent) was used for all measurements presented here.

Experimentally, we do not measure the fluorescence lifetimes or the rotational correlation times directly. The polarized components of the fluorescence emission decays are measured, using polarizers arranged vertically and horizontally in the excitation and emission light paths, and the lifetimes and rotational correlation times are extracted from these curves. Different combinations of the polarized decay curves contain all information needed to recover the fluorescence lifetime(s) and rotational correlation time(s) of the sample. The data set for each anisotropy decay experiment consists of four decay curves:

a) a lamp decay curve L(t);

b) a vertical emission decay component V(t);

c) a horizontal decay component H(t);

d) a 'Q-shift' sample, chosen as a single exponential lifetime standard.

The Q-shift sample serves two purposes:

a) a test of the instrument's performance and stability during the experiment.

b) provide a measure of the time shift of the detection system due to differing wavelengths between excitation and emission [52].

III.c. Single curve and global curve analysis.

Each experimental curve is fitted using a nonlinear least squares search, based on the Marquardt algorithm [53]. When decay curves are analyzed one at a time, the term 'single curve' analysis is used. In single curve analysis (Figure 20), the mathematical parameters

that describe the fit are completely independent from each other.

When certain relationships are known (or postulated) to exist between different data sets, single curve analysis might not yield the same answer for a given parameter, across all experiments. This is due to correlation between the parameters. To investigate possible effects of parameter variation, values can be fixed during single curve fitting, to determine whether or not the other parameters will still be physically meaningful. This is not an efficient way of optimizing a parameter across several experiments, and it does not guarantee that the best solution to the data sets will be found. Using global analysis techniques, it is possible to analyze a series of experiments simultaneously. All of the parameters are varied simultaneously, converging on the best solution of all experiments. Figure 21 shows a set of four experiments, with global analysis strategy being applied to the two lifetime terms τ_1 and τ_2.

Single Curve Analysis of Fluorescence Decay Data

Free Model - All Parameters Independent

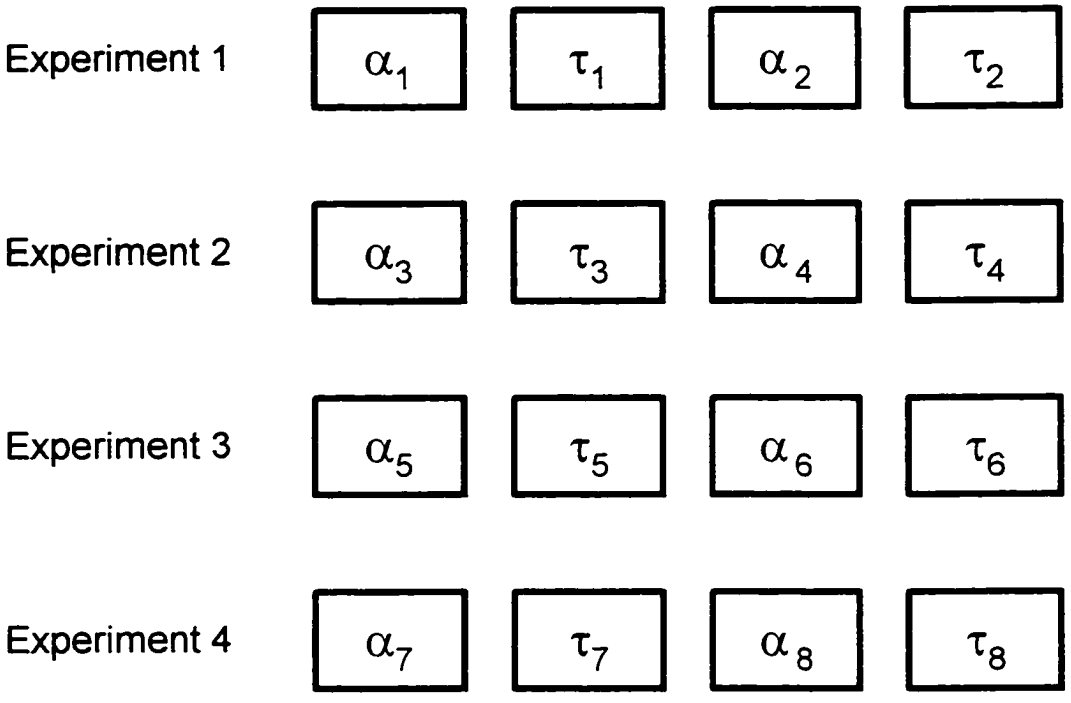

Figure 20. Diagram of single curve analysis of four separate experiments. In this example, each curve is fitted to a double exponential decay law, which requires four independent parameters. For four experiments, a total of sixteen independent parameters must be fitted.

Global Analysis of Fluorescence Decay Data

Global Model - Lifetime Values are Linked

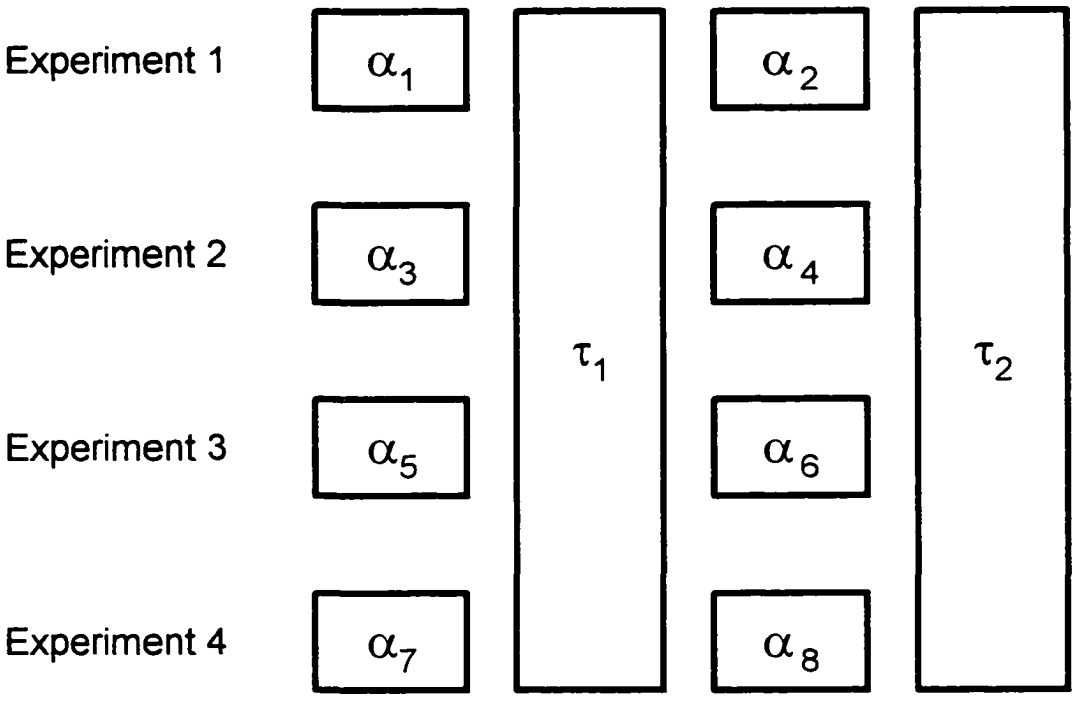

Figure 21. Diagram of global data analysis for a set of four experiments. In this example, a known relationship exists between each lifetime, τ_1 and τ_2. The number of fitting parameters is reduced by 'linking' lifetimes across experiments. The value of the lifetimes are varied simultaneously for all four experiments during the curve fitting process, converging on the unique value that best satisfies all four experiments.

III.d. Compensation for Q (Zero-Time) Shift of the Detector.

Recall that the Q-shift represents the time-shift of the detector which occurs when photons of different wavelength (energy) impinge on the photocathode [54]. The Q-shift is determined by fitting the reference compound to a single exponential decay law, making the Q-shift a parameter in the fit. The lamp decay curve, L(t), and the reference decay curve, R(t), are used in this fitting process. The lamp profile L(t) is mathematically 'shifted' along the time axis, until the best fit to a single exponential decay is obtained. The value of Q, in units of decay channels, obtained at the best-fit (minimum χ^2) is reported by the fitting engine along with the best-fit fluorescence lifetime. The actual value of the time shift (ns) is obtained by the product of the Q-shift (channels) and the timing calibration (ns/channel), but since the data are usually fitted in terms of channel number, we use the Q-shift in units of channels. Generally, greater differences between excitation and emission wavelength show larger Q-shifts. The timing calibration of the experiment is also important, with faster timescales showing larger Q-shifts. For longer time range experiments (e.g. 0.8 ns/channel) such as pyrene in aqueous solution, the magnitude of Q is generally very small. The Q-shift value is valid for this experiment if the reference compound was fitted successfully, with a good statistical fit, proper lifetime value, and clean (random) plots of the weighted residuals and autocorrelation. If the Q-shift reference curve cannot be fitted properly, chances are good that the time-resolved instrument system was not properly prepared or operated. Examples of improper operation might include:

a) too high a count rate on the emission detector, causing systematic errors due to pulse pileup;

b) improper adjustment of timescale and delay lines, causing the decay curve to be placed in the wrong region of the multichannel analyzer;

c) lamp operating conditions such as gas pressure, repetition rate, discharge voltage and synchronization PMT not optimized;

d) lamp instability, due to eroded electrodes. If the electrodes have just been cleaned, they should be allowed to 'burn-in' until the excitation pulses are stable (usually 1-2 hours is sufficient).

e) background count rate too high (correlated dark counts), possibly due to humidity in the emission photomultiplier housing (our system uses a purge gas flow to flush the housings), or high voltage power supply incorrectly set or unstable;

f) maladjusted discriminators, on either timing channel (START or STOP)

g) failure of a cable, cable connector or component.

If the Q-shift standard experiment is valid, we write down the value of Q, and proceed to fit the polarized decay curves of the sample.

III.e. Compensation for optical polarization bias of fluorescence emission.

In addition to the Q-shift, an additional correction term is needed to compensate for instrument bias introduced by the different efficiencies of optical gratings when vertical and horizontally polarized light passes through the monochromator. Known as the G factor, it equals [55]:

$$grating\ factor = G = \frac{I_{HH}}{I_{HV}} \quad (37)$$

The subscripts on terms of intensity I indicate the excitation and emission polarizer orientations, respectively. The G-factor is measured on our instrument before and after the experiment, by integrating the counts over the entire multichannel analyzer window for a period of 100 seconds for each polarizer orientation. (The actual unknown sample is used for these measurements). From these data, both the G-factor and the steady-state emission anisotropy are calculated and printed with the experiment log. The average value of G is computed and used for analysis of the polarized decay curves. In all cases, the G-factor was very close to unity.

III.f. Fitting Methods.

Whether single curve or global fitting is used, the curve fitting itself may be performed using different methods. Two general approaches have been used to fit the data.

III.f.1. Method I. - Sum and Difference of polarized decay curves.

1) A sum curve S(t)is constructed from the measured V(t) and H(t) decay curves:

$$S(t) = G*I_{VV}(t) + 2*I_{VH}(t) \quad (38)$$

2) S(t) is fitted to a sum of exponentials:

$$S(t) = \sum_i \alpha_i e^{\frac{-t}{\tau_i}} \quad (39)$$

The number of components, I, is set at the beginning of the fitting process. During the fitting, the preexponentials (α_i) and lifetimes (τ_i) are varied. The alpha terms (α_i) represent the contribution of each lifetime term (τ_i) to the total fluorescence intensity. The fractional percent contribution of each component (f_i) may be calculated using Equation 40 :

$$f_i = \frac{\alpha_i \tau_i}{\sum_i \alpha_i \tau_i} * 100\ \% \quad (40)$$

It is useful to express a multiexponential decay in terms of an average fluorescence lifetime, $<\tau>$, defined as the weighted average of the individual lifetimes:

$$<\tau> = \sum_i f_i \tau_i = \frac{\sum_i \alpha_i \tau_i^2}{\sum_i \alpha_i \tau_i} \quad (41)$$

3) A difference curve D(t) is formed from the measured V(t) and H(t) decay curves:

$$D(t) = G * I_{VV}(t) - I_{VH}(t) \quad (42)$$

4) A model for the rotational motions is proposed, and expressed as a sum of exponentials:

$$r(t) = \sum_j \beta_j e^{-\frac{t}{\varphi_j}} \quad (43)$$

5) The D(t) curve is fitted to the product of r(t) and s(t):

$$D(t) = r(t) * s(t) = \left(\sum_j \beta_j e^{-\frac{t}{\varphi_j}}\right) * \left(\sum_i \alpha_i e^{-\frac{t}{\tau_i}}\right) \quad (44)$$

The lifetime parameters (the *I* sets of α and τ terms) are held constant during the fitting process for the *j* sets of β and ϕ terms. The preexponentials (β_j) and rotational correlation times (ϕ_j) are varied in the r(t) expression. To model a hindered rotation, an r_∞ term is included in the fit. An extra (β,ϕ) term is included in the model, with the magnitude of this last ϕ fixed to a large value compared to the fluorescence lifetime. For the analyses presented here, a typical value of 10,000 nanoseconds was used.

Figure 22 shows an example of the calculated sum (S(t)) and difference (D(t)) curves of the polarized fluorescence emission of perylene in glycerol, using 410 nm excitation. These sum and difference curves were calculated pointwise from the polarized emission decay curves. Figure 22 also shows a plot of the emission anisotropy decay, r(t), calculated as the difference D(t) divided by the sum S(t), yielding the convolved anisotropy decay. The instrument response has not yet been removed from the anisotropy decay in Figure 22. At longer times, the noise in the measured anisotropy decay increases because the intensity of emission is decreasing, and the difference between the V(t) and H(t) curves is decreasing. Using τ_F = 4.7 ns for perylene in glycerol, the fluorescence intensity will have decayed for

five time constants over the timing channel range:

$$channels\ spanned = \frac{5\ \tau_F}{tcal\ (ns/chan)} = \frac{5 * 4.7\ ns}{0.0883\ ns/chan} = 266\ channels \quad (45)$$

in which *tcal* is the timing calibration of the TAC/MCA for the particular experiment, expressed in nanoseconds per channel. The measured emission anisotropy decay information is useful only over the range where there is emission of fluorescence.

In equations 39 and 43, the functions are convolved with the lamp profile. This is necessary to correct for the distortion of the data by the lamp profile and detector response, since the lamp flash has a finite duration and the PMT has a finite response time. This is not a serious limitation, since by measuring the lamp and decay profiles under identical conditions, the correct decay parameters will be recovered by iterative reconvolution.

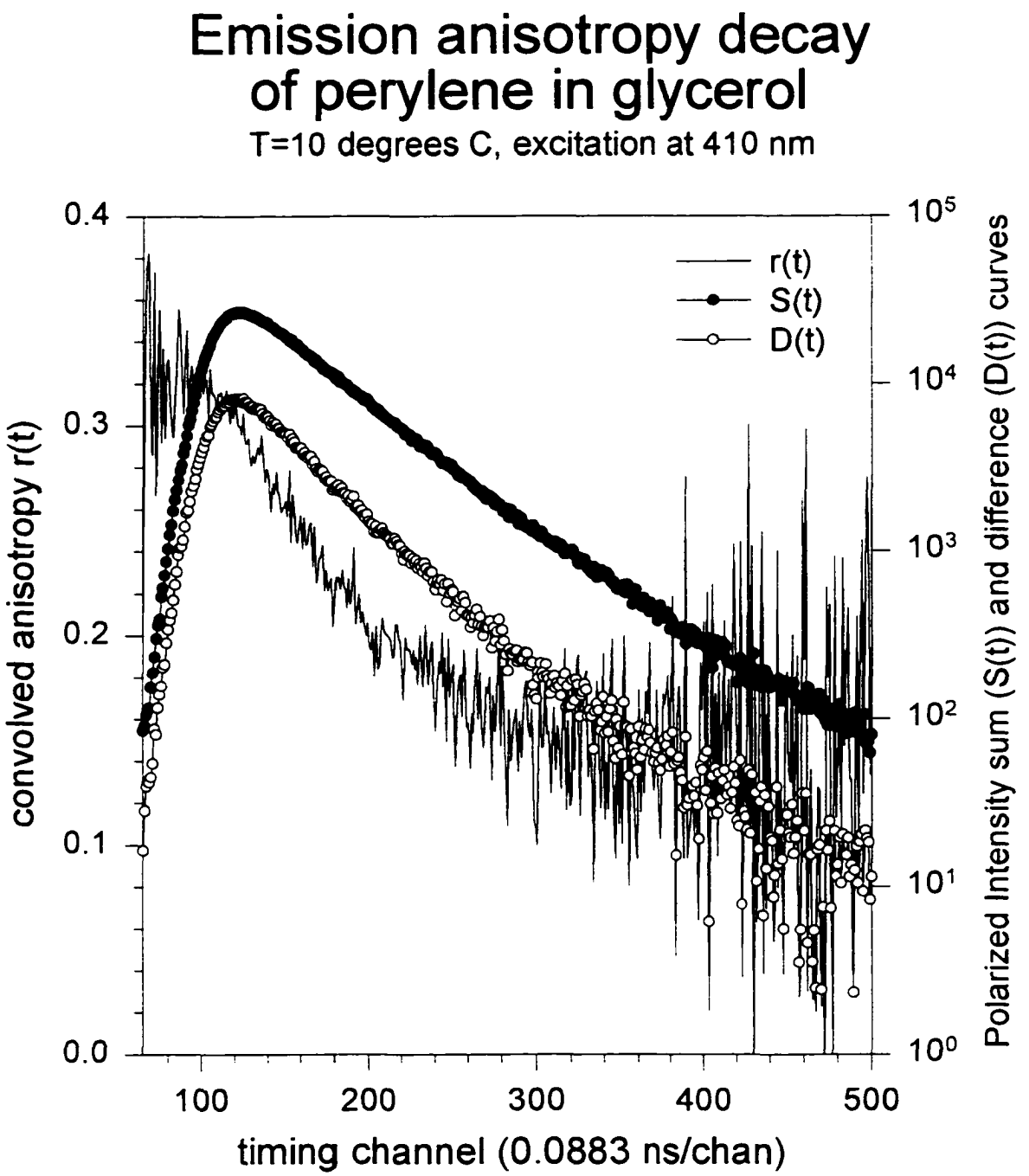

Figure 22. Perylene in glycerol. Starting with the polarized intensity decay curves in Figure 15, the sum S(t) and difference D(t) are calculated point-by-point. The anisotropy decay, r(t), is positive over the lifetime of the excited state, since the difference curve D(t)=V(t)-H(t) is always positive.

III.f.2. Method II - Vector Analysis.

When the anisotropy is very low, the V(t) and H(t) curves will be similar in magnitude, making the difference between them low in magnitude. As an example, Figure 23 shows a pair of polarized decay curves whose sum is high, but their difference is very low. This low number of counts in the difference curve can introduce errors in the rotational parameters, since the precision is lowered. One way to increase the magnitude of the difference between the curves is to extend the counting time of the experiment, but this has practical limitations. The flashlamp stability and sample stability will become factors limiting the length of an experiment.

An alternate method of analyzing the polarized data is available, in which the rotational components are determined from the raw V(t) and H(t) curves [56], rather than from their difference. This method uses a systems analysis approach, treating the two data sets as a vector [57]. The fitting expressions for the anisotropy decay become:

$$I_V(t) = \sum_i s_i(t) \, [1 + 2r_i(t)] \, / \, 3 \qquad \textbf{(46)}$$

$$I_H(t) = \sum_i s_i(t) \, [1 - r_i(t)] \, / \, 3 \qquad \textbf{(47)}$$

Each of these expressions is reconvolved with the lamp profile and compared to the experimental data. The vector analysis method has several advantages, including:

a) the V(t) and H(t) data are not subtracted, improving the result of the fit, especially when the difference between the polarized decay curves is low.

b) it is not necessary for the total intensity parameters (the S(t) expression of Equation 39) to be held constant in the analysis. Both the intensity and rotational parameters may be optimized together.

c) the statistical weights are simplified, since the actual measured data are being analyzed, rather than a mathematical function (sum or difference) of the raw data. (The sum and difference expressions are not Poisson weighted, rather, the weights are the propagated errors of the individual curves [56].)

In the studies presented here, a combination of both fitting techniques was used. Generally, the method of sums and differences was used for the single-curve analysis of the data. Vector analysis was used for all global analyses. For both techniques, the intensity parameters were fixed during the rotational analysis.

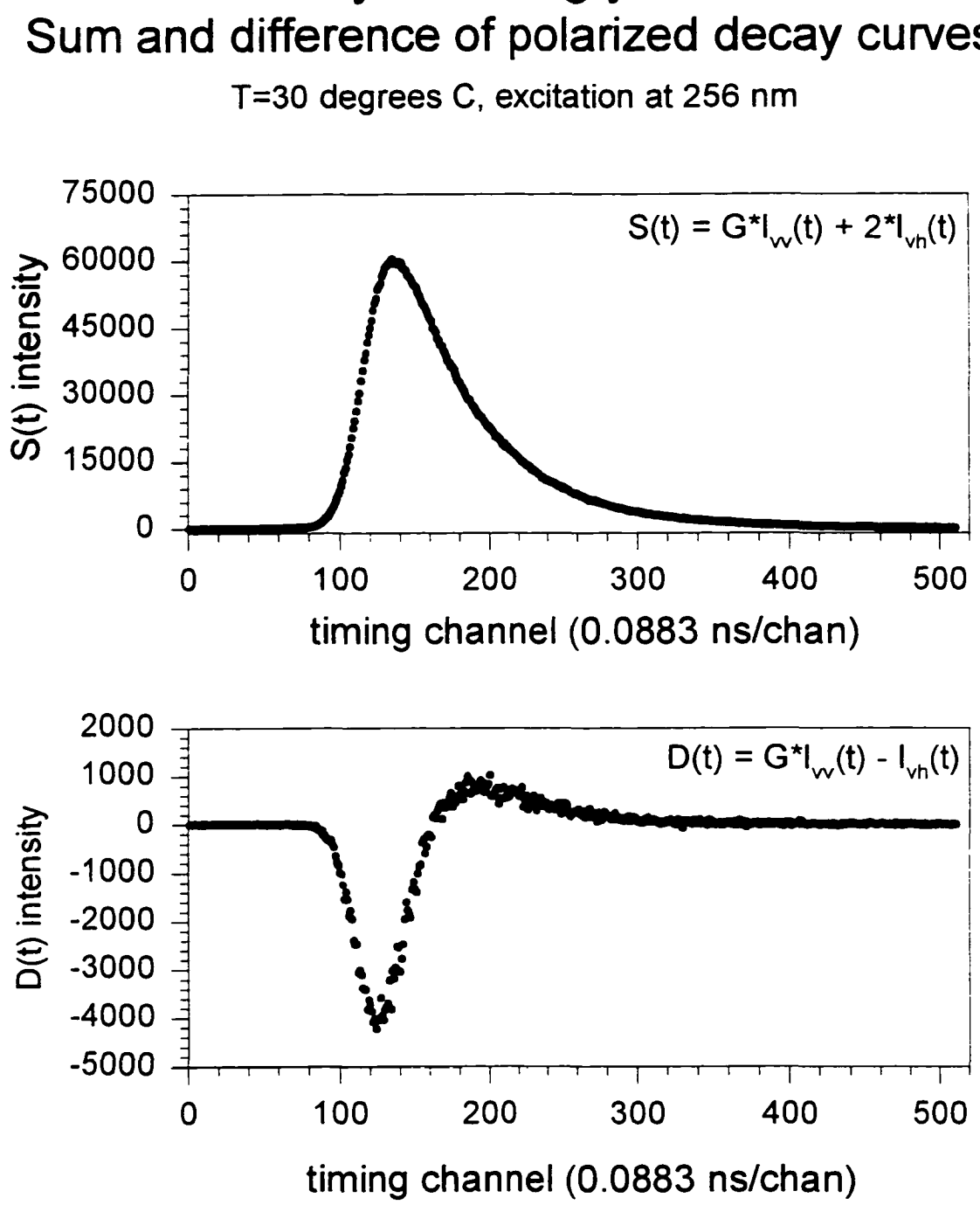

Figure 23. Starting with the polarized intensity decay curves in Figure 16, the sum S(t) and difference D(t) are calculated point-by-point. The anisotropy is initially negative, since the difference curve D(t)=V(t)-H(t) is initially negative, becoming positive and finally decaying towards zero.

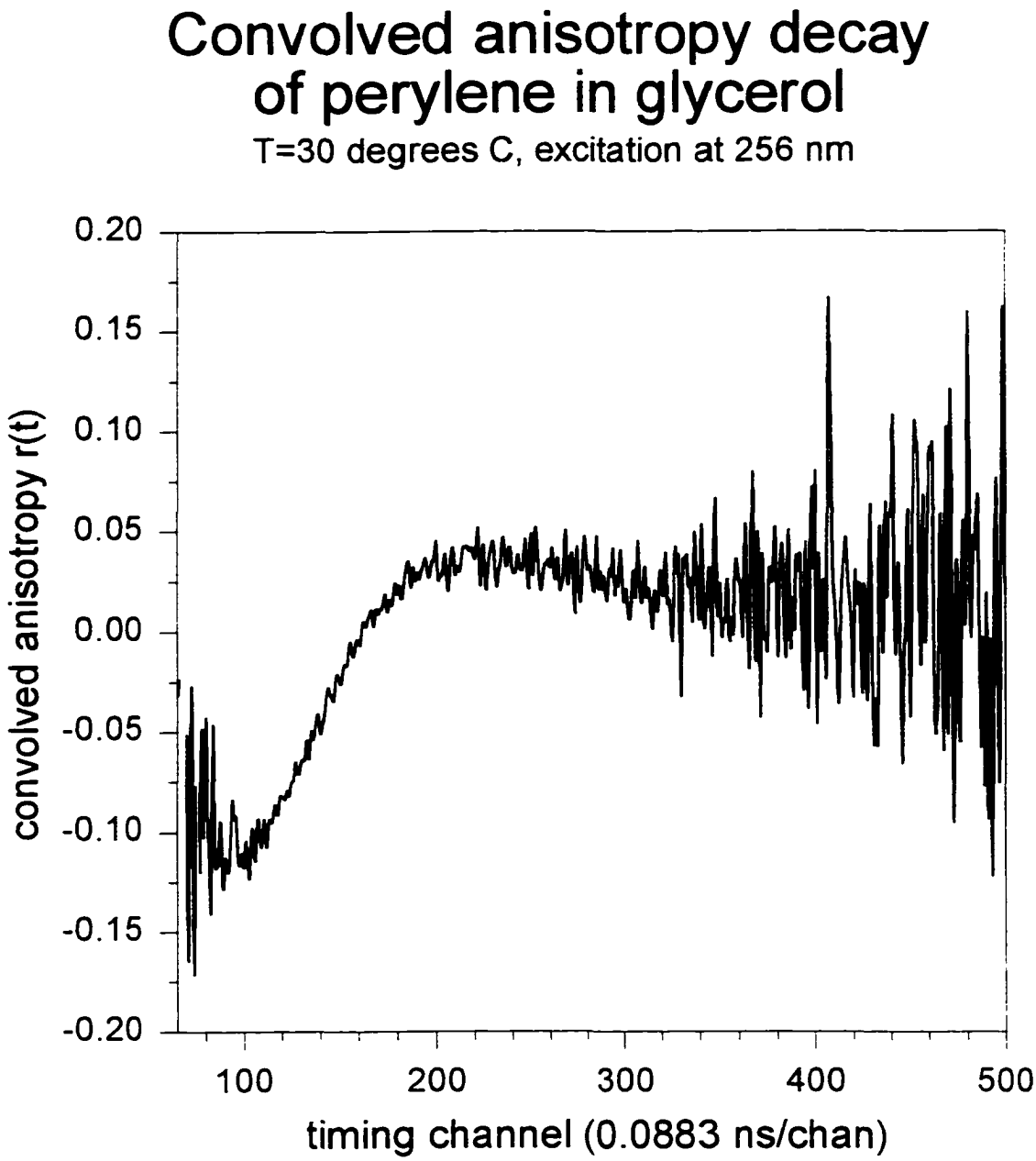

Figure 24. Calculated anisotropy decay r(t), from the sum and difference of the polarized emission decay curves in Figure 23. Notice that the anisotropy is initially negative.

III.g. Nonlinear Least Squares Fitting.

Data analysis using sums and differences, or vector analysis approaches, use a least-squares fitting technique. In least-squares regression analysis, the weighted sum of the squares of the deviations of the experimental points $y(t_i)$ and the calculated fitting function $Y(t_i)$ are minimized [58]:

$$\chi^2 = \sum_{i-1}^{n} W_i [y(t_i) - Y(t_i)]^2 \quad \textbf{(48)}$$

The statistical weights W_i are estimated to be the reciprocal of the number of counts in the i^{th} data point. Then, Equation 48 becomes

$$\chi^2 = \sum_{i=1}^{n} \frac{[y(t_i) - Y(t_i)]^2}{I(t_i)} \quad \textbf{(49)}$$

It is important to use the raw, uncorrected amplitude $I(t_i)$ as a more accurate representation of the variance [59], rather than after any background subtraction.

III.h. Criteria for judging goodness of fit.

To evaluate the goodness of fit between the fitting functions and the data, three statistical parameters were used.

III.h.1. Reduced chi-square, χ^2_v.

The first parameter is the magnitude of the reduced chi-square, χ^2_v :

$$\chi_v^2 = \frac{\chi^2}{(n_2 - n_1 + 1 - p)} \qquad (50)$$

in which n_1 and n_2 represent the starting and ending channel of the data fitting range. The p term indicates the number of variable parameters in the fitting function. For exact Poisson statistics, the reduced chi-square value should equal 1.00, but it turns out that TCSPC data have a slight non-Poisson noise contribution [60] which allows values from 0.8 to 1.2 to be considered as good. It has been stated that reduced chi-square values of 1.5 are still 'reasonably close' to 1 [59]. In practice, chi-square values can be numerically acceptable, even when the fit is unsuccessful, and additional criteria are used along with the reduced chi-square statistic to evaluate the fit.

III.h.2. Plot of the weighted residuals.

The second parameter used to evaluate the fit is a plot of the weighted residuals. The difference between the decay curve and the fitted curve, weighted properly, will show a nonrandom deviation when the fit to the data set is poor. The weighted residual is calculated, channel by channel, using the equation:

$$\textit{residual of channel } i = \sqrt{W_i}\,[I_0(t_i) - Y(t_i)]. \qquad (51)$$

Adding the appropriate weights W_i of the data gives:

$$residual\ of\ channel\ i\ =\ r(t_i)\ =\ \frac{I_0(t_i)\ -\ Y(t_i)}{\sqrt{I(t_i)}} \qquad (52)$$

A good fit will show random distribution about zero.

III.h.3. Autocorrelation of the weighted residuals.

A further test of the goodness of fit is the autocorrelation of the weighted residuals:

$$Cr_j\ =\ \frac{\frac{1}{m}\sum_{i=n_1}^{n_1-m-1} r(t_i)\ r(t_{i-j})}{\frac{1}{n_3}\sum_{i=n_1}^{n_2}[r(t_i)]^2} \qquad (53)$$

with

$$n_3\ =\ n_2\ -\ n_1\ +\ 1 \qquad (54)$$

A successful fit will show an autocorrelation plot with high frequency, low amplitude oscillations about zero. The combination of all three parameters, magnitude of the reduced χ^2_ν, the appearance of the plots of weighted residuals and autocorrelation of weighted residuals, are always used together to judge the success of the fit.

III.i. Implementation of Data Analysis Software.

The original FORTRAN source code for the analysis programs was acquired from Prof. L. Brand of the Johns Hopkins University. The programs were originally written for

an HP E-1000 series minicomputer, running under an operating system known as RTE-III. In all cases, the fitting functions are sums of exponentials, and a nonlinear least squares search based on the Marquardt algorithm is used.

Table VIII. Original set of curve fitting programs.

Program Name	Fitting Method Supported
FIX (HP1000 Minicomputer)	Single curve SUM analysis
DIFX (HP1000 Minicomputer)	Single curve DIFFERENCE analysis
TFIT (HP1000 Minicomputer)	Global VECTOR analysis for Lifetimes
AFIT (HP1000 Minicomputer)	Global VECTOR analysis for Anisotropy Decay

The single curve analysis programs, FIX and DIFX, were originally ported to the IBM PC environment by Dr. Andrej Kowalczyk of the Institute of Physics, N. Copernicus University in Torun, Poland. Graphics were rewritten to work under the EGA/VGA standard using PASCAL graphics libraries.

Global curve fitting routines (TFIT and AFIT) have also been ported to the IBM PC environment. Large global analyses on a 486dx PC required recompiling the FORTRAN programs as Microsoft Windows applications, to allow the use of extended memory. The DOS applications generated by the MS Fortran 5.1 compiler are restricted to use conventional memory only (0.64 Mb), limiting the number of experiments to about 6 at a time. Microsoft provides a set of tools to generate a QuickWin application without having to modify the original FORTRAN code. The increased memory space available using this method removed the space restriction on the number of experiments and fitting parameters.

Section IV. - Mathematical Models for Anisotropic Rotations of Perylene.

Three rotational models were considered for each system. Each model uses global analysis, but differs in the linkage between parameters. In all cases, the rotational correlation times are linked along isotherms.

IV.a. Model I: the 'Free Beta' Model.

In the 'Free-Beta' Model, the rotational correlation times are linked along isotherms. The preexponentials are allowed to vary independently, and are not linked in any way to each other. This model can include a residual anisotropy term for hindered rotation.

IV.b. Model II: the 'Linked-Beta' Model.

In the 'Linked-Beta' Model, the rotational correlation times are linked along an isotherm, as in the 'Free-Beta' Model, but in addition, the values of the preexponential terms are constrained as well. Using photophysical considerations, it is logical to 'link' the preexponential terms that arise when a given excitation wavelength is used. The rationale for this is that the preexponential terms are simple functions of the angle between the absorption and emission oscillators of the perylene molecules, which are, in turn, governed by the excitation wavelength. This model can include residual anisotropy, but when it does, the residual anisotropy term is never linked to any other parameter.

Single Curve Analysis of Anisotropy Decay Data

Preexponentials are free to vary independently
Rotational correlation times are free to vary independently
Hindered motions are free to vary independently

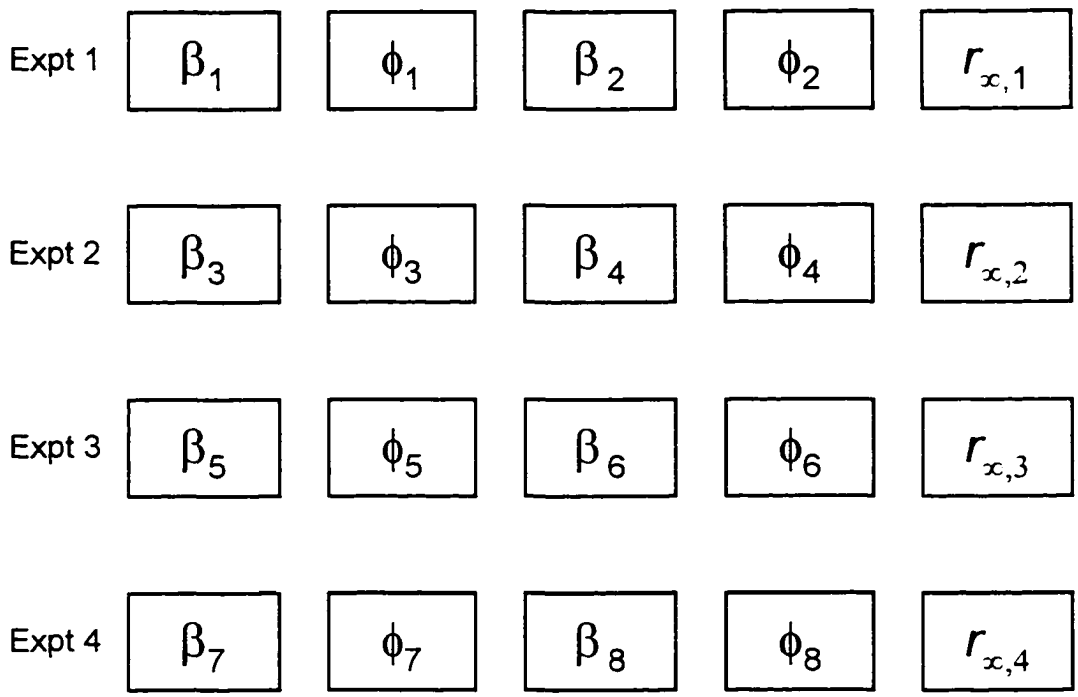

Figure 25. Single curve analysis of multiple data sets results in recovery of completely independent parameters. The solution obtained in this way may not be unique, due to a high degree of correlation between the parameters.

Global Analysis of Anisotropy Decay Data

Model 1 - 'Free Beta' Model

Preexponentials are free to vary independently
Rotational correlation times are linked along Isotherms
Hindered motions are free to vary independently

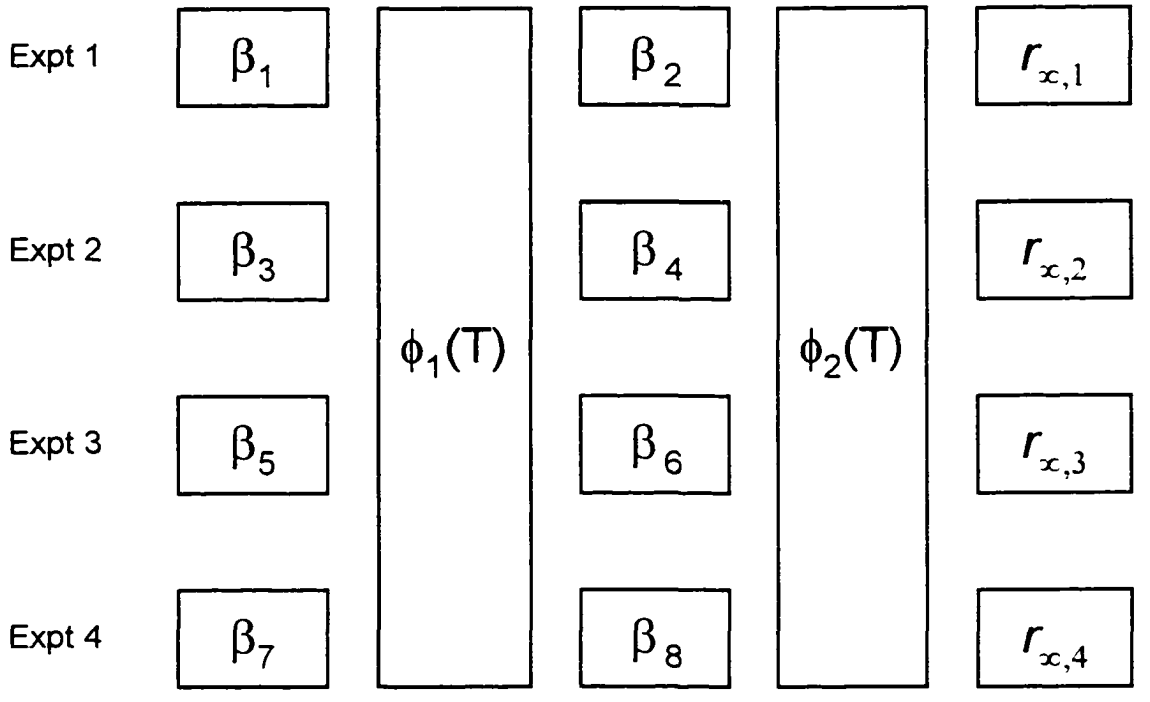

Figure 26. Logical relationship of anisotropy decay parameters in the 'Free Beta' Model. Rotational correlation times (φ's) are linked along isotherms. All other parameters are allowed to vary independently during the global analysis.

Global Analysis of Anisotropy Decay Data

Model 2 - 'Linked Beta' Model

Linked Preexponentials across Wavelength Sets
Linked Rotational Correlation Times along Isotherms

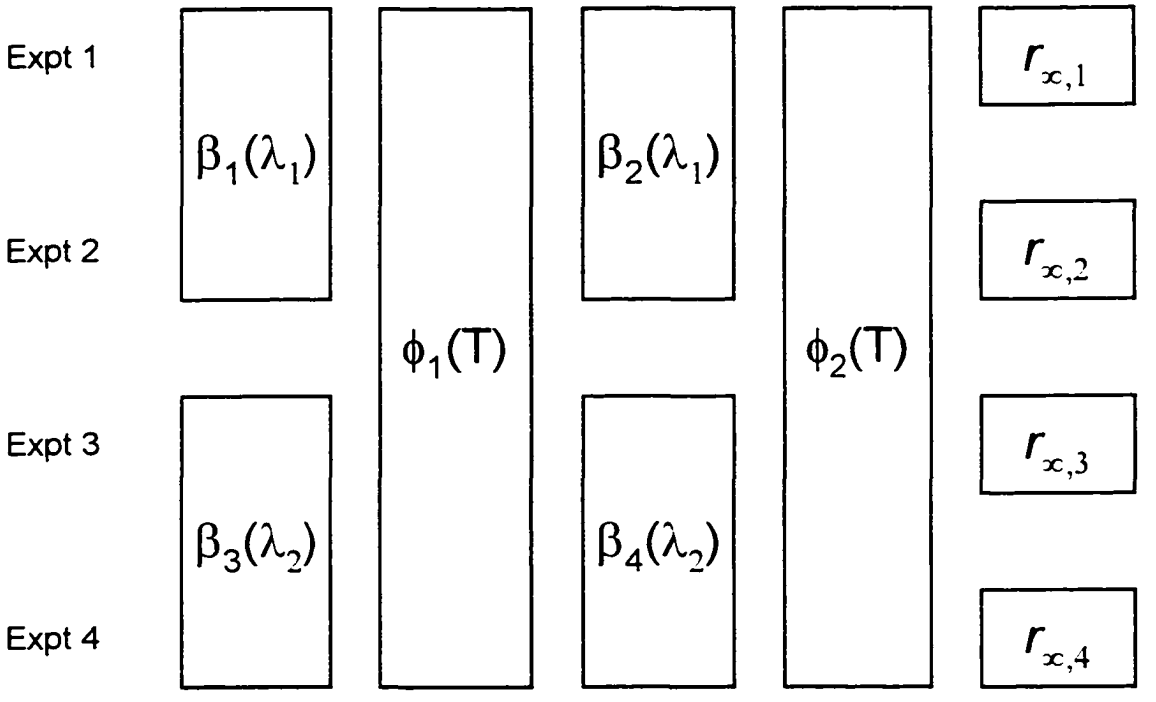

Figure 27. Anisotropy parameters for the 'Linked Beta' Model. At each excitation wavelength, preexponential terms (β's) are linked. Along isotherms (encompassing multiple excitation wavelengths), the rotational correlation times (φ's) are linked, as in the 'Free Beta Model'.

IV.c. Model III: the 'Temperature-Dependent Beta' Model.

This model is a new approach to the treatment of hindered anisotropic rotations, developed in this Thesis. In the 'Temperature-Dependent Beta Model', allowances for the effect of the residual anisotropy term on the remaining preexponentials are considered. Specifically, in hindered anisotropic media, the sum of the preexponentials and a residual anisotropy term do not add to a constant value, which should be the limiting anisotropy. Since the residual anisotropy is temperature dependent, then *one or more of the preexponentials must also be temperature dependent*, so that their sum is a constant at any temperature. This model correctly converges to the linked beta model, when the residual anisotropy terms reduce to zero, as in an isotropic solvent system.

Global Analysis of Anisotropy Decay Data

Model 3 - 'Temperature Dependent Beta' Model

Preexponentials are functions of temperature
Rotational correlation times are linked along Isotherms
Hindered motions are not linked

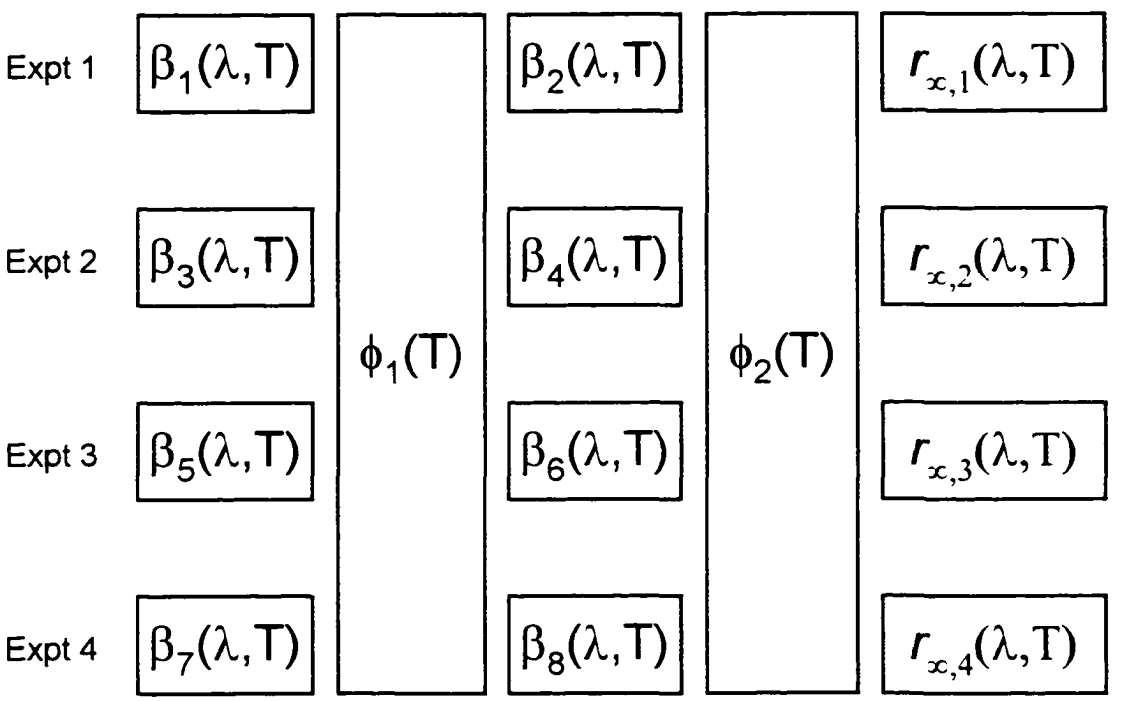

Figure 28. The 'Temperature Dependent Beta Model'. This model constrains the values of the preexponentials (β's) to functions of temperature and excitation wavelength. As in all other global analyses performed on these data sets, the rotational correlation times (φ's) are 'linked' along isotherms. Notice that the residual anisotropy (r_∞) terms, required to allow for hindered motions, are not constrained.

Section V: Materials and Methods.

V.a. Fluorescent dyes and standard reagents.

Perylene, CAS number 198-55-0, was obtained from Aldrich, compound number P1,120-4, purity 99+ percent, FW 252.32 g/mol, mp 277-279 °C, lot number 12504BY and was used as received. A stock solution of 1.0×10^{-4} M perylene in ethanol was prepared by mass. This stock solution was stored in a freezer at -10°C, in a brown glass bottle to minimize photodegradation.

Glycerol was obtained from EM Science (Gibbstown, New Jersey), OmniSolv grade (lot number 33347, purity 99.84 percent, water content 0.019 percent, UV cutoff 203 nm), and was used as received.

V.b. Phospholipids.

The phospholipid 1,2-ditetradecanoyl-sn-glycero-3-phosphocholine (DMPC) was obtained from Sigma Chemical Company (St. Louis, MO), compound number P-0888, lot number 70H8353. It was used as received, after verifying purity by TLC, using silica gel plates and chloroform/methanol/water (65:25:4 v/v) as the solvent [61].

The phospholipid 1-stearoyl-2-caproyl-sn-glycero-3-phosphorylcholine (C18:C10-PC) was synthesized in this laboratory by Dr. M. Straher, according to the method of Ali, *et al.* [62]. One acyl chain is 18 carbons long, and the other is 10 carbons long. The acyl chains of this asymmetric lipid are known to interdigitate below the phase transition temperature. This excludes the possibility of the perylene molecules from positioning themselves between the bilayer leaflets.

Stock solutions of phospholipids were prepared by dissolving a known mass of phospholipid in chloroform. Since commercially available chloroform may contain up to 1 percent of ethanol as a stabilizer [63], purification was required. The chloroform was washed with water, dried over $CaCl_2$ dessicant, and fractionally distilled using standard organic chemistry techniques. Typically, small batches of phospholipid stock were prepared, containing a total of approximately 50 milligrams of phospholipid dissolved in 5.0 milliliters of solvent. This preparation yielded a stock solution of approximately 10 milligrams phospholipid per milliliter of $CHCl_3$. Solutions of phospholipids were sealed in small scintillation vials fitted with Teflon lined caps. The vials were wrapped in aluminum foil to minimize exposure to light and stored in a freezer at -10 °C.

V.c. Preparation of SUV samples.

Small unilamellar vesicles (SUVs) were prepared by cosonication of perylene with the appropriate phospholipid. Typically, 1.0 ml. of the stock phospholipid in chloroform was pipetted into a small sonication vial. Knowing the stock phospholipid concentration, the required volume of perylene stock solution was calculated so that the desired labeling ratio (mol Phospholipid / mol Perylene) was achieved. In all experiments, the perylene dye content (labeling ratio) was 1:200 (mol perylene:mol phospholipid) or lower, to minimize gross perturbation of the phospholipid bilayer matrix by the perylene dye [64]. Using the approximation that a phospholipid SUV labeled at 0.20 mol% contains roughly 5 dye molecules per 2500 phospholipid molecules [65], the effect of perturbation is expected to be minimal. The solvents were removed by directing a gentle stream of dry nitrogen gas

over the solution in the sonication vial. The remaining solvent was removed by placing the sonication vial into a vacuum dessicator for at least 1 hour, maintaining a vacuum of better than 2 torr as measured by a McLeod gauge. The resulting dry film of phospholipid and perylene was suspended in 3.0 ml. of TRIS buffer (0.01M TRIS.HCl in 0.1M NaCl, pH 8.50 at 25°C), and gently vortexed to bring all material into suspension. This resulted in a turbid solution, which had a slight pale green color.

Sonication and separation of SUVs.

The turbid solution, consisting of an aqueous suspension of phospholipid and perylene, was sonicated above the phase transition temperature (T_c) of the respective phospholipid [66] (DMPC: T_c = 23.8°C; C(18):C(10)-PC: T_c=19.8°C). A Heat Systems Ultrasonics Processor Model W-225 (Heat Systems Ultrasonics, Inc., Farmingdale, New York), fitted with a 0.5" diameter C2 ultrasonic horn operating at 20 KHz, was used to sonicate the phospholipid suspension. Each sample was subjected to four cycles of sonication, consisting of three minutes sonicator 'on' time, followed by three minutes sonicator 'off' time. The reason for the intermittent sonication cycles is to reduce the possibility of oxidation of the phospholipids caused by overheating the solution. The turbid solutions became opalescent, usually by the second or third sonication cycle. The total sonication time was usually twelve minutes.

The resultant SUVs were isolated from the sonication products by ultracentrifugation, using a Beckman AIRFUGE (Beckman Instruments, Palo Alto, California) air driven ultracentrifuge operating at 84,000 rpm (approximately 70,000*g*). The

titanium particles and multilamellar species formed during the sonication process are separated as precipitate, appearing at the edges of the rotor lining. The supernatant liquid contains the small unilamellar vesicles, which were carefully removed from the rotor using a Pasteur pipette.

V.d. UV Absorption Spectra.

Absorption spectra of the labeled SUV fractions were obtained using a Hewlett-Packard 8452A Diode Array Spectrophotometer (Hewlett Packard Company, Palo Alto, California). Samples were diluted with the same TRIS buffer used in the preparation. The absorbance of the solutions, measured at the long wavelength absorption peak of perylene, was about 0.10 absorbance units above the SUV baseline. The unlabeled SUV baseline was typically 0.1 - 0.15 absorbance units at the same wavelength of observation. This dilution is necessary to avoid inner-filter [67] and potential concentration quenching effects, which would distort the recovered lifetimes.

V.e. Steady-State Fluorescence Measurements.

Steady-state emission spectra and anisotropy measurements were obtained using either a Perkin-Elmer MPF-2A Fluorescence Spectrometer or a Perkin-Elmer LS-50B Fluorescence Spectrometer (Perkin-Elmer Corporation, Norwalk, Connecticut). For each experimental system, a curve of the steady state emission anisotropy, <r>, versus temperature was obtained using three different excitation wavelengths. For the phospholipid systems, the temperature ranges were 0°C to 30°C, chosen to include temperatures below

and above the phase transition for each phospholipid. For each excitation wavelength and temperature, four polarized intensity measurements were taken (I_{VV}, I_{VH}, I_{HH} and I_{HV}) on labeled samples and phospholipid blanks. For each polarized intensity component, the corresponding blank value was subtracted, and the steady state anisotropy was calculated using:

$$<r> = \frac{G*I_{VV} - I_{VH}}{G*I_{VV} + 2*I_{VH}} \quad (55)$$

$$G = \frac{I_{HH}}{I_{HV}} \quad (56)$$

where G is an instrumental factor [55] which corrects for the difference in instrument response to vertical and horizontally polarized light. The subscripts VV,VH,HH and HV refer to the orientation of the excitation and emission polarizers in the light path, respectively.

V.f. Time-resolved fluorescence anisotropy measurements.

Time-resolved emission anisotropy decay curves were measured on the time-resolved fluorometer described in this Thesis. Samples were excited using an IBH System 5000 Coaxial Nanosecond Flashlamp (IBH Consultants Ltd., Scotland, U.K.). For 410 nm excitation, the lamp was filled with UHP grade nitrogen, at a pressure of 0.8 bar, and the

electrode spacing was typically 0.6 mm. The discharge potential was about 5.9 kV at a repetition rate of 24 kHz. These conditions produced instrumental pulses measuring approximately 2.5 - 3.0 ns FWHM as measured by a Phillips XP2020Q photomultiplier.

For excitation at 256 nm, the lamp was filled with 0.4 bar of deuterium. An electrode spacing of 1.5 mm, a discharge voltage of 4.9 kV and a pulse repetition rate of 17 kHz yielded stable operation, as judged by the appearance of the rf signal detected using a small loop antenna placed near the discharge chamber. The pulses obtained using deuterium gas under these conditions were about 1.8 - 2.4 ns FWHM, and were stable for several days.

For each sample, a series of polarized emission decay curves were collected, in which the temperature was automatically varied over a range specified by the user. For the perylene in glycerol experiments, the range varied from 10°C to 30°C, in 5°C increments. For the phospholipid SUV preparations, the temperature ranged from 0°C to 30°C, including temperature points below and above the phase transition for each phospholipid. For n temperatures, there are n lamp profiles, n V(t) decays, n H(t) decays and n standard fluorophore curves (needed for the determination of the Q-shift). Perylene dissolved in ethanol was used as a reference compound, since it exhibits a single exponential decay time (τ_F = 4.6 ns). In addition, perylene in ethanol matches the excitation and emission wavelengths of the perylene labeled SUVs perfectly, making it an ideal reference standard for these measurements. The temperature was measured periodically during the acquisition, and the average temperature was recorded and saved with each data set's output file on disk.

V.g. Data analysis.

V.g.1. Single curve analysis. Each data set was analyzed using nonlinear least-squared fitting, based on the Marquardt algorithm. The fitting functions adopted for the lifetime (total intensity parameters) were sums of exponentials. For the anisotropy decay curves, the fitting functions were also sums of exponentials, and, for the phospholipid systems, included a residual anisotropy term (r_∞) to allow modeling the hindered rotation of perylene in the phospholipid matrices. The combination of the recovered single curve data analysis results in a matrix which has no linkage between any of the fitted parameters. Due to the high degree of correlation between parameters, the solution obtained by simple single curve analysis may not be unique.

V.g.2. Global curve analysis. For each experimental system, data were assembled and analyzed simultaneously in a global analysis. Certain parameters were linked according to photophysical considerations, as well as the specific model under consideration. Global analysis of a complex heterogeneous decay surface allows optimization of the recovered parameters, especially when these fitted parameters show a high degree of correlation.

Section VI. Results and Discussion.

VI.a. Perylene in isotropic solvent systems.

Glycerol is an isotropic medium. The rotational motions of perylene have been studied in pure glycerol using multiple excitation wavelengths and temperatures [11]. Additional work, using 257nm laser excitation on a series of glycerol / water mixtures [25] was performed to reveal the magnitude of preexponentials associated with the rotational correlation times of perylene. In glycerol solvent, analysis of the time-resolved emission anisotropy decay curves reveals two rotational correlation times, corresponding to two different combinations of in-plane and out-of-plane motions. Using two excitation wavelengths (corresponding to the $S_0 \neg S_1$ and $S_0 \neg S_2$ transitions) allows the rotational correlation times to be overdetermined. As the temperature of the solution is increased, the diffusion coefficients of perylene increase, appearing as lowered values for the rotational correlation times. Knowing that the rotational correlation times are simple functions of the viscosity (and therefore, the temperature), the rotational correlation times can be 'linked' along isotherms, using different excitation wavelengths. This allows a unique solution for the value of the rotational correlation times at each temperature.

The work of Barkley, *et al.* [11] was repeated here, using the lifetime instrument described in this Thesis, for two reasons. First, the perylene/glycerol system is relatively simple to prepare experimentally, and is stable over many days. This system may be used as a test for the instrument, and of the global analysis software which is required for analysis of the more complex systems studied in this work. The goal was to perform a series of experiments, using multiple temperature/excitation wavelength sets, and fit the data

GLOBALLY, a data procedure which was not available to Barkley, *et al.* at the time they performed their classic experiments. In Barkley's study, common parameter sets were obtained *manually*. Beechem, *et al.* later reanalyzed the data using global analysis, and the results were found to be in agreement with the original (manual) search for the best-fit parameters [68].

A second motivation for repeating the measurements of perylene in glycerol included a baseline measurement of the true values for the preexponential terms (β_i) in an *isotropic* solvent system. These baseline data were needed for validation of the instrument hardware and software, before the more complex *anisotropic* phospholipid systems were measured.

In *isotropic* solvents such as glycerol, no rotational barriers are present. The data were analyzed globally using Model II- the 'Linked-Beta' Model, in which the preexponential (β_i) terms were linked across temperature for a given excitation wavelength. Preexponential (β_i) terms were entirely 'linkable' across the temperature range, at each excitation wavelength, consistent with the photophysics of perylene rotating in an isotropic medium. Table IX and Figure 29 show the results of the global analysis of these experiments. The plots express each preexponential term and rotational correlation time as functions of temperature. These results, combined with the intensity decay (fluorescence lifetime) parameters, contain all of the information describing the dynamics of the emission anisotropy decay, i.e. anisotropy vs. time. Figure 31 shows a family of curves of the decay of the emission anisotropy as functions of time, calculated using the globally recovered parameters from Table IX at each temperature and excitation wavelength. The early time portion of the curves reflect the fast in-plane motions of perylene, and the longer time

regions show the slower, out-of-plane motions. It is important to note that, in the long time limit, the emission anisotropies tend to zero. Therefore, no residual anisotropy term (r_∞) representing hindered motion of the fluorophore is needed to describe the rotational behavior.

The absence of hindered rotation ($r_\infty = 0$) can be interpreted as an 'order parameter' of zero. It is expected that an isotropic oil would not have any structural 'order', and the rotational motions of a fluorophore would not be hindered along any particular diffusion axis. Therefore, no residual anisotropy (r_∞) term is expected.

Table IX. Recovered anisotropy decay parameters for Perylene in Glycerol.

Temp, °C	λ_{ex}, nm	β_1	ϕ_1, ns	β_2	ϕ_2, ns
10	410 256	0.238 -0.241	15.9 15.9	0.090 0.090	115 115
15	410 256	0.238 -0.241	9.08 9.08	0.090 0.090	70 70
20	410 256	0.238 -0.241	6.01 6.01	0.090 0.090	34.8 34.8
25	410 256	0.238 -0.241	3.88 3.88	0.090 0.090	22.1 22.1
30	410 256	0.238 -0.241	2.56 2.56	0.090 0.090	14.3 14.3

Notice that the individual β_i have values which exceed the theoretical limits for r_0, but that their *sum* produces the correct values for r_0. Adding the recovered β_i values gives:

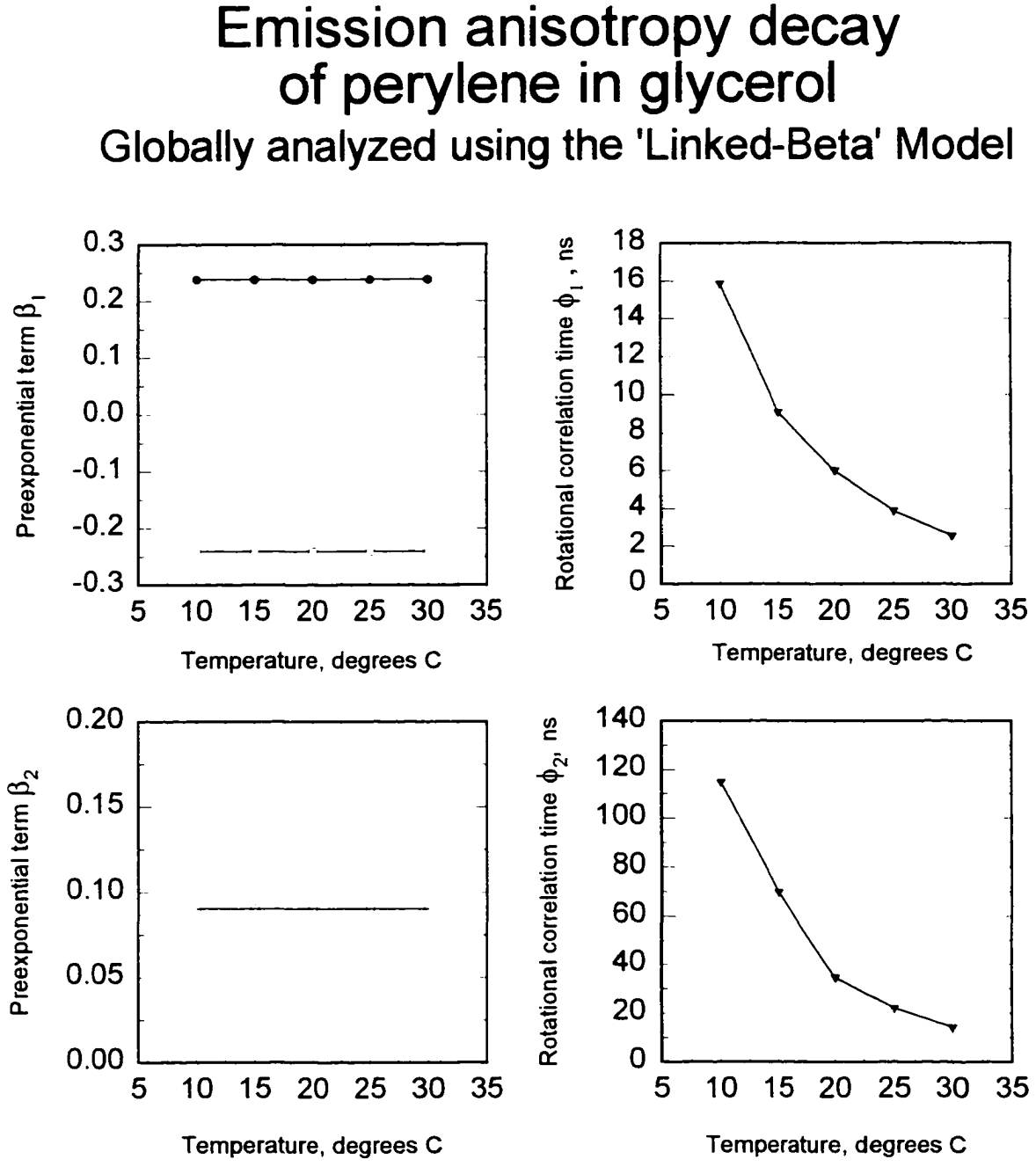

Figure 29. Global analysis of perylene in glycerol. Two excitation wavelengths were used across five temperatures, resulting in ten experiments. At each excitation wavelength, the preexponential terms are linked. At a given temperature, the rotational correlation times are linked, since they are functions of the solvent viscosity and hydrodynamic volume, independent of the excitation wavelength.

$$r_{0,410nm} = \sum \beta_i = \beta_1 + \beta_2 = (+0.238) + (+0.090) = +0.328 \quad (57)$$

$$r_{0,256nm} = \sum \beta_i = \beta_1 + \beta_2 = (-0.241) + (+0.090) = -0.151 \quad (58)$$

These values agree with those reported in the literature (see Table I) of +0.335 and -0.165, which were measured using excitation wavelengths of 410nm and 252 nm, respectively.

The rotational rates of perylene in glycerol were calculated from the rotational correlation times, obtained by global analysis. A plot of these rotational rates, as well as the ratio between them, is shown in Figure 30. Both the in-plane and out-of-plane rates increase steadily with temperature, as the viscosity of the bulk glycerol solvent decreases. The ratio between the rotational rates remains nearly constant at 10:1 in-plane:out-of-plane.

The fitted anisotropy decay functions of perylene in glycerol, as functions of temperature and excitation wavelength, are presented in Figure 31. As the temperature increases, the fast in-plane motion becomes more prominent in the early time portions of the decay, followed by the slower, out-of-plane depolarizing motion of perylene.

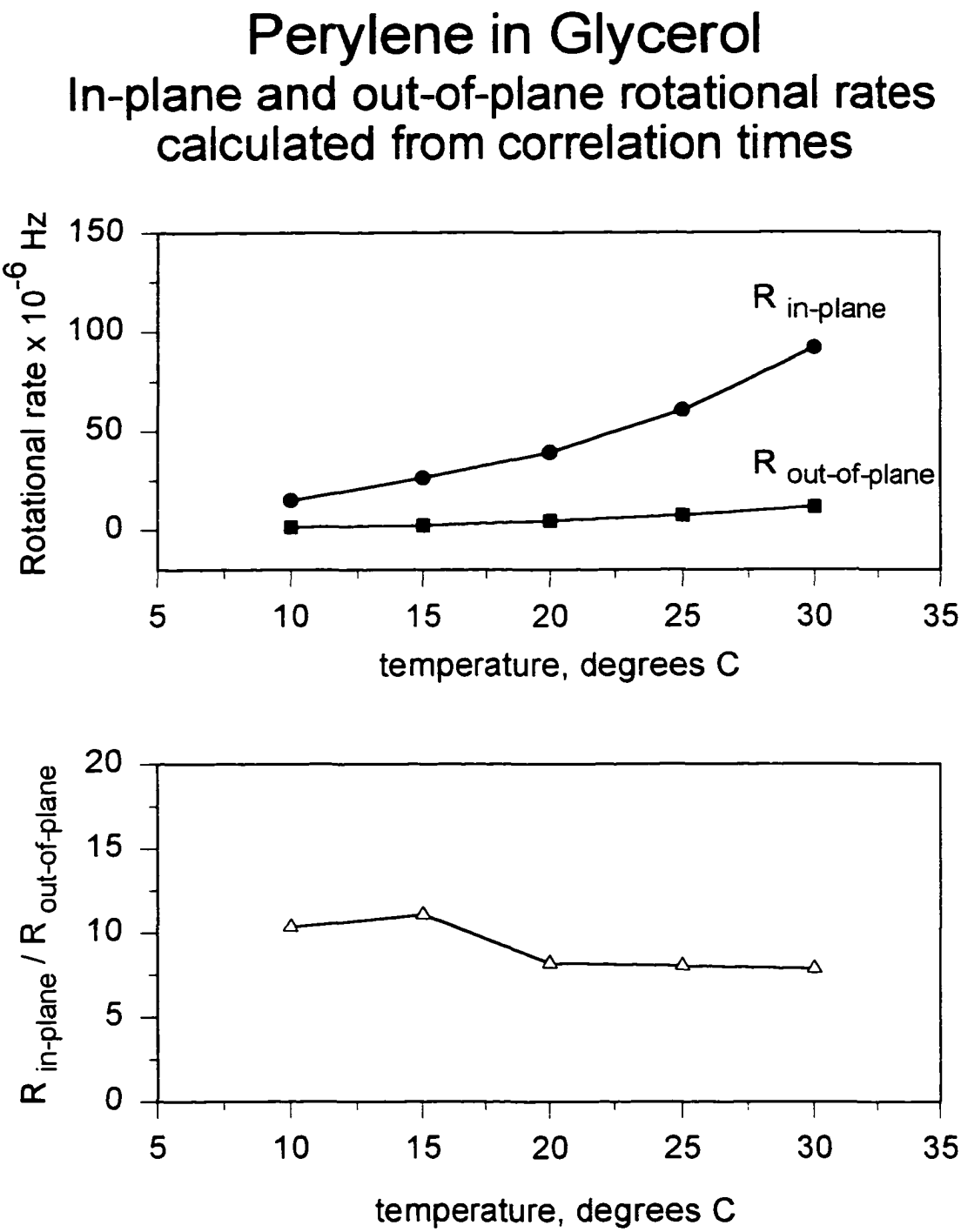

Figure 30. Rotational rates of perylene in glycerol, as a function of temperature. The rotational rates were calculated using the globally recovered rotational correlation times. Notice that the ratio of in-plane to out-of-plane rotational rates is nearly constant in the isotropic glycerol solvent.

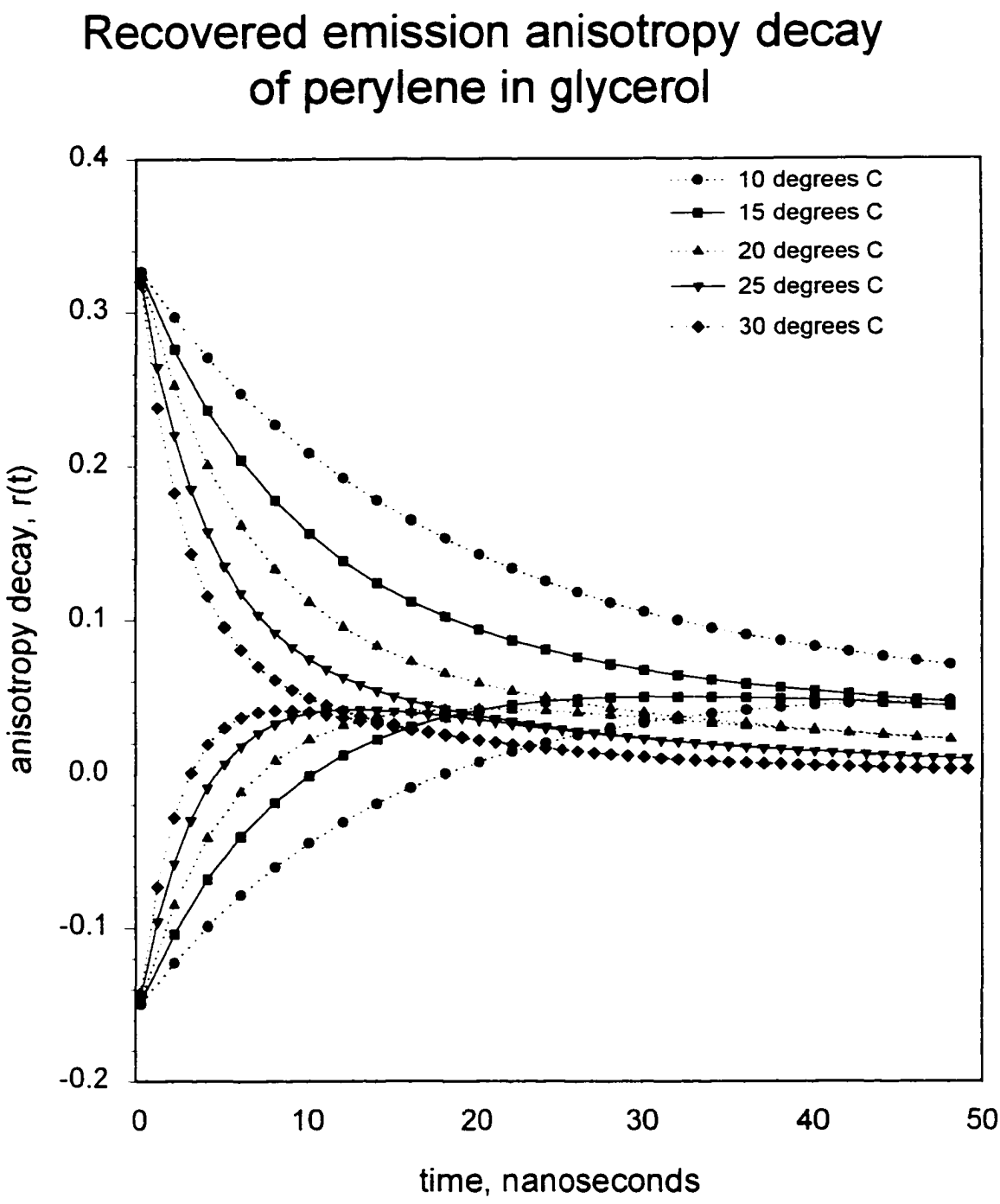

Figure 31. Reconstructed time course of anisotropy, as a function of temperature and excitation wavelength. Using the rotational parameters (preexponential and rotational correlation times) recovered by global analysis, the function $r(t)=\sum_I \beta_i \exp(-t/\varphi_i)$ was constructed, over the time interval from zero to fifty nanoseconds. The temperature ranged from 10°C to 30°C, in 5°C intervals.

VI.b. Perylene in Anisotropic Solvent Environments.

In the last section, the anisotropic rotations of perylene in an isotropic solvent system were examined in detail. The results obtained agreed well with those already available in the literature [11,25,68], providing a performance test of the instrument and software described in this Thesis. In this section, the rotational behavior of perylene in anisotropic solvent systems of phospholipid bilayers will be described in detail.

VI.b.1. System 1 - Asymmetric C(18):C(10)-PC SUVs.

VI.b.1.1. Steady-state emission anisotropy.

Excitation using 410 nm shows a sharp decrease in the emission anisotropy, reaching a minimum value near 20°C, the phase transition temperature. Above this temperature, the emission anisotropy remains fairly constant, at a value of approximately +0.04. This residual anisotropy, even at temperatures above the phase transition temperature, indicates that there is some persistent hindrance to rotation in the phospholipid bilayer. Since both in-plane and out-of-plane motions are detected using 410 nm excitation, it is unclear whether the in-plane, out-of-plane, or both, motions are restricted.

Excitation with 256 nm light, using the negative anisotropy band, shows an initially negative anisotropy, reaching a maximum, and becoming asymptotic near 20°C. A different combination of in-plane and out-of-plane motions is revealed by using 256 nm excitation, and the restricted motion cannot be assigned to purely in-plane or out-of-plane hindrance using the steady-state data alone.

Referring to the excitation anisotropy spectrum of perylene (Figure 5), we find that

the wavelength at which r_0 equals 0.1 occurs near 315 nm. This wavelength corresponds to the excitation wavelength that will allow only the out-of-plane motions to be observed, as will be described in a later section. When 315 nm excitation is used, the emission anisotropy of perylene in the asymmetric C(18):C(10)-PC appears fairly constant with temperature. The significance of this observation is that the out-of-plane motion of perylene within the phospholipid bilayer is relatively unchanged as the phase transition is reached. The implication is that the out-of-plane rotational motion of perylene is not very sensitive to structural changes in the phospholipid acyl chains, as the system undergoes a melt transition. The in-plane motion of the probe appears to be more sensitive to the environment. There is also the lingering question: Why does the anisotropy remain at a constant nonzero value at temperatures above the phase transition? At high temperatures, the phospholipid would be expected to reduce to a disordered, isotropic environment such as glycerol.

Since the steady-state data represent time averaged values, time-resolved measurements are necessary to further unravel this system. Resolution of the discrete in-plane and out-of-plane motions of perylene in the phospholipid bilayers provides further insight.

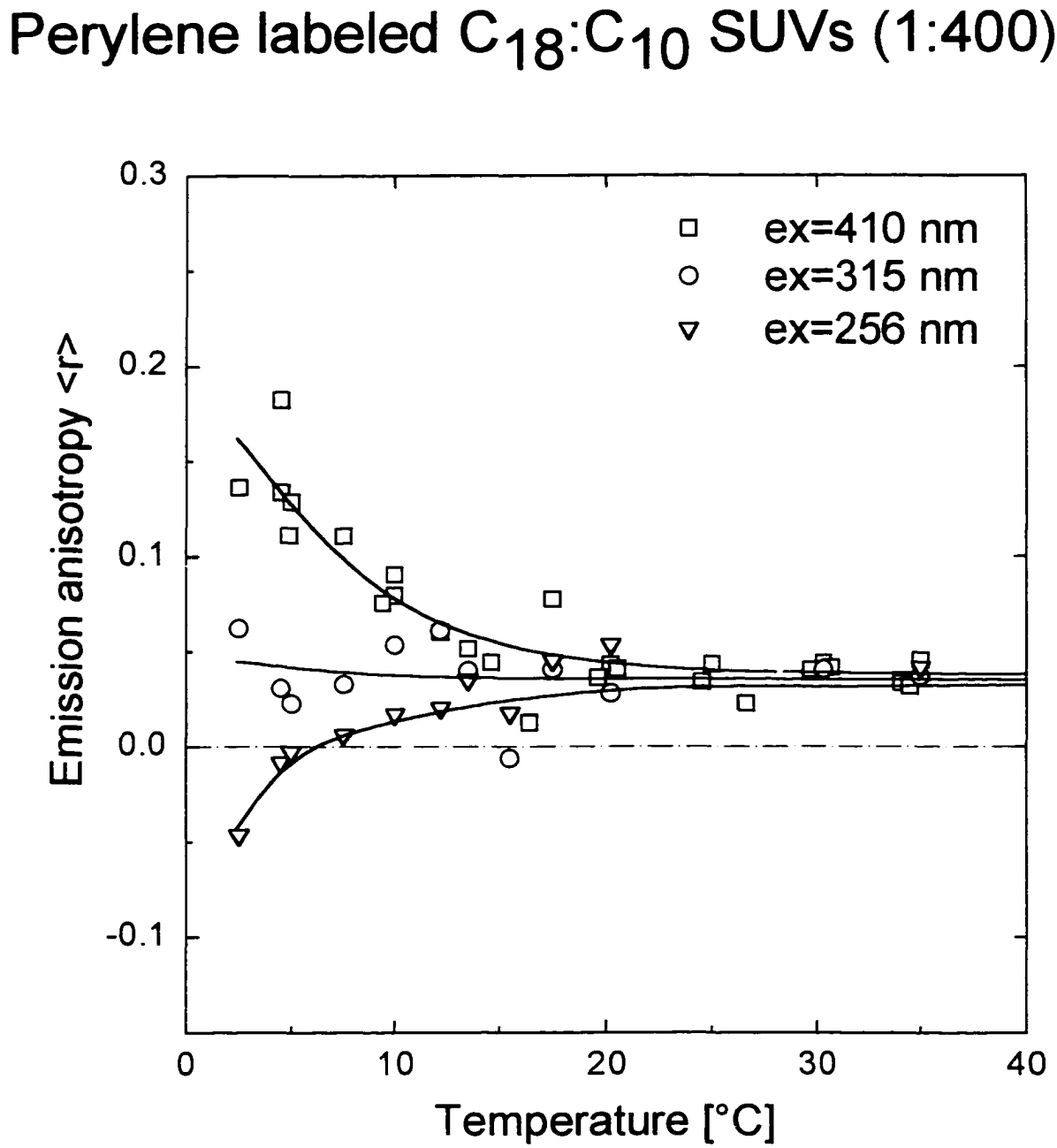

Figure 32. Steady-state emission anisotropy of perylene embedded in the asymmetric phospholipid C(18):C(10)-PC. Excitation into the positive band (410nm) and the negative band (256nm) show different combinations of in-plane and out-of-plane motions. Excitation using 315nm is selective to out-of-plane motions only. As the temperature is increased through the phase transition (19°C), the out-of-plane motion does not appear to change as strongly as the in-plane motions.

VI.b.1.2. Time-Resolved Emission Anisotropy.

Time-resolved emission anisotropy decay experiments were performed on the perylene labeled C(18):C(10)-PC phospholipid system. A total of 16 experiments were performed, using 6 temperatures and 2 excitation wavelengths. The fluorescence lifetimes were described by double and triple exponential decay laws, and showed a slight decrease with increasing temperature. The average lifetime values, obtained using Equation 41, are presented in Table X.

Table X. Average Fluorescence Lifetimes of Perylene in C(18):C(10)-PC
<τ> values were calculated using Equation 41.
Errors are standard deviations of 2 or more determinations at each temperature.

Temperature	Average Fluorescence Lifetime, <τ>
3 °C	6.53 +/- 0.10 ns
5 °C	6.59 +/- 0.23 ns
10 °C	6.52 +/- 0.20 ns
15 °C	6.23 +/- 0.14 ns
25 °C	6.10 +/- 0.03 ns
30 °C	6.06 +/- 0.04 ns

Single curve analysis of the decay data required two rotational correlation times plus an r_∞ term to achieve a proper fit. Examination of the sum and difference decay curves (Figures 33 and 34), along with the convolved anisotropy curves shows the hindered motion clearly. At 3 °C, the convolved anisotropy decay using either 410 nm (Figure 35) or 256 nm (Figure 36) excitation shows nonzero asymptotic values at long times.

Global analysis of the C(18):C(10)-PC data.

Several global analysis models were considered for the rotational dynamics of the system, to account for the hindered anisotropic rotation expected in the phospholipid bilayer matrix.

Global Model I: 'Free Beta' Model.

The preexponentials β_1(410 nm), β_1(256 nm), β_2(410 nm) and β_2(256 nm) are completely unrestricted in the global analysis. Each rotational correlation time was linked as a function of temperature, across the excitation wavelengths, i.e. $\varphi = \varphi(T)$ alone. This is justified since the rotational correlation times are functions of temperature and viscosity, independent of the excitation wavelength, fluorescence intensity and lifetime parameters.

In the 'Free-Beta' Model, no constraints are placed on the hindrance (r_∞) terms describing the hindered rotational motion of the fluorophore. To model a hindered rotation, an additional beta term was allowed in the fitting function, with a correlation time fixed to a value of 10,000ns, i.e., the rotation would not occur on the fluorescence timescale of the molecule. Figure 37 shows the results of the global fit using this model. The global reduced chisquare (χ^2_v) was 1.28 for the analysis.

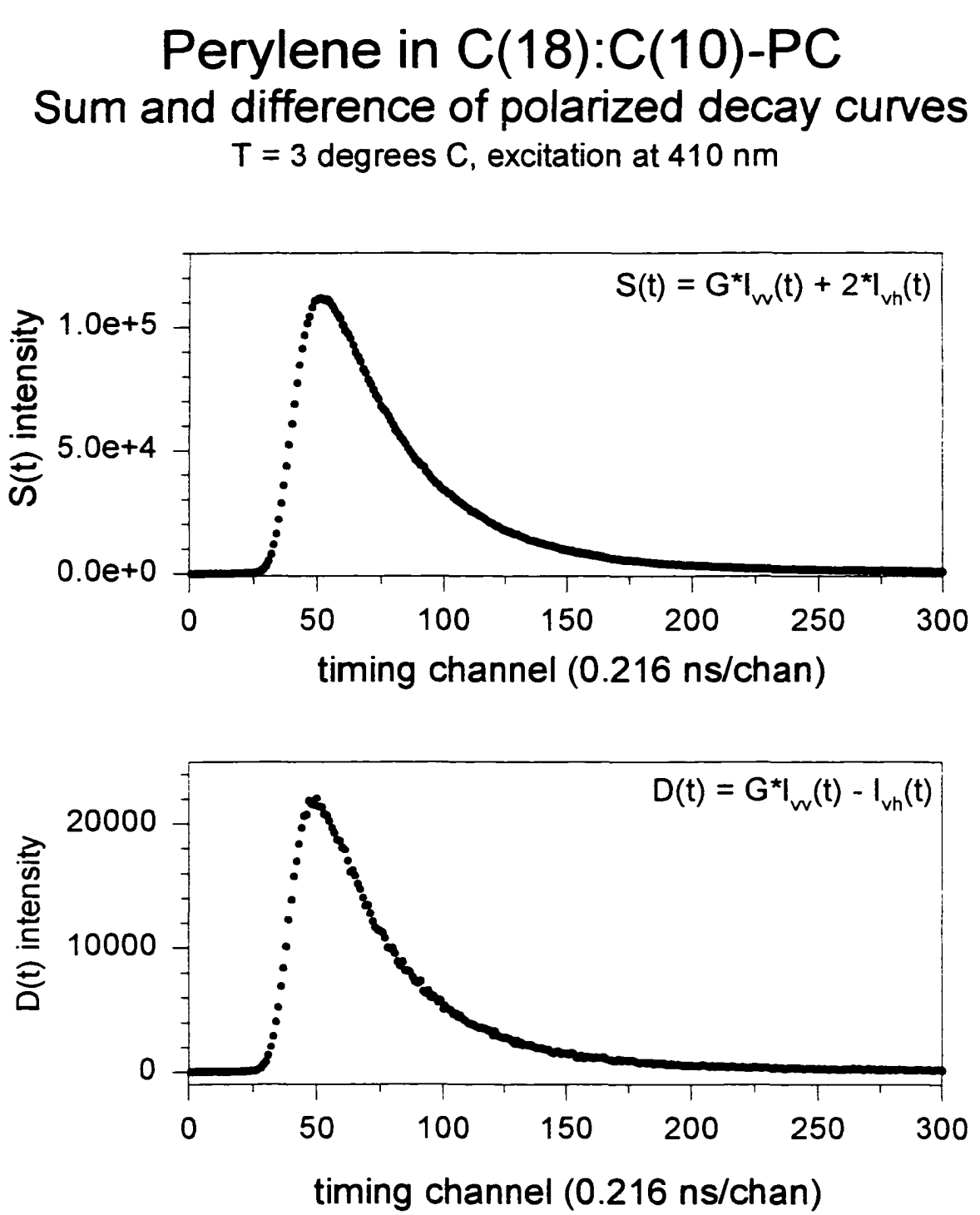

Figure 33. Asymmetric phospholipid C(18):C(10)-PC labeled with perylene. Sum (S(t)) and difference (D(t)) of polarized decay curves, using excitation into the positive band (410 nm).

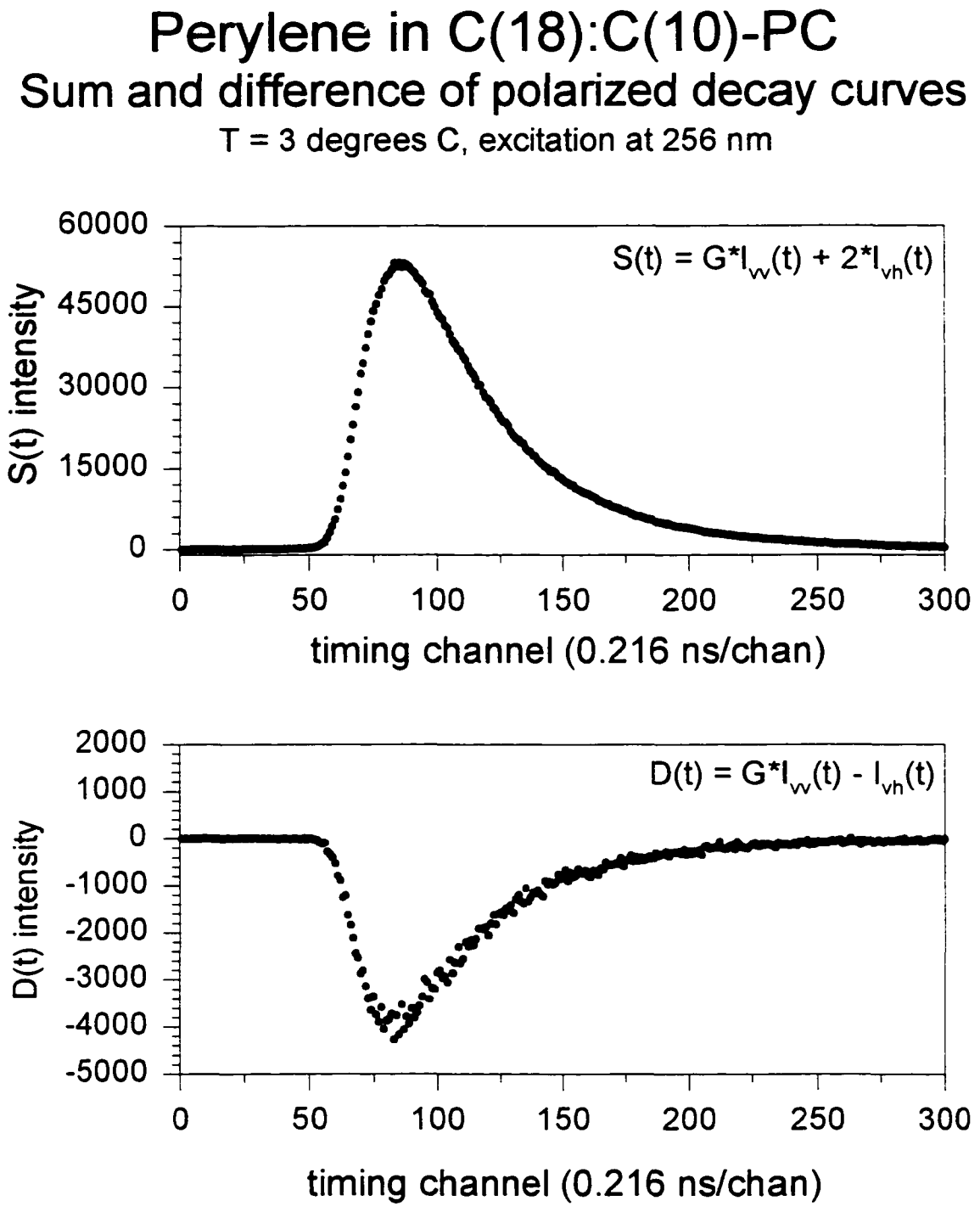

Figure 34. Asymmetric phospholipid C(18):C(10)-PC labeled with perylene. Sum (S(t)) and difference (D(t)) of polarized decay curves, using excitation into the negative band (256 nm). Notice that the difference curve (D(t)=V(t)-H(t)) is negative, resulting in negative anisotropy values.

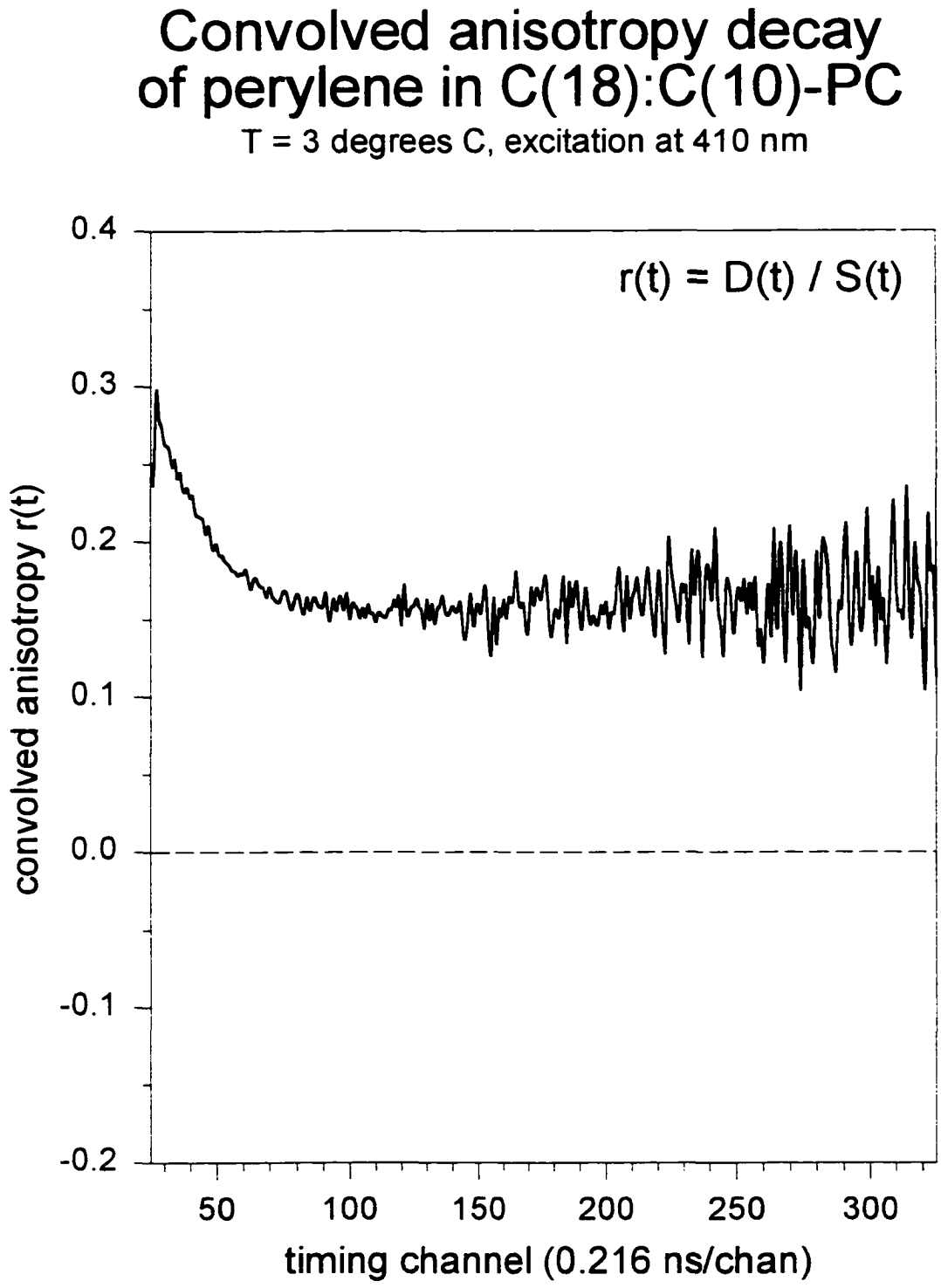

Figure 35. Convolved anisotropy decay of perylene in C(18):C(10)-PC. Using positive excitation (410 nm), the hindrance to the rotational motion is seen as a nonzero, asymptotic anisotropy at longer times.

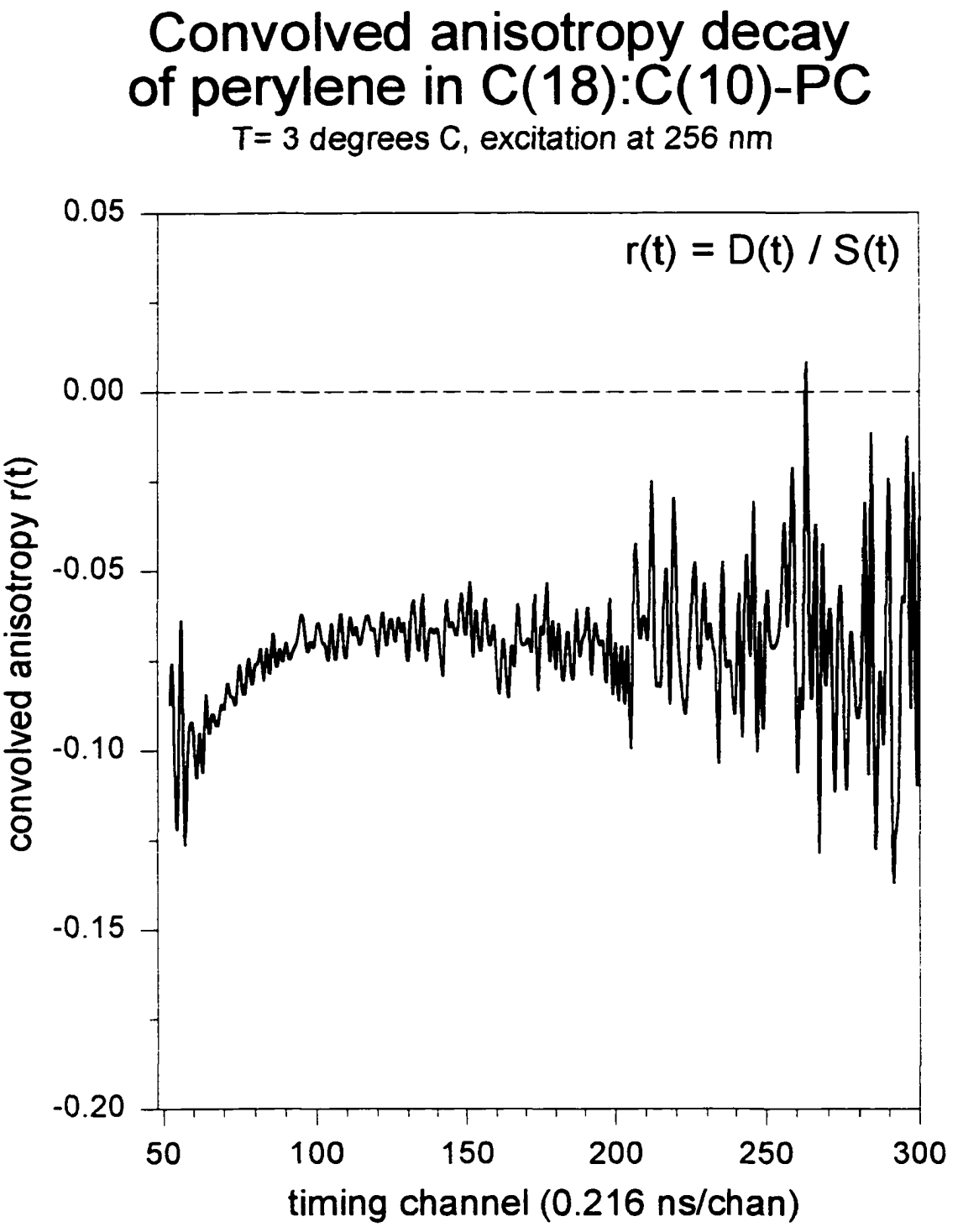

Figure 36. Convolved anisotropy decay of perylene in C(18):C(10)-PC. Using excitation at 256 nm, the hindrance to the rotational motion is seen as a negative, asymptotic anisotropy value at longer times.

Evaluation of Model 1 - 'Free-Beta' Model.

The β_1 terms using 410 nm excitation show a slight trend towards increasing values as the temperature is increased. At 3 degrees, the recovered $\beta_1(410)$ is near 0.12, and increases to approximately 0.23 at 30 degrees, which is above the phase transition. The $\beta_1(256)$ terms show a very slight decrease in their magnitudes as the temperature is increased. The rotational correlation time, φ_1, which corresponds to β_1, decreases smoothly as the temperature is increased. Physically, φ_1 corresponds to a combination of in-plane and out-of-plane rotational rates. At higher temperatures, the value for the rotational correlation time approaches 0.2 ns. This value is in accordance with results obtained by Lakowicz for a gel-phase phospholipid [28]. A value of 0.2 nanoseconds is probably below the time resolution of our current instrumentation, and the absolute magnitude probably cannot be extracted from these data. It is possible to deduce that the in-plane motion is extremely fast, anisotropic and partially hindered. The rationale for the partial hindrance argument becomes more apparent when the data are plotted as functions of anisotropy vs. time. Such plots follow in the next section.

The recovered β_2 terms are similar in magnitude for both excitation wavelengths, having values near 0.05. The value for this term appears somewhat lower at lower temperatures, but the error in the value is high, due to the high degree of correlation between the parameters, as well as their low magnitudes.

The second rotational correlation time, ϕ_2, representing the out-of-plane motions exclusively, decreases rapidly in the temperature range 0 to 10 degrees, and then remains

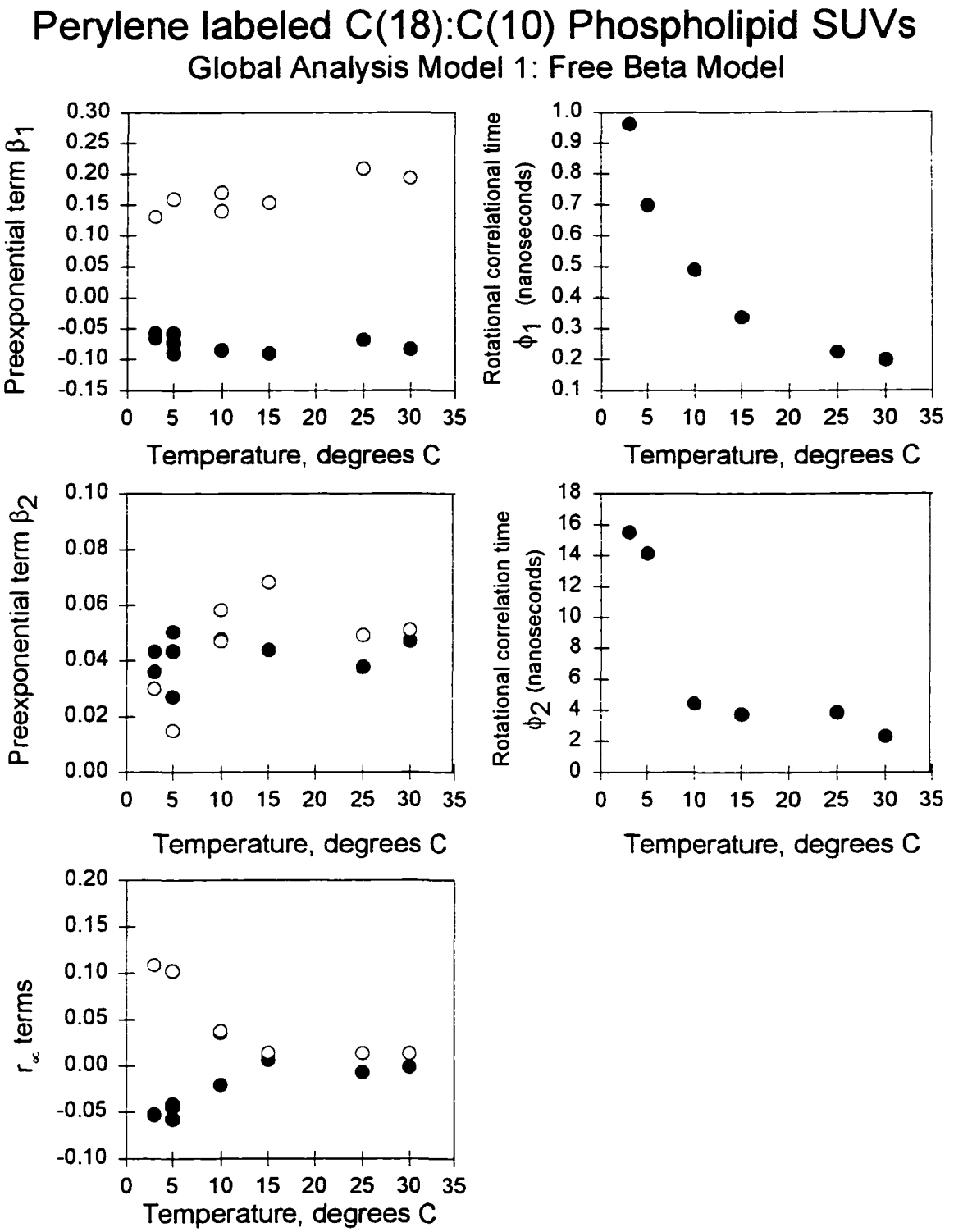

Figure 37. Global analysis of perylene in C18:C10-PC using Model 1 (Free Beta model). In this analysis, only the rotational correlation times were linked at each temperature. No other constraints were placed on the system.

relatively constant with further increases in temperature.

The hindered rotation (r_∞) terms, at both excitation wavelengths, reveal large restrictions below the phase transition temperature (19°C), and show the same trend as the second rotational correlation time.

Knowing that the photophysics of perylene allows linkage of preexponential terms in isotropic solvents [11,25,68] such as glycerol, we applied Model II - the 'Linked-Beta' Model - to the data sets.

Global Model II: the 'Linked-Beta' Model.

The preexponentials β_1(410 nm), β_1(256 nm), β_2(410 nm) and β_2(256 nm) are linked across constant excitation wavelength experiments in the global analysis. Each rotational correlation time was linked as a function of temperature, across multiple excitation wavelengths, i.e. $\phi = \phi(T)$ alone. As in Model I, this is justified since the rotational correlation times are functions of temperature and viscosity, independent of the excitation wavelength, fluorescence intensity and lifetime parameters.

As in the 'Free-Beta' Model, no constraints were placed on the hindrance (r_∞) terms describing the hindered rotational motion of the fluorophore. Figure 38 shows the results of the global fit using the 'Linked-Beta' Model. The global reduced chisquare was 1.29 for the analysis.

Evaluation of Model II - 'Linked-Beta' Model.

The 'Linked-Beta' Model, applied to the C(18):C(10)-PC data sets, was fitted

reasonably well on statistical grounds, as judged by a global reduced chisquare value of 1.29. However, the recovered values for the linked β terms, at both wavelengths, are different from those recovered from the perylene in glycerol system. Reviewing the data for perylene in glycerol at both excitation wavelengths, and comparing it to the asymmetric C(18):C(10)-PC data, reveals changes in the magnitudes and ratios of the preexponential terms. These results are presented in Table XI.

Table XI. Recovered values for 'linked' beta terms for perylene in glycerol and C(18):C(10) PC SUVs.

Solvent system	linked β_1 410	linked β_2 410	$\Sigma\beta_{410}$	β_1/β_2 410	linked β_1 256	linked β_2 256	$\Sigma\beta_{256}$	β_1/β_2 256
Glycerol	0.238	0.090	0.328	2.64	-0.241	0.090	-0.151	2.68
C(18):C(10)-PC	0.148	0.040	0.188	3.70	-0.069	0.052	-0.017	1.33

The lower magnitude of the preexponential terms is not due to an instrumental artifact or a mathematical normalization problem within the analysis program. Both of these concerns were eliminated, since the perylene in glycerol system had been measured on the same instrument, using the same analysis software, yielding correct results. A possible explanation involving a heterogeneous distribution of perylene within the bilayer may be considered for *symmetric* phospholipids such as DMPC. However, since the acyl chains of the asymmetric phospholipid are known to interdigitate below the phase transition, the possibility of multiple partitioning regions has been eliminated.

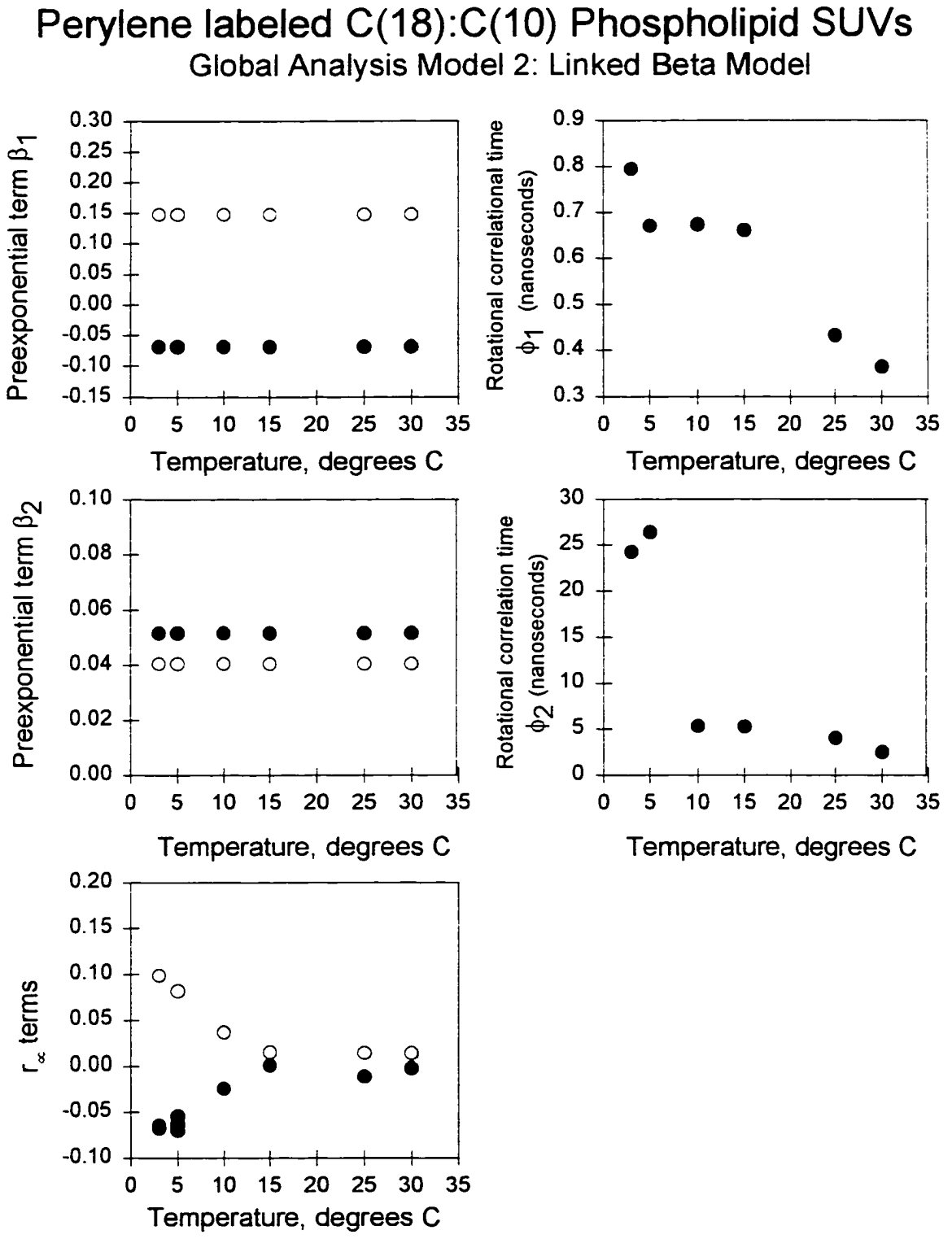

Figure 38. Global fitting of C(18):C(10)-PC using the 'Linked-Beta' Model. Notice the magnitudes of the recovered linked β terms are lower than those recovered in the isotropic glycerol system, for both excitation wavelengths.

Using the recovered rotational correlation times, the in-plane and out-of-plane rotational rates were calculated. Figure 39 shows a plot of these rotational rates, as well as the ratio between them, R_{ip}/R_{op}. For isotropic glycerol, this ratio is approximately 10:1 over the range from 10°- 40°C [11,25]. We had measured similar values for perylene in glycerol using the instrumentation described in this Thesis (Figure 30). In the C(18):C(10)-PC bilayer, we observe this ratio to be approximately 80:1 at 0°C, decreasing sharply to 12:1 at 10°C. Above this temperature, the ratio remains reasonably constant, and closer to the isotropic value of 10:1. For this ratio to decrease, either the rate of in-plane rotation is decreasing, or the out-of-plane rate is increasing. Since the temperature is being increased, a reduction of the in-plane rate does not seem likely.

Referring to the steady-state emission anisotropy (Figure 31), we see that the out-of-plane motion, observed using 315 nm excitation, remains nearly constant. These results appear to conflict with the time-resolved measurements over the same temperature range, which indicate that the rotational correlation time associated with the out-of-plane motion is changing with temperature.

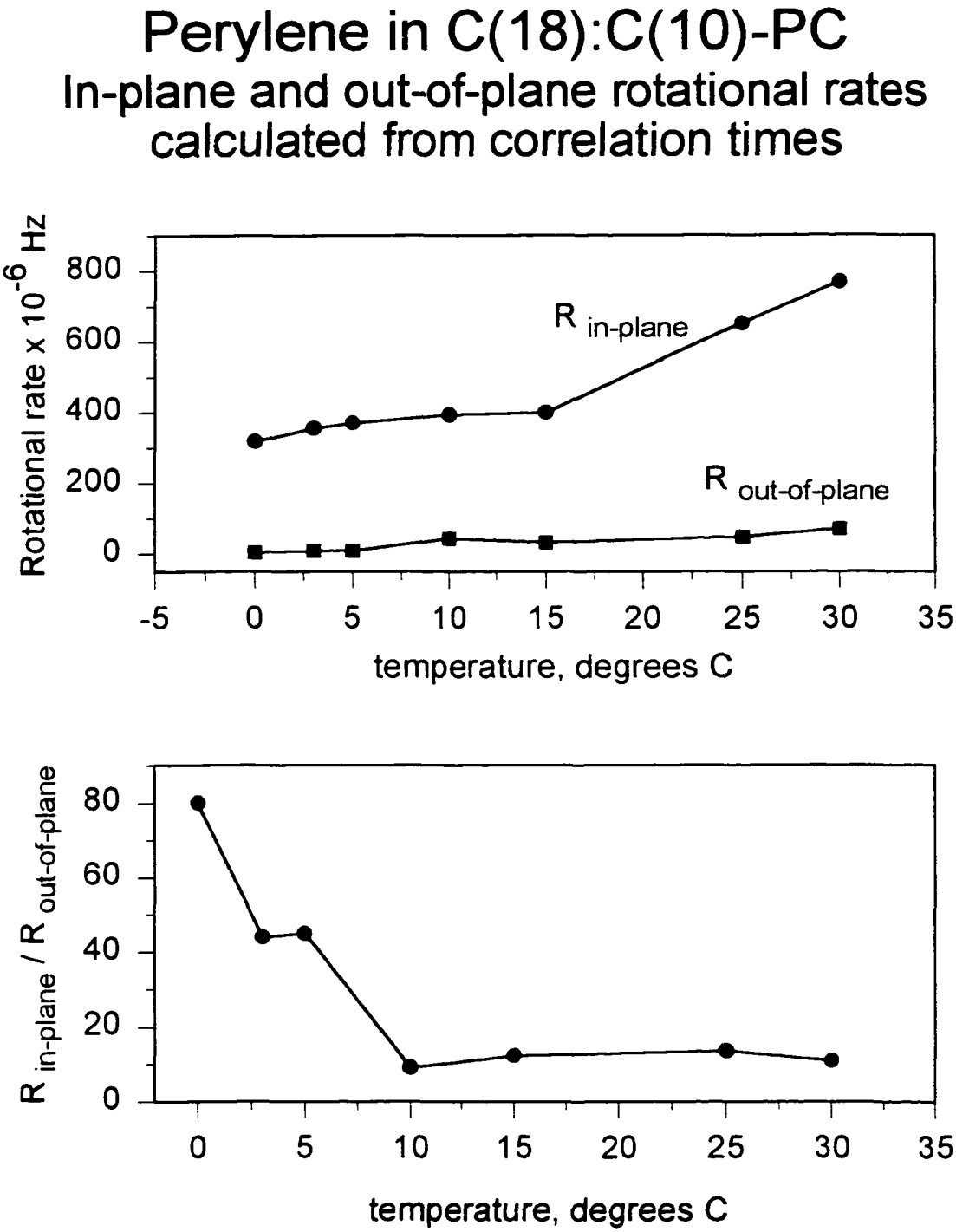

Figure 39. Rotational rates of perylene in the asymmetric phospholipid C(18):C(10)-PC as a function of temperature. Notice that the rotational rates of perylene in the asymmetric phospholipid do not show a nearly constant ratio of $D_{\|}$ to $D_{\perp}$ (see also Figure 30).

VI.b.2. System 2 - Symmetric DMPC: C(14):C(14)-PC SUVs.

DMPC is a symmetric, C(14):C(14) phospholipid. It is commercially available. When labeled with perylene, the possibility of heterogeneity of probe location within the DMPC bilayer exists. Perylene can possibly align itself along the acyl chains, or locate itself between the bilayer leaflets. Most likely, a combination of both can be expected. The anisotropic rotations of perylene would be different in these regions, resulting in an even more complex decay than the asymmetric phospholipid system. By comparing results of the symmetric vs. asymmetric phospholipid systems, we wish to evaluate the extent of probe heterogeneity and partitioning within the bilayer.

As with the asymmetric phospholipid, steady-state and time-resolved emission anisotropy data were collected using multiple excitation wavelengths and temperatures. The same approach to data collection and analysis was used for DMPC as for the asymmetric C(18):C(10)-PC, so the results will be stated here without further elaboration.

VI.b.2.1. Steady-state emission anisotropy.

Steady-state emission anisotropy measurements using three excitation wavelengths are shown in Figure 40. Excitation using 410 nm shows a gradual decrease in the emission anisotropy, reaching a minimum value near 25°C. Above this temperature, the emission anisotropy remains fairly constant at approximately 0.03, indicating that there is some persistent hindrance to rotation.

Excitation with 256 nm light shows an anisotropy that is initially negative, crossing through zero near 18 °C, and continuing with a positive slope until approximately 25 °C.

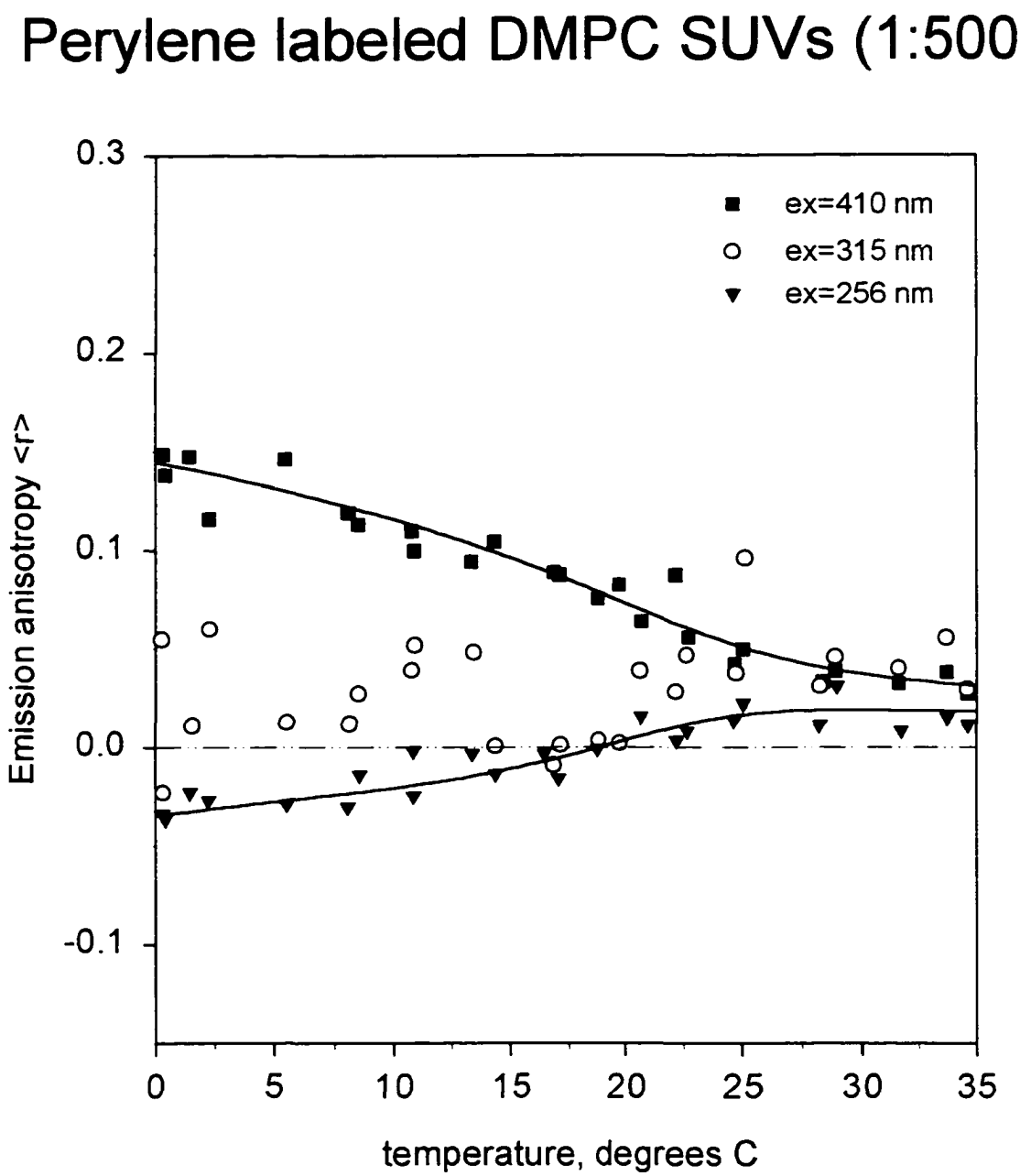

Figure 40. Steady state emission anisotropy of perylene in DMPC SUVs, as functions of excitation wavelength and temperature. Excitation using 315 nm, selective for out-of-plane rotations of perylene, reveals little change with temperature. The 410 nm and 256 nm profiles elicit different combinations of in-plane and out-of-plane rotations.

Above 25 °C, the anisotropy becomes asymptotic at approximately 0.02. As with the asymmetric C(18):C(10)-PC phospholipid in the last section, the origin(s) of the restricted motion(s) cannot be assigned uniquely using only the steady-state data .

When 315 nm excitation is used, the emission anisotropy of perylene in DMPC appears fairly constant with temperature. The data show significant scatter, because the absorption of perylene is near a minimum at 315 nm. Recall that the wavelength at which r_0 equals 0.1 (315 nm for perylene) allows out-of-plane rotations to be observed exclusively. The significance of this observation is that the out-of-plane motion of perylene within the phospholipid bilayer is relatively unchanged as the phase transition is reached. The implication is that the out-of-plane rotational motion of perylene is not greatly affected, as the phospholipid bilayer undergoes a phase transition. As observed with C(18):C(10)-PC, the *in-plane* motion of the probe appears to be more sensitive to the local phospholipid environment.

VI.b.2.2. Time-Resolved Emission Anisotropy.

Single curve analysis of the time-resolved emission anisotropy decays of perylene in DMPC revealed two rotational correlation times and a residual anisotropy (r_∞) term. Global analysis of the data was performed as described above. The fluorescence lifetime was fitted using double- and triple-exponential decay laws, and the average lifetimes of perylene in DMPC are presented in Table XII. A small decrease in the fluorescence lifetimes was observed with increasing temperature.

Table XII. Average Fluorescence Lifetimes of Perylene in DMPC
<τ> values were calculated using Equation 41.
Errors are standard deviations of 3 or more determinations at each temperature.

Temperature	Average Fluorescence Lifetime, <τ>
5 °C	7.40 +/- 0.99 ns
10 °C	6.93 +/- 0.40 ns
15 °C	6.74 +/- 0.23 ns
20 °C	6.81 +/- 0.29 ns
25 °C	6.37 +/- 0.02 ns
30 °C	6.20 +/- 0.02 ns

As with the asymmetric C(18):C(10)-PC phospholipid, different models were applied to the data.

Global Model I: 'Free-Beta' Model.

The logic of the 'Free-Beta' Model was applied to 19 experiments in which DMPC was used as the phospholipid. Recall that, in the 'Free-Beta' Model, the rotational correlation times are linked along isotherms. All other parameters are free in the global analysis.

The preexponential terms for both excitation wavelengths behave similar to those of the C(18):C(10)-PC system. This is expected, since the same excitation and emission wavelengths were used. Interpretation of the rotational correlation times is more complex in this system. The phase transition of DMPC occurs at 23.8°C, but the anisotropy decay results indicate local environment changes at temperatures well below this. Comparison of the r_∞ terms, at low temperatures, for DMPC and the asymmetric C(18):C(10)-PC bilayer

systems shows lower values for the DMPC system. Possible interpretations include partitioning of perylene between the bilayer leaflets, where the acyl chains are less ordered. The differences in the rotational correlation time profiles between the two phospholipid systems may indicate an even more complex decay

.Global Model II: 'Linked-Beta' Model applied to DMPC/Perylene.

Recall that the 'Linked-Beta' Model links the preexponentials β_1(410 nm), β_1(256 nm), β_2(410 nm) and β_2(256 nm) at constant excitation wavelengths, and the rotational correlation times along isotherms, i.e. $\phi = \phi(T)$. No constraints were placed on the hindrance (r_∞) terms describing the hindered rotational motion of the fluorophore. Figure 42 shows the results of the global fit of perylene in DMPC using the 'Linked-Beta' Model. The global reduced chisquare was 1.31.

Evaluation of Model II - 'Linked-Beta' Model.

The 'Linked-Beta' Model provided a good fit to the perylene in DMPC data, as judged by a global reduced chisquare value of 1.31. Even with satisfactory fitting statistics, the 'Linked-Beta' Model does not appear to provide a complete description of the rotational behavior of perylene in the phospholipid, for the following two reasons:

a) The recovered values for the linked β terms at both wavelengths are too low in magnitude, compared with perylene in glycerol.

b) The sum of the preexponentials and the hindered component do not add to a

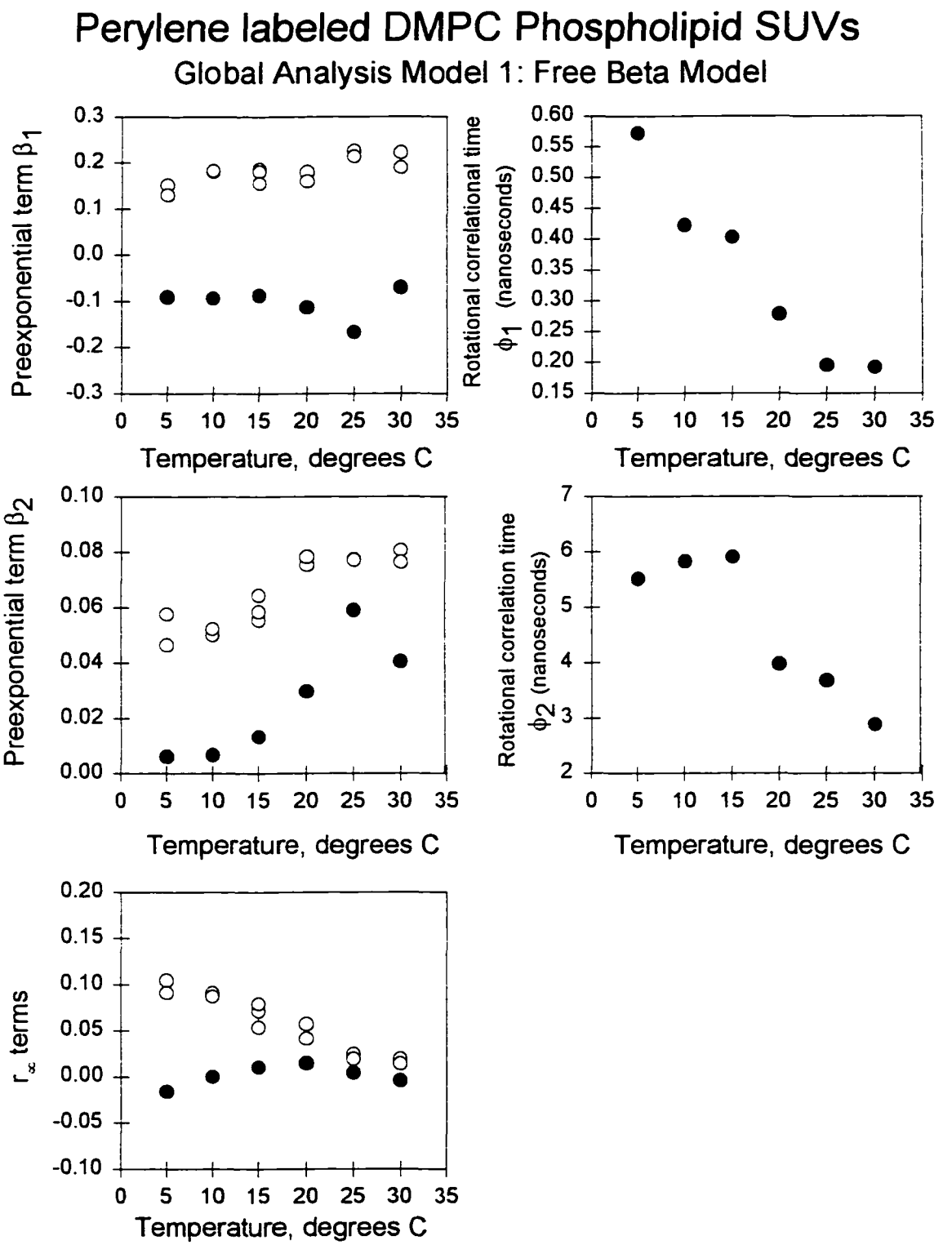

Figure 41. Global analysis of the DMPC/perylene system. The 'Free-Beta Model' was used, linking only the rotational correlation times at each temperature.

constant value at each temperature. This sum should equal the limiting anisotropy for the excitation wavelength used. This is not the case for the phospholipid systems, until the hindrance term becomes zero. Only then will the sum of the two remaining preexponentials equal a constant, but its magnitude will still be too low, since the 'Linked-Beta' model recovers preexponentials too low in magnitude.

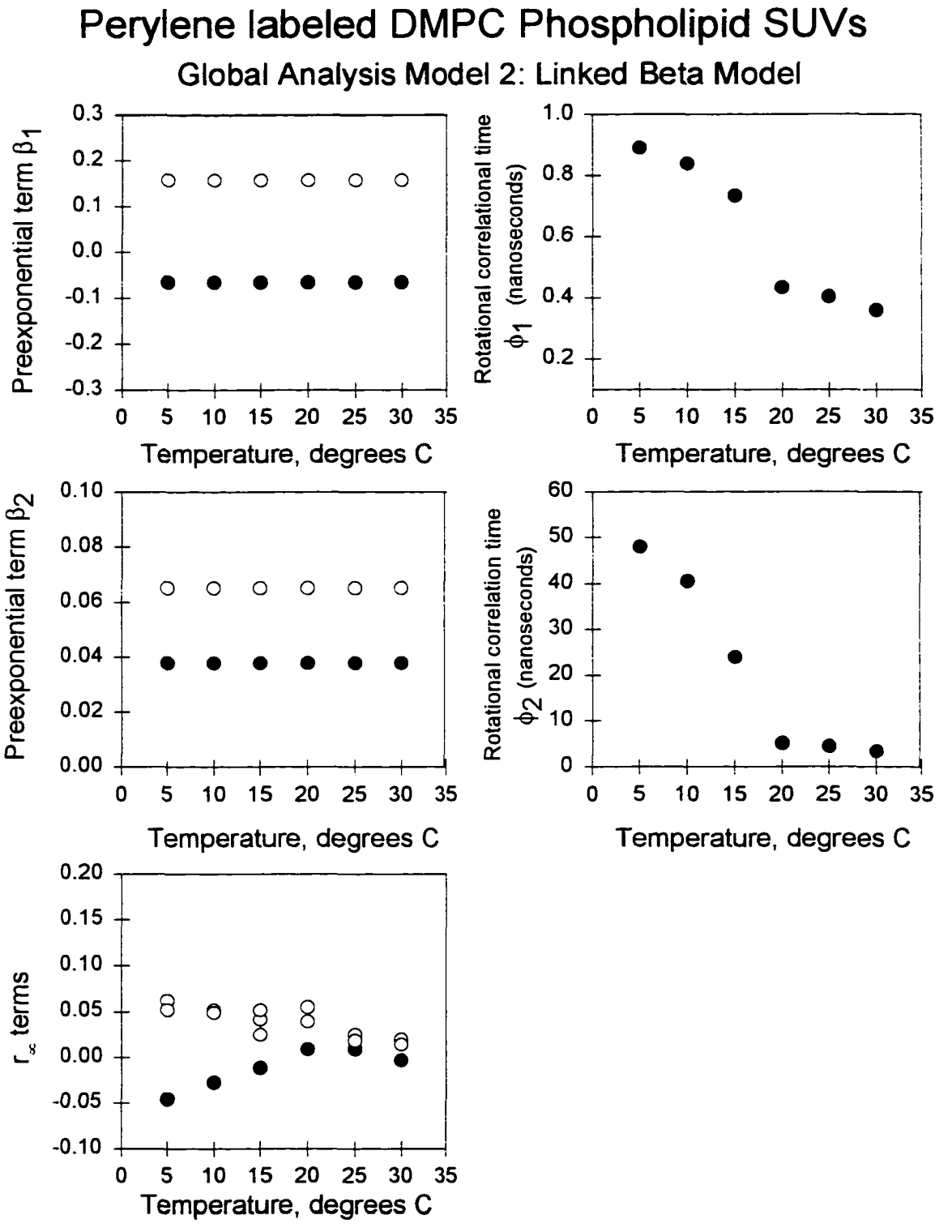

Figure 42. Global analysis of DMPC in perylene using the 'Linked-Beta' Model. In the DMPC phospholipid, the 'Linked-Beta' Model recovers preexponential terms (β_1 and β_2) that are too low, compared with the results obtained for perylene in glycerol.

Section VII. Rationale for a Temperature Dependent Beta Model.

The general expression for anisotropy decay with a hindered motion (Equation 24) expresses the hindrance as a constant term. However, the values for r_∞ we recovered from the global analysis of perylene embedded in phospholipid bilayers are strongly dependent on temperature. These r_∞ values decrease in magnitude as the temperature is increased, tending to zero near the phase transition temperature of the phospholipid. Comparing the results of global analysis of perylene in glycerol and the phospholipid bilayer systems shows some discrepancies in the preexponential terms and rotational correlation times that are not easily rationalized.

What the asymmetric C(18):C(10)-PC and the symmetric DMPC phospholipid systems have in common, differing from the isotropic glycerol solvent system, is that they are *anisotropic solvent environments*, with nonzero r_∞ terms below their respective phase transitions.

Neither of the two models discussed so far (the 'Free-Beta' and 'Linked-Beta' Models) properly account for the temperature dependence of the r_∞ terms, and its effect on the other preexponential terms. This observation is not expected on purely photophysical grounds.

For *anisotropic, hindered rotations in anisotropic environments*, we need to propose a more detailed model. In the following section, expressions which can account for temperature dependent preexponentials will be derived. The values obtained for these modified preexponentials will be fixed in a global analysis of the same data sets to which the previous two models have been applied, to reevaluate the magnitude of the rotational

correlation times as functions of temperature.

The temperature difference between the experimental temperature (T_{exp}) and the lipid phase transition temperature (T_c) can be used as an independent variable to quantitate the value of r_∞ expected at a certain temperature, for a given phospholipid. Denoting this temperature difference (T*) as:

$$T^* = T_{exp} - T_c \tag{59}$$

we can rewrite the expression for the decay of r(t) (Equation 24), making the r_∞ a temperature dependent function:

$$r(t,T^*) = (r_0 - r_\infty(T^*)) \sum_i \beta_i e^{\frac{-t}{\varphi_i(T^*)}} + r_\infty(T^*) \tag{60}$$

This expression is valid for a given wavelength of excitation, since variation of the excitation wavelength may alter r_0. Rewriting Equation 60 to emphasize this wavelength dependence gives:

$$r(t,T^*,\lambda_{ex}) = (r_0(\lambda_{ex}) - r_\infty(T^*,\lambda_{ex})) \sum_i \beta_i(\lambda_{ex}) e^{\frac{t}{\varphi_i(T^*)}} + r_\infty(T^*,\lambda_{ex}) \tag{61}$$

The effect of r_∞ should decrease as the lipid approaches the transition temperature, and, in the high temperature limit, r_∞ should tend to zero as the solvent system becomes isotropic.

Equation 61 implies that, for an *anisotropic* medium such as a phospholipid bilayer below the phase transition, the anisotropy decay range is reduced from that of an equivalent

fluorophore rotating in an *isotropic* solvent system. An unhindered fluorophore can show an anisotropy decay from r_0 to zero. The same fluorophore, in a hindered environment, can decay only from r_0 to r_∞, which will be less than the range of the isotropic solvent system.

For an *isotropic* solvent system:

$$r_\infty = 0 \quad \textit{Isotropic Solvent System} \tag{62}$$

and temperature will not affect the recovered values of the preexponential terms, since there is no hindrance to rotation. Previously, theoretical discussions of temperature dependent preexponentials have been published in the literature, but these temperature dependencies were not due to contributions of hindered rotation [26]. Rather, the temperature dependence is a result of librational motions (low frequency torsional motions).

In summary, comparing the equations of unhindered and hindered motion:

$$\sum_i \beta_i = \beta_1(\lambda_{ex}) + \beta_2(\lambda_{ex}) = r_0 \quad \textit{Unhindered} \tag{63}$$

and

$$\sum_i \beta_i = \beta_1(\lambda_{ex},T) + \beta_2(\lambda_{ex},T) + r_\infty(T) = r_0 \quad \textit{Hindered} \tag{64}$$

it is apparent that one, or both, of the recovered β_i must be temperature dependent when hindrance to rotational motion is present. Since the r_∞ terms are temperature dependent, the sum of the remaining two β terms must equal the difference between r_0 and r_∞ at a given temperature.

VII.a. Preexponentials as Functions of Wavelength and Hindered Motion.

Equation 64, at first appearance, may seem to violate the photophysics of the perylene molecule. After all, the molecular energy levels are not affected by possible hindrance to rotation, so why should the preexponential terms that describe the oscillator directions be affected by these hindered motions? We know that the magnitude of the fundamental anisotropy depends on photoselection and the angle between the molecular dipoles, and that this fundamental anisotropy is the sum of preexponential terms defined above. There are cases in which the magnitude of the preexponential terms can be made to vary, while maintaining the correct sum, and therefore not violating the fundamental photophysics of the molecule.

Brand, *et al.* [16] have defined an expression for depolarization of an ellipsoidal rotator in an *isotropic* solvent, which alters the preexponential terms (β_i) as functions of the excitation wavelength. The model assumed that the molecule has both its absorption and emission dipoles perpendicular to the symmetry axis (as does perylene). Their expression is:

$$r(t) = 0.3\ (2f - 1)\ e^{-(4D_{\parallel} \cdot 2D_{\perp})\,t} + 0.1\ e^{-6D_{\perp}t} \qquad (65)$$

in which the f parameter represents the fractional $S_0 \rightarrow S_1$ absorption.

When $f=1$, the quantity

$$\beta_1 = 0.3 * (2(1)-1) = +0.3 \qquad (66)$$

corresponds to a transition which is fully $S_0 \rightarrow S_1$.

When $f = 0$, the quantity

$$\beta_1 = 0.3 * (2(0)-1) = -0.3 \quad (67)$$

corresponding to complete S_0-S_2 absorption.

It is possible to mix the two transitions, so that equal contributions of collinear and orthogonal dipoles are involved. This may be simulated by setting $f = 0.5$:

$$\beta_1 = 0.3 * (2(0.5)-1) = 0.0 \quad (68)$$

causing the first preexponential term to vanish. For perylene, this simulates an excitation wavelength of 315 nm, which has an r_0 value of +0.1, corresponding to the out-of-plane contribution to the rotational motions. Brand, *et al.* used these equations to describe the changes in the preexponential terms which would occur if the angle between absorption and emission dipoles (experimentally, the excitation wavelength) was varied. Using Equation 65, simulation of the effects of changing the in-plane and out-of-plane motions of disklike molecules at various excitation wavelengths is possible, by setting different values for D and $D_\perp$, and varying the f term from 0 to 1.

The expression of Brand, *et al.* does not allow for the simulation of hindered motion in its current form. There is no term describing the relationship between the preexponentials when an r_∞ term is present, as would be observed when angular barriers to rotation are present. By simulating cases when φ_2 is infinite, Brand, *et al.* were able to view the shapes of anisotropy decay curves including totally hindered out-of-plane motion, without explicitly

defining an r_∞ term. In those simulations, the magnitudes of the preexponentials were determined by using different values of *f* in Equation 65.

Changes in preexponential terms as rotational motions become hindered have been derived by Wahl for a *sphere* (isotropic rotor) of revolution spinning on one axis and experiencing angular barriers to rotation along the other axis [20]. In Wahl's simulation, angular barriers to rotation caused the magnitude of the preexponential terms to vary, *yet the sum of the preexponential terms and the r_∞ (hindrance) remained constant.*

We need an expression that accounts for changes in the value for r_∞ as a function of temperature as well as the excitation wavelength. The r_∞ term, which reflects the extent of hindered rotation, is a function of the physical state of the phospholipid bilayer at a given temperature and excitation wavelength. At low temperatures, the phospholipid bilayer presents an anisotropic solvent which will cause restricted motions in the in-plane and/or out-of-plane rotations of perylene. The resolution of the relative amount of in-plane and out-of-plane hindrances in the phospholipid bilayers is a difficult problem, partly due to the fact that we can only directly observe a net hindered rotation term r_∞, which is the sum of the r_∞(in-plane) and r_∞(out-of-plane). At higher temperatures, the phospholipid bilayer undergoes a phase transition, and becomes less of an anisotropic solvent environment. At sufficiently high temperatures, the phospholipid bilayer loses its anisotropic nature, and the probe order parameter $(r_\infty / r_0)^{1/2} \rightarrow 0$. Under these conditions, embedded dye molecules such as perylene will rotate as if they were in a nearly isotropic solvent.

Our new model must correctly recover a temperature dependent set of betas, without violating the photophysics of the molecule. The sum of the recovered preexponential terms

at any temperature and excitation wavelength must add to the expected r_0. Starting with Equation 64, we can write an equation that accounts for changes in the beta terms at a given excitation wavelength:

$$p(T^*)\beta_1(\lambda_{ex}) + q(T^*)\beta_2(\lambda_{ex}) + r_\infty(\lambda_{ex}, T^*) = r_0 \quad \textbf{(69)}$$

in which p(T*) and q(T*) will be temperature dependent functions describing the different effect of temperature and hindered rotation on the preexponential terms. Equation 69 is true for all cases, isotropic and anisotropic. It is a general equation which holds for lipids with T_c as well as those that are fluid. An example of a fluid phospholipid is DOPC [15]. The p(T*) and q(T*) expressions should have no effect at high temperatures (significantly above the phase transition for the phospholipid under investigation):

$$p(T^*) \rightarrow 1 \quad (T^* \rightarrow 0) \quad \textbf{(70)}$$

$$q(T^*) \rightarrow 1 \quad (T^* \rightarrow 0) \quad \textbf{(71)}$$

$$r_\infty(T^*) \rightarrow 0 \quad (T \gg T_c) \quad \textbf{(72)}$$

reducing Equation 69 to the isotropic case (Equation 63).

To form a function for the temperature dependence of the preexponentials, the following strategy was used. We have two excitation wavelengths, namely 410 nm and 256 nm. These different excitation wavelengths affect the magnitude of β_1, β_2 and r_∞ at each

wavelength. Each excitation wavelength will have its own set of (β_1, β_2, r_∞) as functions of temperature, such that their sum is r_0. Substituting each of the two excitation wavelengths into Equation 69 shows that six temperature dependent curves will be formed for each anisotropic solvent system.

Beginning with the r_∞ terms obtained from the Free Beta Model, the r_∞ terms at each excitation wavelength were fitted as functions of temperature. Initial r_∞ values were taken from the 'Free-Beta' Model because they were independently obtained, with no constraints on the magnitude of any other preexponential term. The results are summarized at the end of this section.

Fitting of the r_∞ (410 nm) as a function of temperature.

The r_∞ (410) data were fitted as a function of temperature, using a function of the form:

$$r_\infty (410nm, T) = ae^{-bT} \quad (73)$$

This function was chosen because it has the characteristic of vanishing at high values of T, and has no physical significance. Such behavior is physically consistent with the r_∞ term disappearing as a phospholipid bilayer undergoes a melting transition. Using a curve fitting routine in Jandel SigmaPlot, the parameters that described the exponential decrease (Equation 73) of the r_∞ term were determined.

Using another SigmaPlot transform, the difference curve

$$r_0(410nm) - r_x(410nm,T) \quad (74)$$

was formed. The value of r_0(410 nm) was taken from the literature. This difference curve equals the sum of the preexponentials β_1 and β_2 at each temperature:

$$r_0(410nm) - r_x(410nm,T) = \beta_1(410nm,T) + \beta_2(410nm,T) \quad (75)$$

At high temperatures, beyond the phospholipid T_c, the r_∞ term vanishes. Equation 75 then reduces to Equation 63, reflecting isotropic solvent behavior.

Fitting of r_∞(256 nm) as a function of temperature.

A similar procedure was performed using the 256 nm excitation data. For this negative anisotropy band, a rising exponential of the form

$$r_x(256nm,T) = a * (1 - e^{-bT}) + c \quad (76)$$

was chosen for the fitting function. Using Jandel SigmaPlot, the three fitting parameters were obtained, forming the temperature dependence of r_∞ using 256 nm excitation. Taking the value of r_0 at 256 nm from the literature, the difference curve

$$r_0(256nm) - r_x(256nm,T) \quad (77)$$

was formed, representing the sum of the preexponentials as a function of temperature:

$$r_0(256nm) - r_\infty(256nm,T) = \beta_1(256nm,T) + \beta_2(256nm,T) \quad (78)$$

The fitted r_∞ curves for the asymmetric C(18):C(10)-PC are presented in Figures 43 and 44. For the symmetric DMPC system, the results appear in Figures 45 and 46.

The parameters that describe the exponential functions are presented in Table XIII:

Table XIII. Parameters describing fitted r_∞ terms as functions of temperature.

Phospholipid System	Parameter		
C(18):C(10)-PC	*a*	*b*	*c*
410 nm: $r_\infty(T) = a\, e^{-b\,T}$	+0.1766	+0.1401	not used
256 nm: $r_\infty(T) = a\,(1 - e^{-b\,T}) + c$	+0.0963	+0.1693	-0.0961
DMPC	*a*	*b*	*c*
410 nm: $r_\infty(T) = a\, e^{-b\,T}$	+0.1426	+0.0587	not used
256 nm: $r_\infty(T) = a\,(1 - e^{-b\,T}) + c$	+0.1532	+0.3988	-0.1484

Below the phase transition, the difference curve represents the total amount of hindered motion in the system, which arises from contributions from both in-plane and out-of-plane restrictions:

$$r_\infty(T,\lambda_{ex}) = r_{\infty,\ in\text{-}plane}(T,\lambda_{ex}) + r_{\infty,\ out\text{-}of\text{-}plane}(T,\lambda_{ex}) \quad (79)$$

This is easy to visualize, by considering the reduction of the equation when $r_\infty(T,\lambda_{ex})$ vanishes. Then, the expression reduces to zero difference, or zero hindered motion.

If one of the values representing the individual components of the in-plane and out-

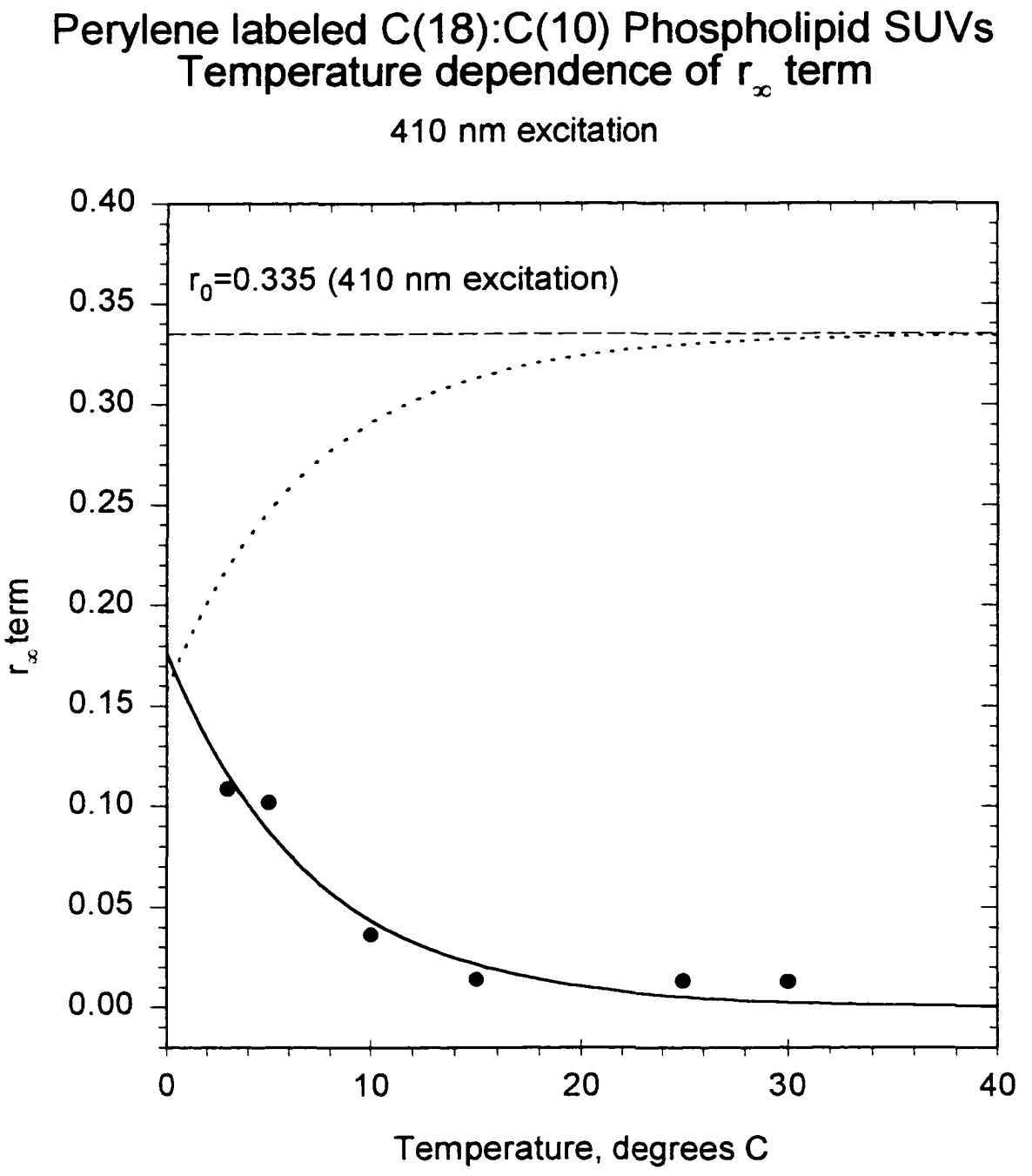

Figure 43. For the asymmetric C(18):C(10)-PC system, the temperature dependence of r_∞ (using 410 nm excitation) was fitted to an exponentially decreasing function. The upper curve represents the difference between the limiting anisotropy (r_0) and the temperature dependent r_∞ curve. At high temperature, the curvature vanishes, as the system changes from a hindered, anisotropic system to an unhindered, isotropic system.

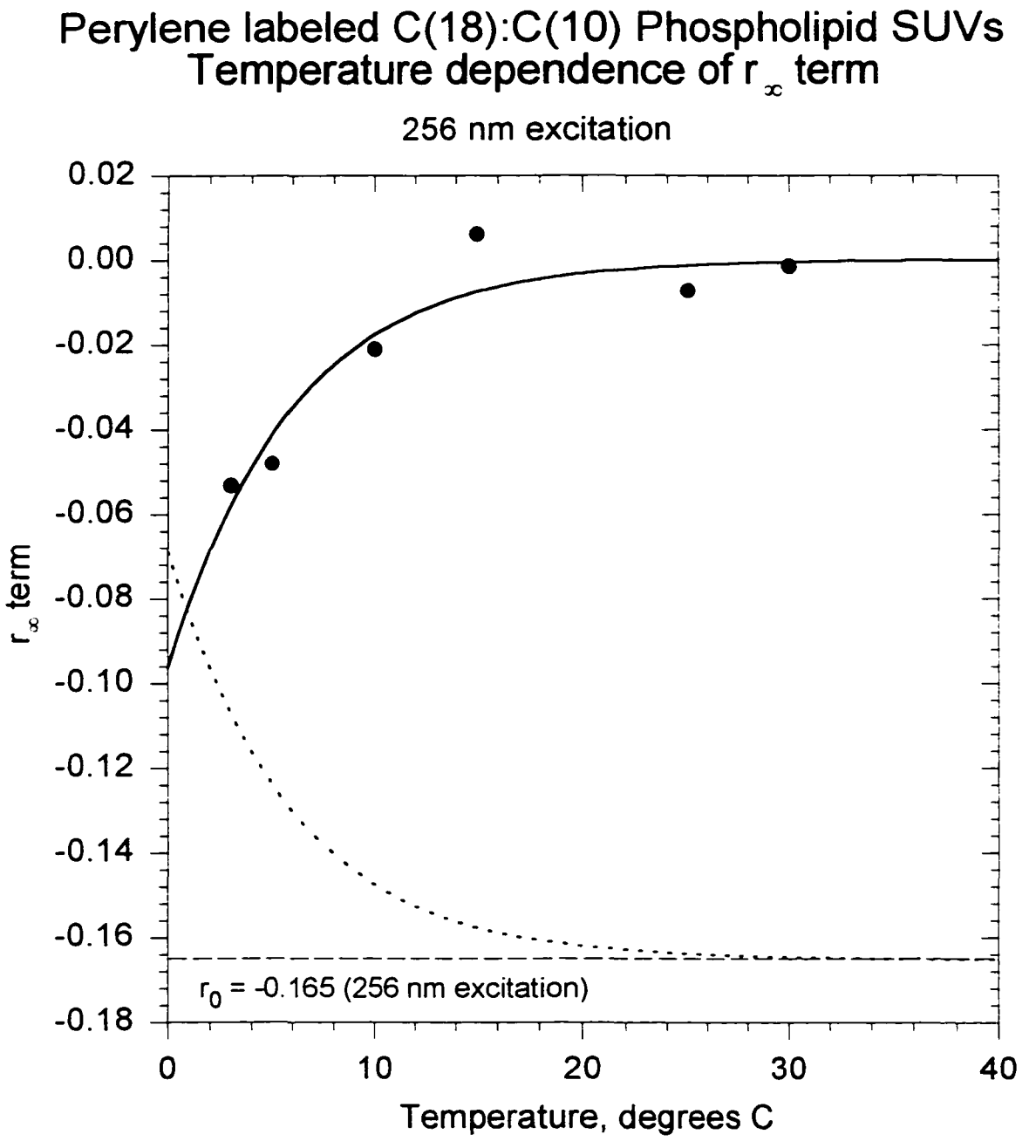

Figure 44. Temperature dependence of r_∞, using 256 nm excitation, asymmetric C(18):C(10)-PC system. The curve was fitted to a rising exponential. The difference between the limiting anisotropy (r_0) and the hindered (r_∞) term shows the predicted value of $\beta_1 + \beta_2$ at 256 nm. Notice that the temperature dependence vanishes at high temperature, at which point $\beta_1 + \beta_2 = r_0$.

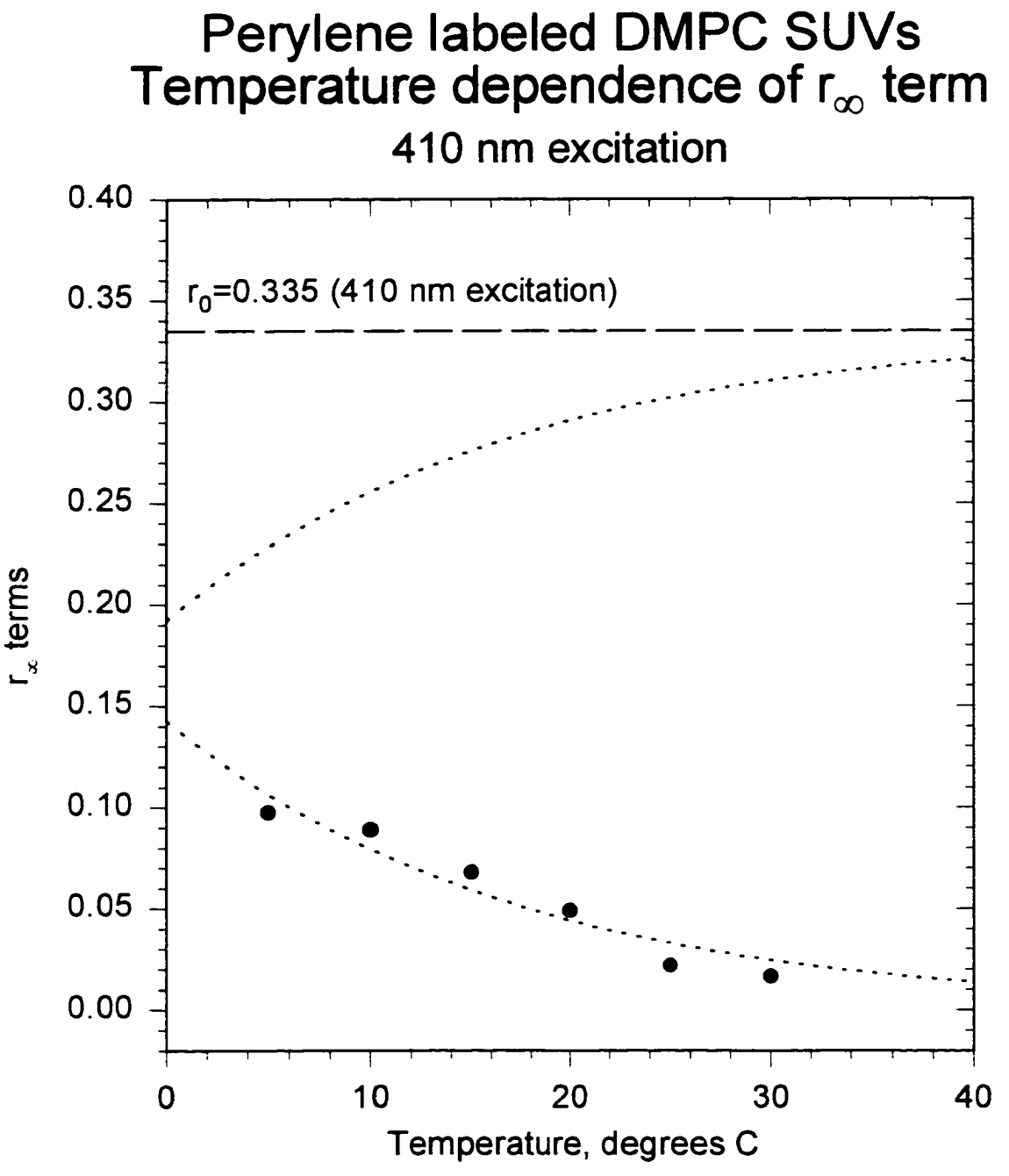

Figure 45. For the symmetric DMPC system, the temperature dependence of r_∞ (using 410 nm excitation) was fitted to an exponentially decreasing function. The expected exponential behavior is not as obvious as in the C(18):C(10)-PC asymmetric lipid. Interpretations include heterogeneous distribution of perylene within the bilayer.

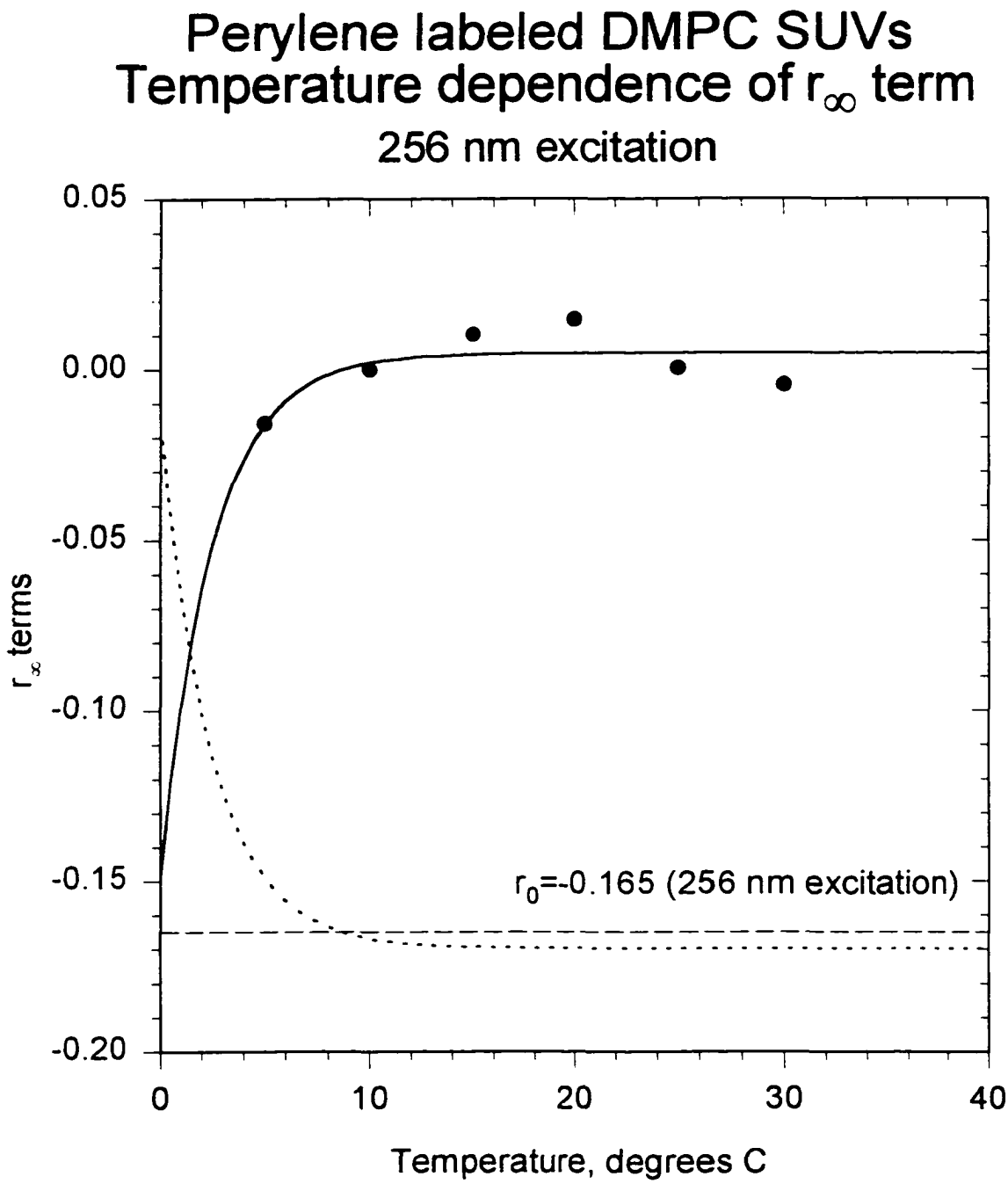

Figure 46. Symmetric DMPC system. The temperature dependence of r_∞ (using 256 nm excitation), fitted to an exponentially increasing function.

of-plane restriction were known, the contributions of the preexponential terms would be known uniquely. Recall that β_1 involves both in-plane and out-of-plane contributions, while β_2 is sensitive to the out-of-plane motion only. If the out-of-plane motion was the only contributor, then $r_\infty = r_{\infty,\text{ out-of-plane}}$, and the difference

$$(0.1 - r_{\infty,out-of-plane}) = \beta_{out-of-plane} \quad \textbf{(80)}$$

would be uniquely known. Molecules such as coronene that have a high symmetry (D_{6h}), have in-plane motions averaged, and measurements of the TREA are sensitive only to out-of-plane motions. For perylene, it is possible to select an excitation wavelength (chosen so that $r_0 = 0.1$) which causes the absorption oscillators to be averaged, therefore averaging the in-plane motions. This occurs at 315 nm excitation in perylene. The experiment would be impractical due to the relatively low absorbance of perylene at 315 nm. With the 256nm and 410 nm excitation wavelengths, we have data which contains different combinations of in-plane and out-of-plane contributions of hindered motion.

The strategy is now, having a curve which represents the *sum* of the preexponentials β_1 and β_2, as functions of temperature, obtain the *unique* solution for $\beta_1(T)$ and $\beta_2(T)$. To do this, we need to separate the total hindered motion into its in-plane and out-of-plane components. Once either term is known, the last one may be determined by difference.

VII.b. Separation of the Components of Hindered Anisotropic Rotation.

The measured r_∞ terms, using either excitation wavelength, are combinations of two hindered motions reflecting the in-plane hindrance, $r_{\infty,\text{in-plane}}$ and the out-of-plane

hindrance, $r_{\infty,\text{out-of-plane}}$. We need to separate each component of the hindered motion, to facilitate the solution of the corresponding preexponential terms which are affected by these hindrance terms. Experimentally, we have data at each temperature, using two excitation wavelengths, thus overdetermining the system. The problem we need to solve involves two unknowns, namely the in-plane and out-of-plane restrictions.

VII.b.1. Theoretical treatments by previous workers.

The separation may be achieved by closer examination of the anisotropy decay functions, viewed as functions of time. Mathematical simulations of anisotropy decay functions performed by Wahl [20] involved an idealized system in which the rotational axis is perpendicular to the plane of the transition dipoles. Wahl's simulation showed that, for such a system, the average value of the anisotropy decay at long times (r_∞) converged to a constant value of 0.1, when rotation was allowed for a full 360 degrees (no angular restriction to the rotation). This simulation is equivalent to fully free in-plane motion and totally hindered out-of-plane motion of perylene, since rotation was only allowed about the axis perpendicular to the transition dipoles. Since both the absorption and emission dipoles of perylene lie in the molecular plane, rotation about an axis perpendicular to this plane indicates an in-plane, or spinning, motion.

Brand, *et al.* have simulated the time course of anisotropy of a disklike fluorophore, rotating in an anisotropic fashion. In these simulations, two rotational correlation times were used to describe the anisotropic motions, and these correlation times were individually varied to assess the effects on the shapes of the anisotropy decay curves. Both positive and

negative anisotropy decay curves were simulated for a disklike fluorophore. The results of Brand, *et al.* demonstrate that the effects of differing in-plane rotational rates should be clearly distinguishable from changes in the out-of-plane rotational rates. An important observation is that the average value of the positive and negative anisotropy decay curves contains information about the out-of-plane rotational rate. If the out-of-plane rotational rate is held constant, and the in-plane rate is varied, the average of the positive and negative curves always gives the same value at later times.

VII.b.2. Computer simulation of anisotropy decay curves.

Following Brand, *et al.* a series of curves were simulated with rotational correlation times similar to those observed for perylene in the asymmetric C(18):C(10)-PC system. Both free and hindered motions were simulated, to see the effects on the anisotropy decay curves (r(t)), using positive and negative excitation anisotropy decays.

To simulate the curves, a FORTRAN program was written to calculate values for the expression for the decay of fluorescence emission anisotropy:

$$r(t) = \beta_1 e^{-\frac{t}{\varphi_1}} + \beta_2 e^{-\frac{t}{\varphi_2}} \qquad \textbf{(81)}$$

In the first series of simulations, the value of ϕ_2, representing the out-of-plane motion of perylene, was left constant at 10.0 ns, while the value of ϕ_1, representing a combination of the in-plane and out-of-plane rotational rates, was varied from 0.4 ns to 1.0 ns. These correlation time ranges are easily observed with perylene ($\tau_F \sim 5$ ns).

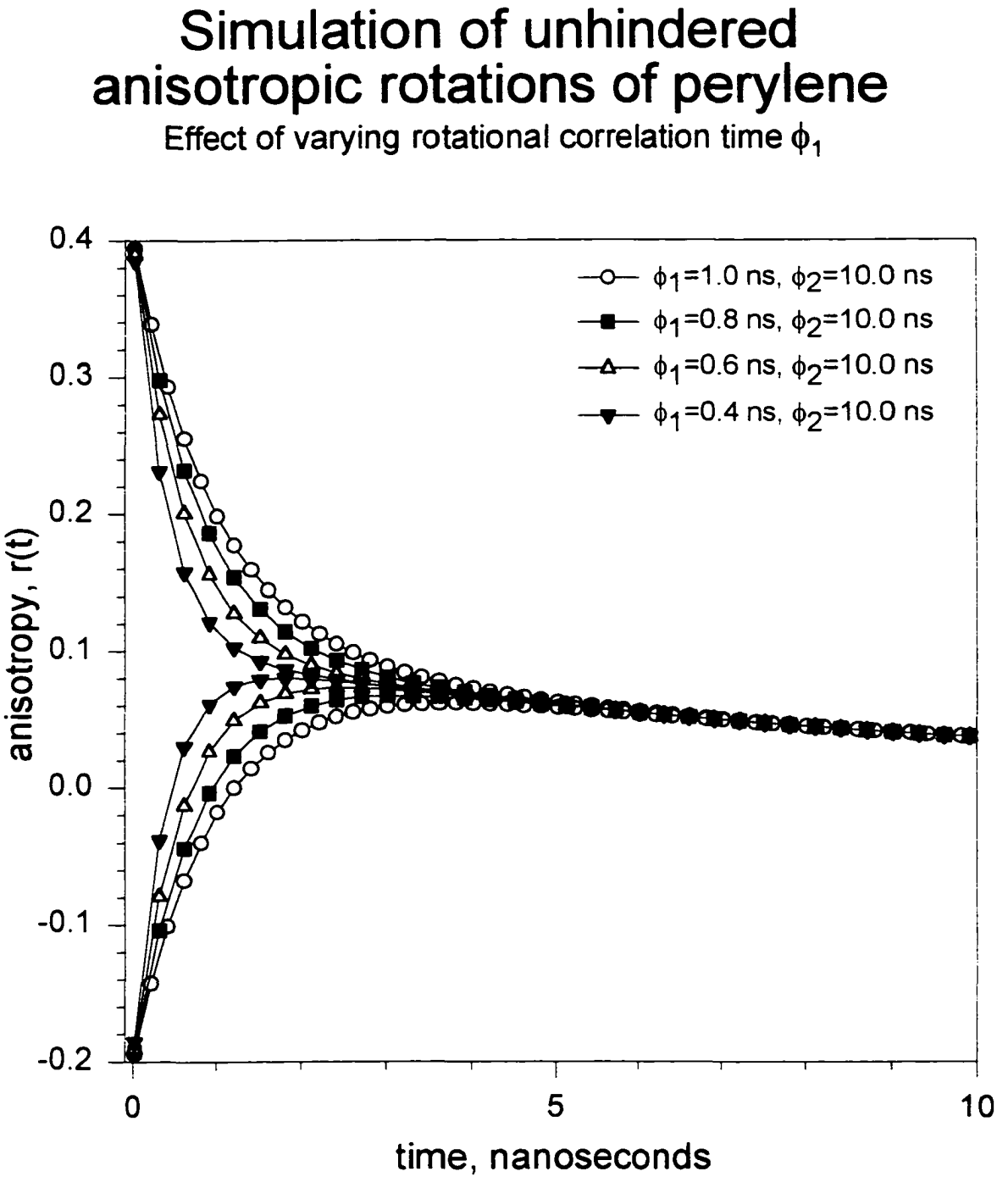

Figure 47. Simulation of unhindered anisotropic rotations of perylene. The value of Φ_2 was left constant at 10 ns, while the value of Φ_1, representing a combination of in-plane and out-of-plane motions, was varied from 0.4 ns to 1.0 ns.

to the fluorescence lifetime. This series of curves, in which only ϕ_1 (mostly in-plane rotations) are varied, is shown in Figure 47. Notice that the average value of each positive and negative anisotropy decay is unchanged, as was the out-of-plane rotational rate.

In the second series of simulated curves (Figure 48), the out-of-plane motions, represented by ϕ_2, were varied, while ϕ_1 was held constant. Here, the opposite trend appears in the curves. The magnitude of the positive and negative anisotropy decay curve average changes as the out-of-plane rotational rate is varied.

In the third simulation, increasing amounts of hindered in-plane rotation, in the presence of a fully hindered out-of-plane rotation was modeled. By adding increasing amounts of hindrance (δ) to the in-plane motion and decreasing the corresponding preexponential ($\beta_1 - \delta$), the sum of preexponential and in-plane hindrance terms remained constant. This simulation was performed using preexponential magnitudes corresponding to both positive ($\beta_1^+ = 0.3$) and negative ($\beta_1^- = -0.3$) anisotropy bands in perylene. The simulation shows that in-plane hindrance does not affect the average of the r_∞ values, which reflect the out-of-plane hindrance to rotation. The results of this hindered simulation is shown in Figure 49.

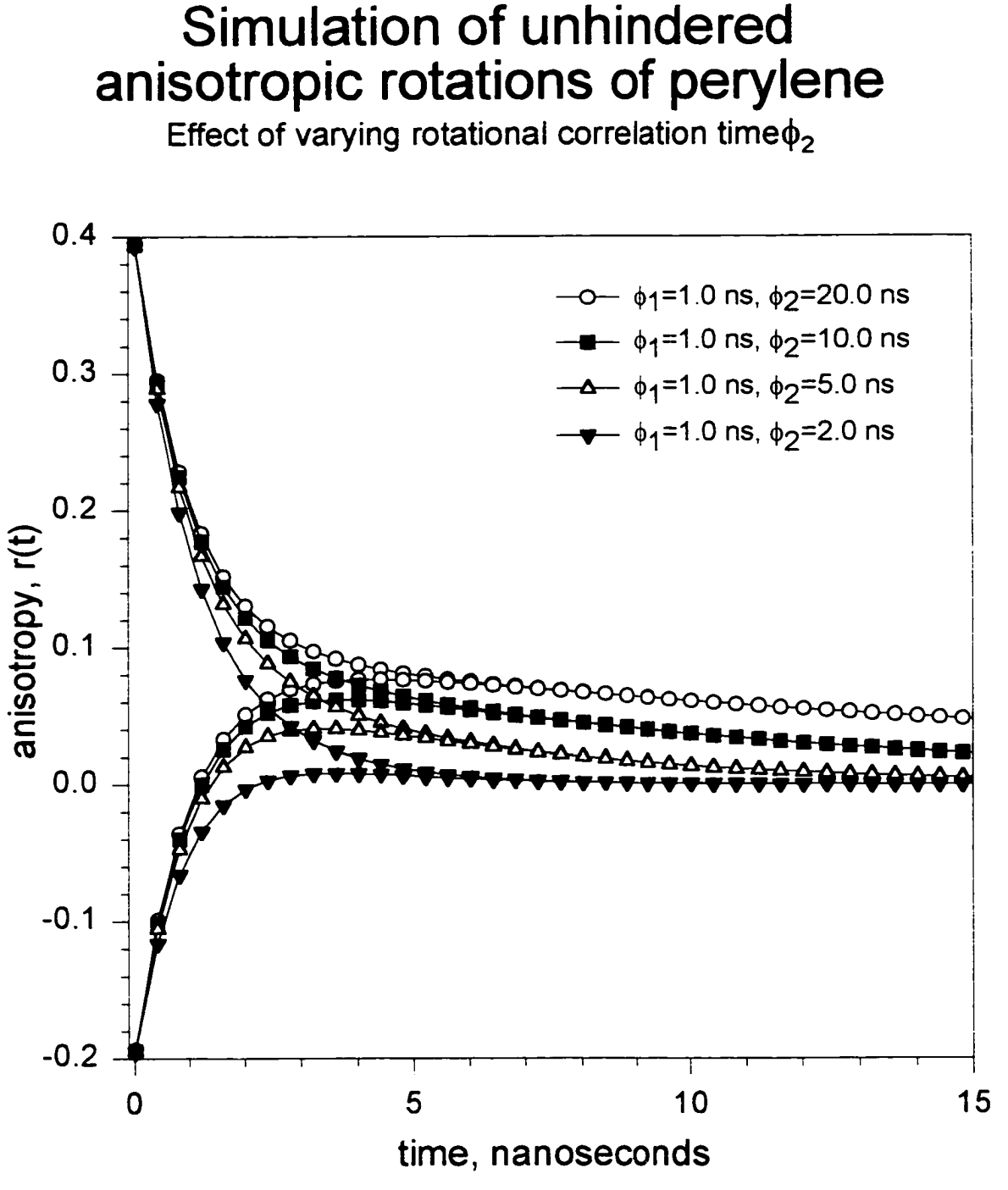

Figure 48. In this simulation, ϕ_2, representing the out-of-plane motion of perylene, was varied from a relatively slow correlation time of 20.0 ns to a faster 2.0 ns correlation time. The value of ϕ_1 was left constant at 1.0 ns in this simulation.

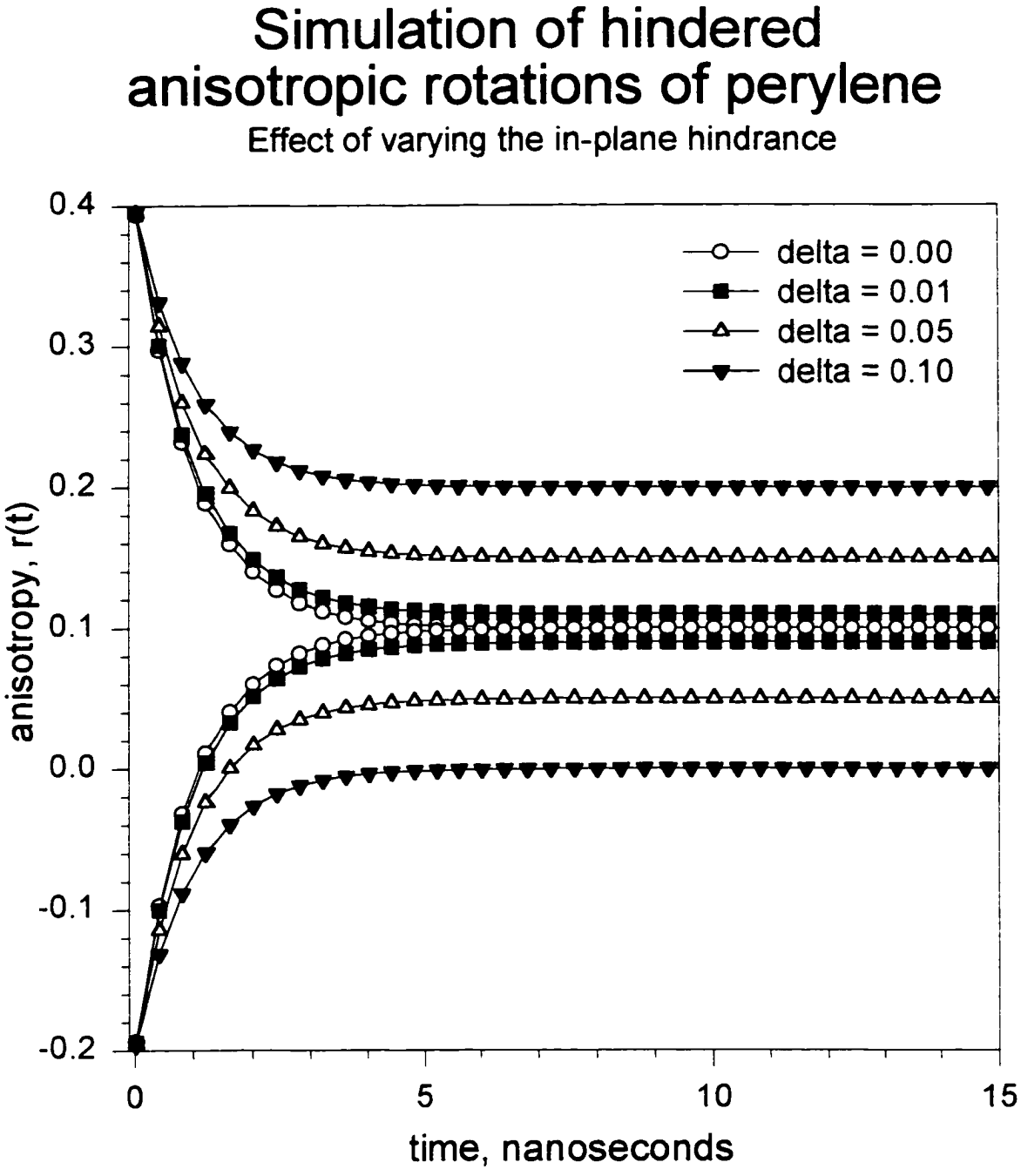

Figure 49. Simulation of hindered anisotropic rotation of perylene. In this simulation, the out-of-plane motion is completely restricted, and the in-plane motion is restricted by varying degrees of δ. The effect of in-plane hindrance shows separation of the ± curves without changing the ± average. This is the mechanism by which the hindered rotations of perylene in phospholipid bilayers may be separated into their component parts.

VII.c. Separation of hindered motions in C(18):C(10)-PC.

The average value of the r_∞ terms at a given temperature yields the out-of-plane hindrance exclusively. Using the fitted values for the r_∞ curves at both wavelengths, values of r_∞ were averaged to obtain the out-of-plane contribution to the hindered motion:

$$r_{\infty,op} = \frac{r_{\infty,410} + r_{\infty,256}}{2} \qquad (82)$$

These results are tabulated below.

Table XIV. Calculation of the out-of-plane hindrance of perylene in C(18):C(10)-PC.

Temp, °C	r_∞ (410 nm)	r_∞ (256 nm)	average = $r_{\infty,\text{out-of-plane}}$
3.0	0.1160	-0.0577	0.0292
5.0	0.0877	-0.0411	0.0233
10.0	0.0435	-0.0175	0.0130
15.0	0.0216	-0.0074	0.0071
25.0	0.0053	-0.0012	0.0021
30.0	0.0026	-0.0004	0.0011

The out-of-plane restriction, given by the +/- average of the time course of the anisotropy decay at long times, becomes smaller with increasing temperature, essentially vanishing at T = 30° (11° above the phase transition for this asymmetric phospholipid).

It is now possible to obtain the unique solution of the system in terms of preexponentials, hindered rotation terms and limiting anisotropies at each excitation wavelength. Since the preexponential term β_2 depends only on the out-of-plane rotation, we can calculate the magnitude of the 'net' β_2 (call it β_2') as the difference between the β_2 recovered for perylene in the isotropic unhindered system and the out-of-plane hindrance:

$$\beta_2' = \beta_2(isotropic) - r_{\infty,out\text{-}of\text{-}plane} \quad (83)$$

The value of β_2 recovered by global analysis of perylene in glycerol was +0.090. Using the values of the out-of-plane restriction from Table XIV, the temperature-dependent preexponentials $\beta_2'(T)$ were calculated using Equation 83. The results are presented in Table XV:

Table XV. Temperature-dependent β_2' terms for perylene in C(18):C(10)-PC.

Temp,°C	$\beta_{2,isotropic}$	$r_{\infty,op}$	$\beta_2' = \beta_{2,isotropic} - r_{\infty,op}$
3.0	0.090	0.029	0.061
5.0	0.090	0.023	0.067
10.0	0.090	0.013	0.077
15.0	0.090	0.007	0.083
25.0	0.090	0.002	0.088
30.0	0.090	0.001	0.089

Having $r_0(\lambda_{ex})$, $\beta_2'(T)$ and $r_\infty(T,\lambda_{ex})$, the net β_1 (β_1') can be calculated by difference, at each wavelength and temperature:

$$\beta_1'(\lambda_{ex},T) = r_0 - r_\infty(\lambda_{ex},T) - \beta_2'(\lambda_{ex},T) \quad (84)$$

The values of these preexponentials, using both excitation wavelengths, are summarized in Table XVI, below. The Table represents the completed set of temperature dependent preexponentials for perylene in the C(18):C(10)-PC phospholipid system.

Table XVI. Temperature dependent β' terms for *asymmetric* C(18):C(10)-PC.

λ_{ex} = 410 nm				
T,°C	**r_0, 410 nm**	**r_∞^+, 410 nm**	**β_2'**	**β_1', 410 nm**
3.0	+0.335	+0.1160	0.0609	+0.1581
5.0	+0.335	+0.0877	0.0667	+0.1806
10.0	+0.335	+0.0435	0.0770	+0.2145
15.0	+0.335	+0.0216	0.0829	+0.2305
25.0	+0.335	+0.0053	0.0879	+0.2418
30.0	+0.335	+0.0026	0.0889	+0.2436
λ_{ex} = 256 nm				
T,°C	**r_0, 256 nm**	**r_∞^-, 256 nm**	**β_2'**	**β_1', 256 nm**
3.0	-0.165	-0.0577	0.0609	-0.1682
5.0	-0.165	-0.0411	0.0667	-0.1906
10.0	-0.165	-0.0175	0.0770	-0.2245
15.0	-0.165	-0.0074	0.0829	-0.2405
25.0	-0.165	-0.0012	0.0879	-0.2517
30.0	-0.165	-0.0004	0.0889	-0.2534

VII.d. Separation of hindered motions in DMPC.

The strategy of using the r_∞ average to reveal the out-of-plane hindrance was applied to the symmetric DMPC system. Using the fitted temperature dependencies of the r_∞, the out-of-plane restriction was calculated using Equation 82. The results are shown in Table XVII:

Table XVII. Calculation of the out-of-plane hindrance for perylene in DMPC.

Temp, °C	r_{∞}^{+}	r_{∞}^{-}	average = r_{∞} .out-of-plane
5.0	0.1068	-0.0161	0.0454
10.0	0.0800	0.0020	0.0410
15.0	0.0599	0.0044	0.0322
20.0	0.0449	0.0048	0.0248
25.0	0.0336	0.0048	0.0192
30.0	0.0252	0.0048	0.0150

Knowing that the isotropic preexponential β_2 has the value +0.090, the net β_2' is calculated by difference using Equation 83:

Table XVIII. Net preexponential terms (β_2') for perylene in DMPC.

Temp,°C	$\beta_{2,isotropic}$	$r_{\infty,op}$	$\beta_2' = \beta_{2,isotropic} - r_{\infty,op}$
5.0	+0.090	+0.04535	0.04465
10.0	+0.090	+0.04098	0.04902
15.0	+0.090	+0.03216	0.05784
20.0	+0.090	+0.02483	0.06517
25.0	+0.090	+0.019195	0.07081
30.0	+0.090	+0.01500	0.07500

Once the out-of-plane hindrance ($r_{\infty,op}$) and the net preexponential term associated with it (β_2') have been assigned, the remaining preexponential (β_1') is determined by difference using Equation 84. The complete set of temperature dependent preexponentials is presented in Table XIX.

Table XIX. DMPC / perylene. Temperature dependent preexponential (β') terms.

λ_{ex} = 410 nm				
T,°C	r_0,λ_{ex}	r_∞^+,λ_{ex}	β_2',λ_{ex}	β_1',λ_{ex}
5.0	+0.335	+0.1068	0.04465	+0.1836
10.0	+0.335	+0.0800	0.04902	+0.2060
15.0	+0.335	+0.0599	0.05784	+0.2173
20.0	+0.335	+0.0449	0.06517	+0.2249
25.0	+0.335	+0.0336	0.07081	+0.2306
30.0	+0.335	+0.0252	0.07500	+0.2348
λ_{ex} = 256 nm				
T,°C	r_0,λ_{ex}	r_∞^+,λ_{ex}	β_2',λ_{ex}	β_1',λ_{ex}
5.0	-0.165	-0.0161	0.04465	-0.1936
10.0	-0.165	+0.00196	0.04902	-0.2160
15.0	-0.165	+0.00441	0.05784	-0.2273
20.0	-0.165	+0.00475	0.06517	-0.2349
25.0	-0.165	+0.00479	0.07081	-0.2406
30.0	-0.165	+0.00480	0.07500	-0.2448

VIII. Tests of the Temperature-Dependent Beta Model.

VIII.a. Global analysis - Temperature dependent preexponentials.

To verify that the 'Temperature-Dependent Beta' Model proposed here represents a valid solution, global analyses was performed in which the preexponentials were fixed to the values predicted using the 'Temperature-Dependent Beta' Model. The rotational correlation times were allowed to vary as functions of temperature. If the goodness of fit, judged by the magnitude of the reduced chisquare, is similar between models, the 'Temperature-Dependent Beta' Model would be favored, since it results in more realistic physical parameters for the data. Specifically, the magnitudes of the recovered preexponentials, in the high temperature limit, must approach the values measured in the isotropic glycerol system, while maintaining the proper sum, at each excitation wavelength, and any temperature.

Plots of the recovered global fitting parameters using the 'Temperature-Dependent Beta Model' are presented below. In each plot, the preexponentials increase smoothly in magnitude as the temperature is raised. At the same time, the r_∞ term, representing the hindrance to rotational motion, is smoothly decreasing. At any temperature, the sum of the preexponentials and the r_∞ equals the fundamental anisotropy. These trends make sense, based on the physical and mathematical requirements of each system.

The asymmetric phospholipid (C(18):C(10)-PC) is presented in Figure 50. The global reduced chisquare was 1.57. For perylene in DMPC, the results are presented in Figure 51. The global chisquare was 1.77 the symmetric DMPC system.

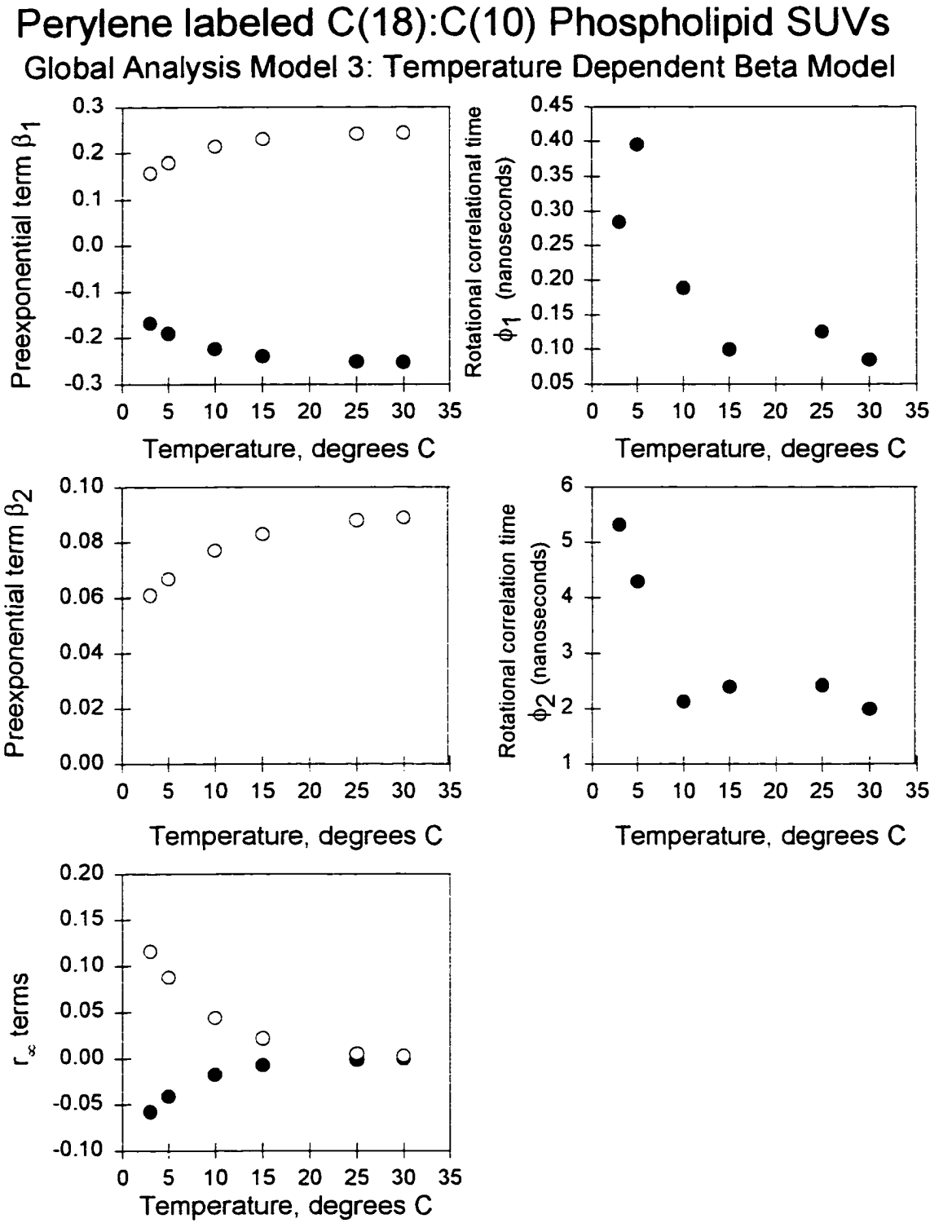

Figure 50. C(18):C(10)-PC / perylene system analyzed using the 'Temperature-Dependent Beta' Model. The values of the preexponentials (β values) were fixed according to the model. Rotational correlation times are linked at each temperature and are free.

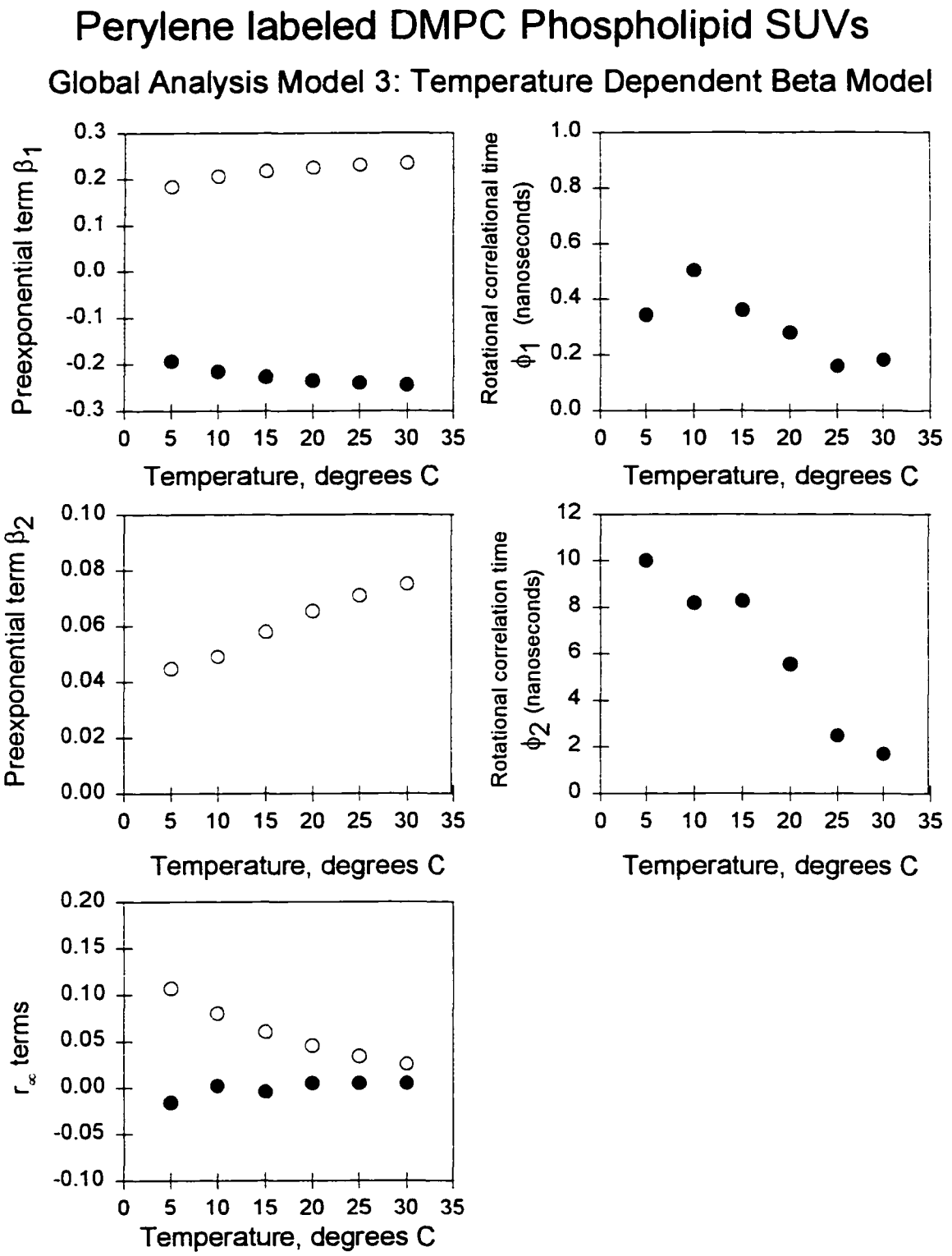

Figure 51. DMPC / perylene system analyzed using the 'Temperature-Dependent Beta' Model. The values of the preexponentials (β values) were fixed according to the model. Rotational correlation times are linked at each temperature and are free.

VIII.b. Comparison with Steady-State Measurements.

As a further test of the model, the temporal parameters of the entire data set, including the lifetimes and rotational dynamics, were used to calculate the expected steady state emission anisotropy. The steady state was recalculated as:

$$\langle r \rangle = \frac{\int_0^t I(t)dt * r(t)dt}{\int_0^t I(t)dt} \qquad (85)$$

using a FORTRAN program (CalcSSEA.for), which accepts lifetime values as ordered pairs of (α,τ) and the rotational dynamics as sets of (β,φ,r_∞) at a given temperature. The program calculates the integrals over a time span of 200 ns, well beyond the lifetime of perylene in phospholipid bilayers.

The steady-state emission anisotropies, recalculated from time-resolved data, are shown in Figure 52 for C(18):C(10)-PC, and Figure 53 for DMPC. The calculated values for the steady-state emission anisotropy agree with measured values, providing support for the 'Temperature-Dependent Beta' Model.

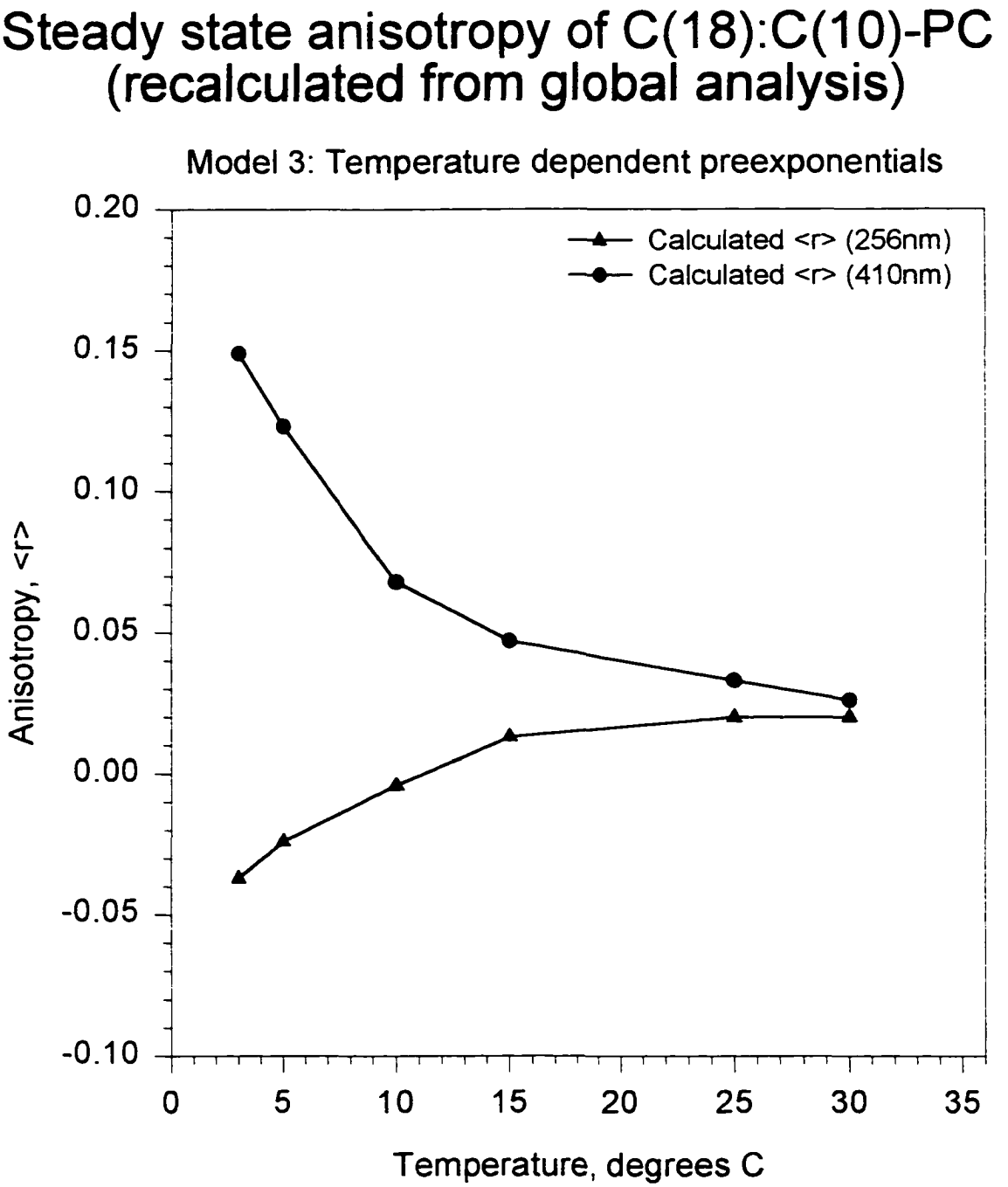

Figure 52. Calculation of the expected steady-state anisotropy, <r>, of perylene labeled C(18):C(10)-PC. Rotational parameters obtained with the 'Temperature-Dependent Beta Model' were used.

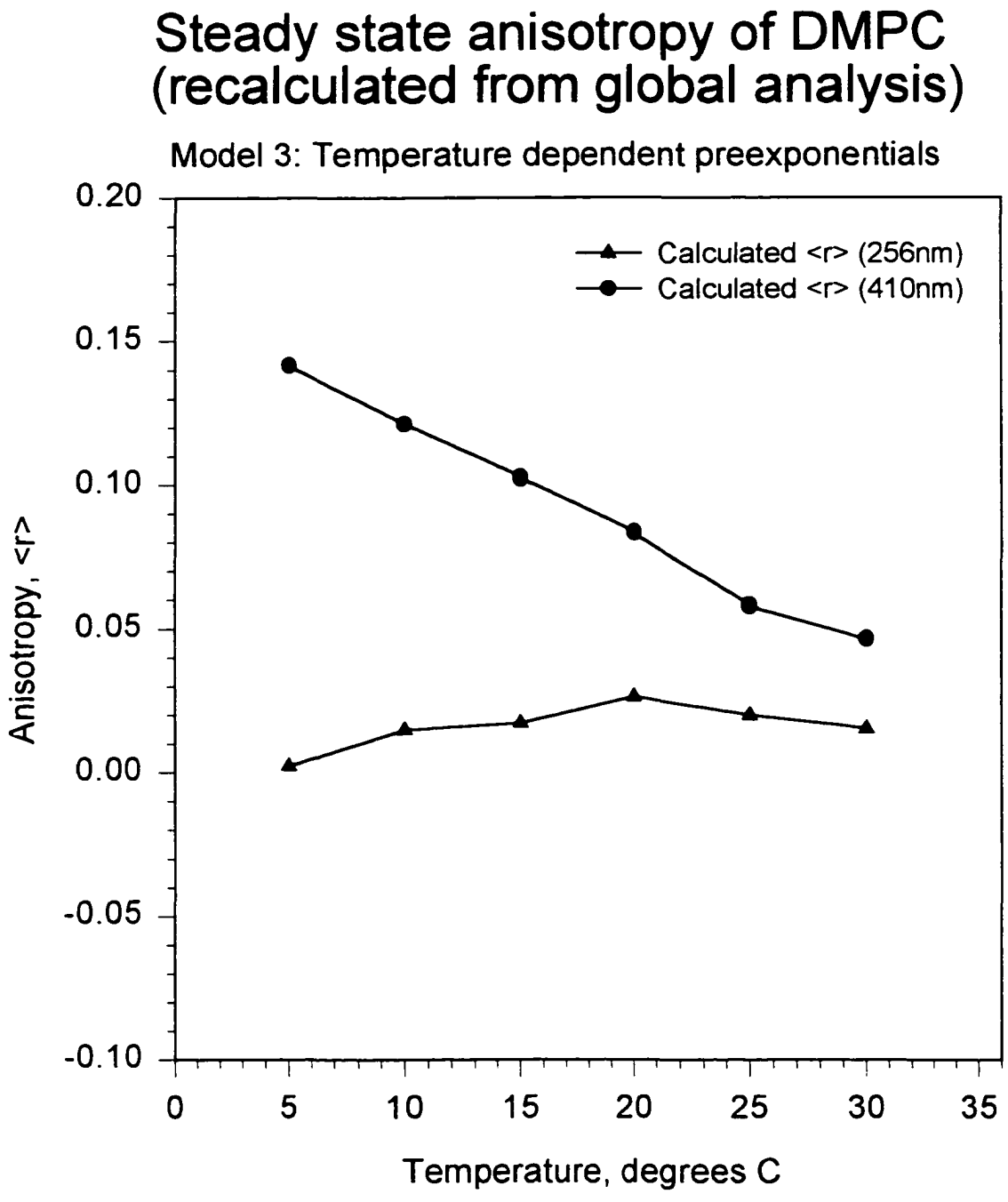

Figure 53. Calculation of the expected steady-state anisotropy, <r>, of perylene labeled DMPC. Rotational parameters obtained with the 'Temperature-Dependent Beta Model' were used.

IX. Discussion.

IX.a. Comparison of Models for Anisotropic Solvents - Phospholipid Systems.

Model I, the 'Free-Beta' Model, shows the relationships of the preexponentials as functions of temperature, without imposing any constraints on their values. The recovered β terms show a large amount of scatter, which is not unexpected, since there is a high degree of correlation among the parameters used to describe the anisotropy decay. For this reason, global analysis of the data should help in recovering a unique set of decay parameters across the entire series of experiments. This is the rationale for incrementing to Model II - the 'Linked-Beta' Model.

The results obtained using the 'Linked-Beta' Model were satisfactory from a statistical viewpoint, but the recovered parameters describing the rotational dynamics are not physically realistic. The magnitude of the recovered preexponential terms are lower than those recovered for the isotropic solvent system. For the same fluorescence probe, perylene, using the same excitation wavelengths, this discrepancy cannot be ignored. Additionally, the 'Linked-Beta' Model does not consider any hindrance to rotational motion, which will affect the magnitude of the sum of the preexponentials. Even though the 'Linked-Beta' Model improves the appearance of the fitted parameters, the results are not consistent with what we already know about the photophysics of perylene and the behavior of phospholipid bilayers. The hindered rotational motions cannot be ignored by simply linking the preexponential terms as functions of wavelength. For these reasons, the 'Temperature-Dependent Beta' Model was developed, which places additional constraints on the model, in a way consistent with both perylene's photophysics and the behavior of the

phospholipid bilayers below and above their phase transition. The 'Temperature-Dependent Beta' Model works for both anisotropic and isotropic solvent systems, since, in the isotropic solvents, the r_∞ terms are zero, and the equations reduce to simple isotropic expressions.

Model III - the Temperature Dependent Beta Model, provides a universal description for complex rotational behavior of the anisotropic rotor perylene in both isotropic and anisotropic solvents.

IX.b. Interpretation of the r_∞ curves as functions of temperature.

The temperature profiles of the r_∞ of the asymmetric C(18):C(10)-PC phospholipid and the symmetric DMPC phospholipid show distinct differences.

The first observation is the decreased magnitude of the r_∞ terms obtained the symmetric DMPC system, especially at low temperature using 256 nm excitation. The immediate thought is, the overall environment of perylene is less restricted in the DMPC system. More freedom of rotation would lower the magnitude of the r_∞ terms. However, there is a problem with this interpretation. The phase transition temperature for DMPC is higher than that for the asymmetric C(18):C(10)-PC system, by approximately five degrees. How can a phospholipid system with a *higher* phase transition present a *less hindered environment* to rotation? The opposite would be expected using this simple picture.

The structure of DMPC bilayers allows for the heterogeneous distribution of perylene within the bilayer. The asymmetric C(18):C(10)-PC bilayer does not allow a heterogeneous distribution, due to the interdigitated lipid chains that exclude the region between the bilayer

leaflets.

These differences are easily visualized when plotted as functions of the temperature difference between the experimental temperature and the phase transition temperature (Equation 59). Comparing r_∞ values at a particular T^* value removes the shift in the temperature axis, due to different phase transition temperatures.

As mentioned earlier, the hindered rotations may be used to calculate the structural 'order' of the phospholipid bilayer [17]. Using Equation 25, the order parameters reported by perylene were calculated, using both 410 nm and 256 nm excitation wavelengths. For the asymmetric C(18):C(10)-PC , the order parameters as a function of the T* is shown in Figure 54, and the DMPC order parameters are presented in Figure 55.

These data clearly suggest that the symmetric DMPC system exhibits heterogeneity of the probe location in the bilayer. A partitioning of perylene within the bilayer could account for these observations. A two-state system is possible, with one population of perylene residing along the lipid chains (exactly as in the C(18):C(10)-PC phospholipid) and a second population lying between the bilayer leaflets. How does this explain the lowered values of the r_∞ terms and order parameters? Assume that, for a given temperature below the phase transition, the environment of perylene molecules aligned with the acyl chains is similar in both the DMPC and C(18):C(10)-PC. This is reasonable, because both bilayers have the same cross sectional thickness (average C(18):C(10) interdigitated = C(14) per leaflet, the same as DMPC). Perylene molecules located along the acyl chains of either phospholipid experience hindered rotation in environments of similar microviscosity and lipid order. It is not unreasonable to expect similar rotational correlation times as well as

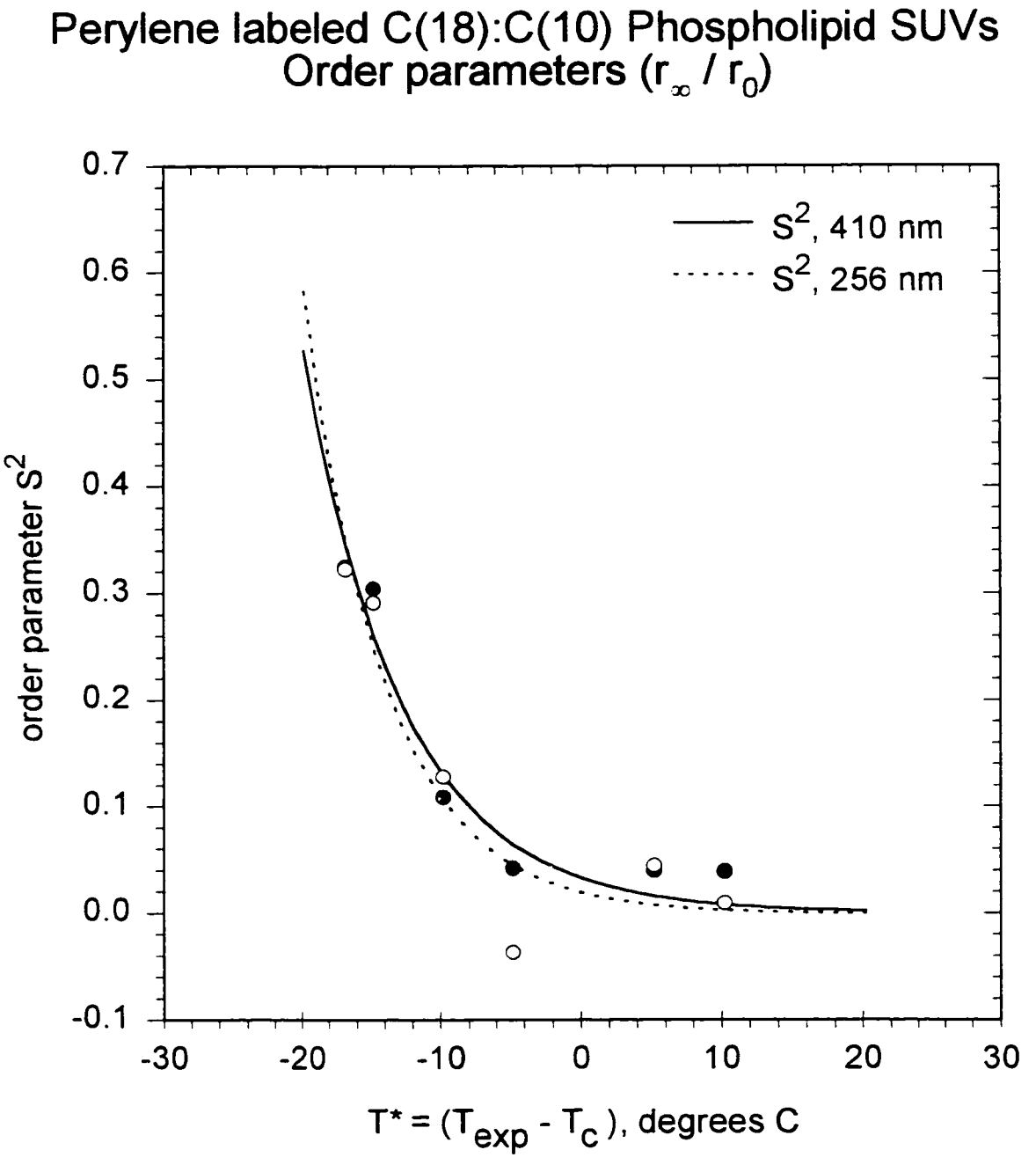

Figure 54. Order parameters of perylene labeled, asymmetric chain C(18):C(10)-PC phospholipid SUVs. The curves represent the fitted $r_\infty(\lambda_{cx},T^*)$ terms, and the points are actual measured r_∞ values divided by the appropriate r_0.

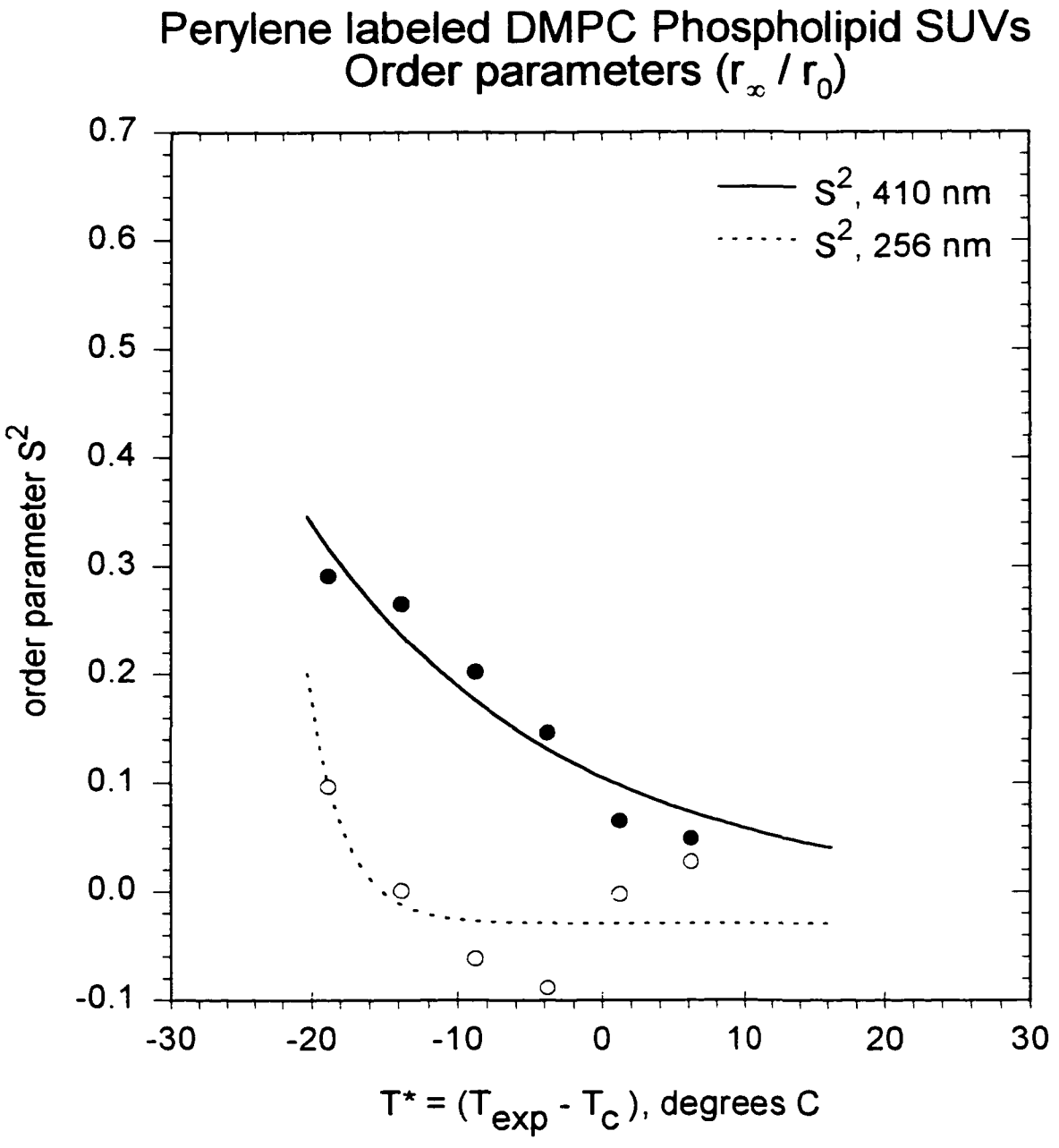

Figure 55. Order parameters of perylene labeled DMPC. The curves represent the fitted $r_\infty(\lambda_{ex},T^*)$ terms, and the points are actual measured r_∞ values divided by the appropriate r_0.

r_∞ terms.

Now, consider an additional population of perylene in the DMPC system, located in the region between the bilayer leaflets. (In C(18):C(10)-PC, this probe fraction would be absent, due to steric considerations). If this population of perylene experiences a different degree of restriction to rotation, these molecules would contribute an additional term to the rotational decay. The net result is the observation of an average environment, which reflects the superposition of the two populations of perylene in the DMPC bilayer. Since the overall r_∞ is lower in magnitude, it indicates that the environment between the DMPC bilayer leaflets presents a lower microviscosity, and less hindrance to rotational motion, than does the local environment of the region along the acyl chains. This comparison between the two phospholipid system provides *evidence of heterogeneous distribution* of perylene in lipid bilayers, and suggests that the region between the bilayer leaflets is *more disordered* than the region along the acyl chains.

The situation may be even more complex. In the last section, we considered the partitioning of perylene in DMPC at one temperature. Extending to a range of temperatures, above and below the lipid phase transition, allows the possibility of a dynamic equilibrium. As the DMPC temperature increases, the relative partitioning of perylene between region I (along acyl chains) and region II (between the bilayer leaflets) may change. So, there is the possibility of four, not two, extremes in which perylene may be found within this system:

Extremes:

I- Along acyl chains, below the phase transition temperature.

II- Between bilayer, below the phase transition temperature.

III- Along acyl chains, above the phase transition temperature.

IV- Between bilayer, above the phase transition temperature.

A continuously changing distribution between all four states would be expected as the temperature is varied. Such redistribution might resemble the four-way diagram in Figure 56.

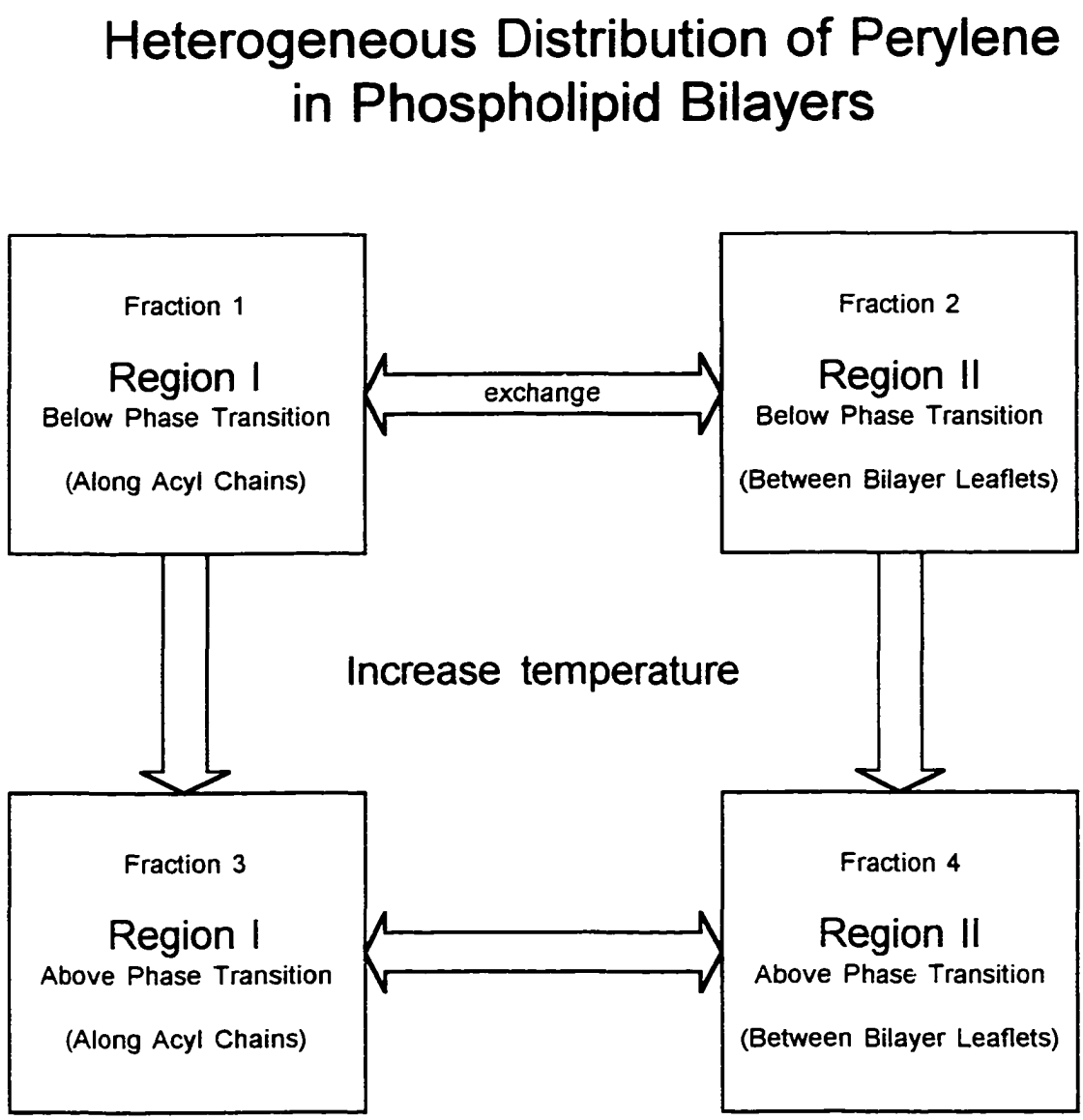

Figure 56. Schematic of heterogeneous distribution of perylene in phospholipid bilayers. The differing regions will have different local environments, resulting in a complex emission anisotropy decay. The symmetric DMPC system shows evidence of this heterogeneous distribution of perylene within the matrix, but the asymmetric C(18):C(10) PC lipid system is probably homogeneous in this regard.

X. Proposed Future Directions of Research.

The anisotropic rotations of perylene have been shown to be useful as probes of complex anisotropic environments, such as phospholipid bilayers. Using the unique spectroscopic properties of perylene, namely, its pair of orthogonal absorption dipoles, as well as its planar D_{2h} symmetry, a unique solution to the problem of hindered anisotropic motion in phospholipid bilayers was obtained.

The two excitation wavelengths used in this research correspond to strong absorptions in perylene. The 410 nm data are relatively easy to collect, even though the emission spectrum of nitrogen (used as the excitation source) is weak above 380 nm. The 256 nm data are difficult, since there are no spectral lines available when nitrogen is used as a filler gas for the lamp. Deuterium gas provides stable pulses in this region, but they are very low in intensity. The relatively high absorption of perylene at 256 nm makes the experiment possible. Recall that these two excitation wavelengths allow the observation of different linear combinations of in-plane and out-of-plane motions of perylene.

An interesting possibility is the use of an excitation wavelength that averages the in-plane motions, revealing only the out-of-plane motion. This technique presents another way to overdetermine one of the rotational correlation times. Such an experiment could help validate the new 'Temperature-Dependent Beta' Model by allowing the direct observation of the preexponential (β_2) associated with the out-of-plane motion exclusively. If this new Model is correct, the magnitude of the preexponential and its associated rotational correlation time should agree with such a direct observation. As described earlier, this would require excitation at 315 nm (the wavelength at which the fundamental anisotropy

equals 0.1). With the flashlamp system, nitrogen has a strong emission line at 315 nm. Unfortunately, the absorption of perylene is very low at 315 nm, making the experiment difficult.

It should be noted that, in some of the experiments, the recovered rotational correlation times were in the subnanosecond time range. The instrument described in this Thesis is estimated to have a lower temporal resolution of well below 1 nanosecond, but recovery of decays with a 200 ps component is questionable, due to limitations of the instrument. Global analysis techniques improve confidence in the recovered values, but it would be useful to confirm some of the measurements on a system capable of lower time resolution. A picosecond dye laser, coupled with appropriate fast detectors, could be used to provide 315 nm excitation as well as the improved temporal resolution. Alternately, the differential phase technique of measuring rotational correlation times could be used to verify the results obtained here. Modulation of a helium-cadmium laser (325 nm and 442 nm) is straightforward and would be a useful tool for excitation of perylene.

Originally, this work sought to investigate the mechanism of the interaction of cholesterol with phospholipid bilayers. Steady-state anisotropy measurements of DMPC/cholesterol bilayers (20 mol% cholesterol) showed complex rotational behavior, the interpretation of which included heterogeneity of phospholipid packing as well as multiple environments of perylene [69]. We performed time-resolved emission anisotropy measurements of DMPC/cholesterol bilayers, attempting to resolve the rotational behavior of perylene [70]. A unique solution proved difficult, due to alternative, equally possible interpretations of the data . This work, using simplified phospholipid systems, may have

partially answered some of the questions needed to solve the interaction of cholesterol with phospholipid bilayers. Anisotropic rotations of fluorophores might be used to study other systems such as liquid crystals and polymers, providing greater detail than is possible using an isotropic probe.

XI. References

1. Einstein, A. *Ann. Physik* **1905**, *17*, 549.

2. Becker R. *Theory and Interpretation of Fluorescence and Phosphorescence*; Wiley: New York, 1969; p 1.

3. Lakowicz, J. R. *Principles of Fluorescence Spectroscopy*; Plenum: New York, 1983.

4. Inman, E. L.; Winefordner, J. D. *Anal. Chem.* **1982**, *54*, 2018-2022.

5. Lakowicz, J. R. *Principles of Fluorescence Spectroscopy*; Plenum: New York, 1983; p. 11

6. Cantor, C. R.; Schimmel, P. R. *Biophysical Chemistry*; Freeman: New York, 1980; Part II, p 434.

7. Lakowicz, J. R. *Principles of Fluorescence Spectroscopy*; Plenum: New York, 1983; p 51.

8. Zannoni, C.; Arcioni, A.; Cavatorta, P. *Chem. Phys. Lipids* **1983**, *32*, 179-250.

9. Lakowicz, J. R.; Knutson, J. R. *Biochemistry* **1980**, *19*, 905-911.

10. Small, E. W.; Isenberg, I. *Biopolym.* **1977**, *16*, 1907-1928.

11. Barkley, M. D.; Kowalczyk, A. A.; Brand, L. *J. Chem. Phys.* **1981**, *75(7)*, 3581-3593.

12. Tao, T. *Biopolym.* **1969**, *8*, 609-632.

13. Lipari, G.; Szabo, A. *Biophys. J.* **1980**, *30*, 489-506.

14. Kinosita, K.; Kawato, S.; Ikegami, A. *Biophys. J.* **1977**, *20*, 289-305.

15. Chong, P. L.-G.; van der Meer, B. W.; Thompson, T. E. *Biochim. Biophys. Acta* **1985**, *813*, 253-265.

16. Brand, L., Knutson, J. R., Davenport, L., Beechem, J. M., Dale, R. E., Walbridge, D. G. and Kowalczyk, A. A. In *Spectroscopy and the Dynamics of Molecular Biological Systems*; P.M. Bayley and R.E. Dale, Eds.; Academic: London, 1985.

17. Heyn, M.P. *FEBS Letters* **1979** *108, 359-364.*

18. Johansson, L. B. A. *Chem. Phys. Lett.* **1985**, *118(5)*, 516-521.

19. Michl, J.; Thulstrup, E. W. *Spectroscopy with Polarized Light*; VCH: New York, 1986; p 335-336.

20. Wahl, Ph. *Chem. Phys.* **1975**, ¯, 210-219.

21. Singer, S. J.; Nicolson, G. L. *Science* **1972**, *1¯5*, 720-731.

22. Cotton, F. A. *Chemical Applications of Group Theory*, 2nd Edition. Wiley: New York, 1971.

23. Turro, N. J. *Modern Molecular Photochemistry*; Benjamin/Cummings: New York, 1978.

24. Knutson, J. R.; Beechem, J. M.; Brand, L. *Chem. Phys. Lett.* **1983**, *102*, 501-507.

25. Christensen, R. L.; Drake, R. C.; Phillips, D. *J. Phys. Chem.* **1986**, *90*, 5960-5967.

26. Zinsli, P. E. *Chem. Phys.* **1977**, *20*, 299-309.

27. Janiak, M. J.; Small, D. M.; Shipley, G. G. *Biochemistry* **1976**, *15(21)*, 4575-4580.

28. Lakowicz, J. R.; Cherek, H.; Maliwal, B. P.; Gratton, E. *Biochemistry* **1985** *24(2), 3¯6.*

29. van Zandvoort, M. A. M. J.; Gerritsen, H. C.; van Ginkel, G.; Levine, Y. K.; Tarroni, R.; Zannoni, C. *J. Phys. Chem. B* **1997**, *101*, 4149-4154.

30. Wolber, P. K.; Hudson, B. S. *Biochemistry* **1981**, *20*, 2800-2810.

31. Vincent, M.; de Foresta, B.; Gallay, J.; Alfsen, A. *Biochemistry* **1982**, *21*, 708-716.

32. Haugen, G. R.; Wallin, B. W.; Lytle, F. E. *Rev. Sci. Instrum.* **1979**, *50(1)*, 64-73.

33. James, D. R.; Siemiarczuk, A.; Ware, W. R. *Rev. Sci. Instrum.* **1992**, *63(2)*, 1710-1716.

34. Birch, D. J. S.; Imhof, R. E. *Rev. Sci. Instrum.* **1981**, *52(8)*, 1206-1212.

35. Birch, D. J. S.; Hungerford, G.; Nadolski, B.; Imhof, R. E.; Dutch, A. D. *J. Phys. E* **1988**, *21*, 857-862.

36. Birch, D. J. S.; Hungerford, G.; Imhof, R. E. *Rev. Sci. Instrum.* **1991**, *62(10)*, 2405-2408.

37. Birch, D. J. S. and Imhof, R. E. In *Topics in Fluorescence Spectroscopy - Vol 1 Techniques;* J. R. Lakowicz, Ed.; Plenum: New York, 1991.

38. Leskovar, B.; Lo, C. C.; Hartig, P. R.; Sauer, K. *Rev. Sci. Instrum.* **1976,** *47(9)*, 1113-1121.

39. Halpern, A. M. *J. Am. Chem. Soc.* **1974**, *96(25)*, 7655-7661.

40. O'Connor, D. V. and Phillips, D. *Time-correlated Single Photon Counting*; Academic: London, 1984; p 108.

41. Morrison, R. *Grounding and Shielding Techniques in Instrumentation*; Wiley: New York, 1967.

42. Lytle, F. E. *Anal. Chem.* **1974,** *46(9)*, 817A-824A.

43. Gedcke, D. A.; McDonald, W. J. *Nucl. Instrum. Meth.* **1967**, *55*, 377-385.

44. Knoll, G. F. *Radiation Detection and Measurement*; Wiley: New York, 1989.

45. O'Connor, D. V.; Phillips, D. *Time-correlated Single Photon Counting*; Academic: London, 1984, p152.

46. Lampert, R. A.; Chewter, L. A.; Phillips, D.; O'Connor, D. V.; Roberts, A. J.; Meech, S. R. *Anal. Chem.* **1983**, *55*, 68-73.

47. Spencer, R. D.; Weber, G. *J. Chem. Phys.* **1970**, *52*, 1654-1663.

48. Eastman, J. W. *Photochem. and Photobiol.* **1967**, *6*, 55-72.

49. Večeř, J.; Kowalczyk, A. A.; Davenport, L.; Dale, R. E. *Rev. Sci. Instrum.* **1993**, *64(12)*, 3413-3424.

50. Kamen, E. *Introduction to Signals and Systems*; Macmillan: New York, 1987; p141.

51. Yguerabide, J. *Meth. Enzymol.* **1972,** *26*, 498-578.

52. Badea, M. G.; Brand, L. *Meth. Enzymol.* **1979**, *61H*, 378-394.

53. Marquardt, D. W. *J. Soc. Ind. Appl. Math.* **1963**, *II(2)*, 431-441.

54. Wahl, Ph. *Biochim. Biophys. Acta* **1969**, *175*, 55-58.

55. Chen, R. F.; Bowman, R. L. *Science* **1965**, *147*, 729-732.

56. Cross, A. J.; Fleming, G. R. *Biophys. J.* **1984**, *46*, 45-56.

57. Gilbert, C. W. In *Time-resolved Fluorescence Spectroscopy in Biochemistry and Biology*; R. B. Cundall and R. E. Dale., Eds.; Plenum: New York, 1983; pp 605-606.

58. O'Connor, D. V.; Phillips, D. *Time-correlated Single Photon Counting*; Academic: London, 1984; p171.

59. Bevington, P. B. *Data Reduction and Error Analysis for the Physical Sciences*; McGraw-Hill: New York, 1969; Chapter II.

60. Grinvald, A.; Steinberg, I. Z. *Anal. Biochem.* **1974**, *59*, 583-598.

61. Davenport, L.; Knutson, J. R.; Brand, L. *Biochemistry* **1986**, *25*, 1811-1816.

62. Ali, S.; Hai-nan L.; Bittman, R.; Huang, C. *Biochemistry* **1989,** *28*, 522-528.

63. Vogel, A. *Vogel's Textbook of Practical Organic Chemistry*; Wiley: New York, 1978; p 267-268.

64. Davenport, L. *Meth. Enzymol.* **1997**, *278*, 487-512.

65. Newman, G. C.; Huang, C. H. *Biochemistry* **1975**, *14*, 3363.

66. Small, D. M. *The Physical Chemistry of Lipids*; Plenum: New York, 1986; p 629.

67. Parker, C. A.; Rees, W. T. *Analyst (London)* **1962**, *87*, 83-111.

68. Beechem, J. M.; Ameloot, M.; Brand, L. *Anal. Instrum.* **1985**, *14*, 379-402.

69. Davenport, L.; Ri, Y. *Biophys. J.* **1990**, *57*, 483a.

70. Targowski, P.; Atzeni, S. H.; Davenport, L. *Biophys. J.* **1993**, *64*, A72.

IMAGE EVALUATION TEST TARGET (QA-3)

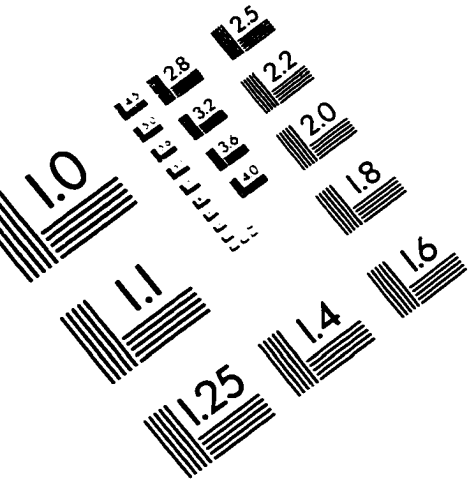

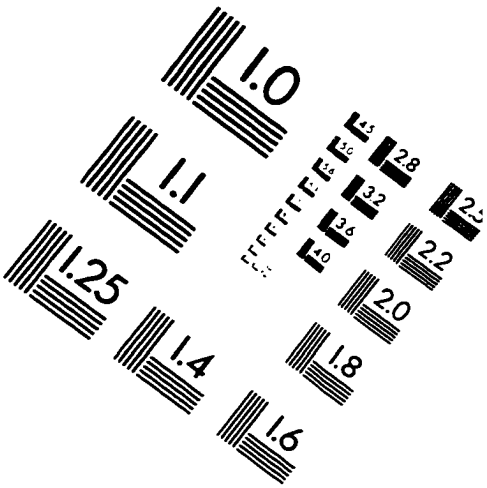

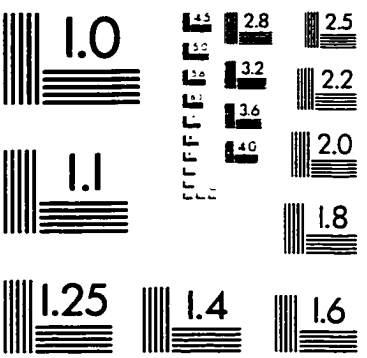

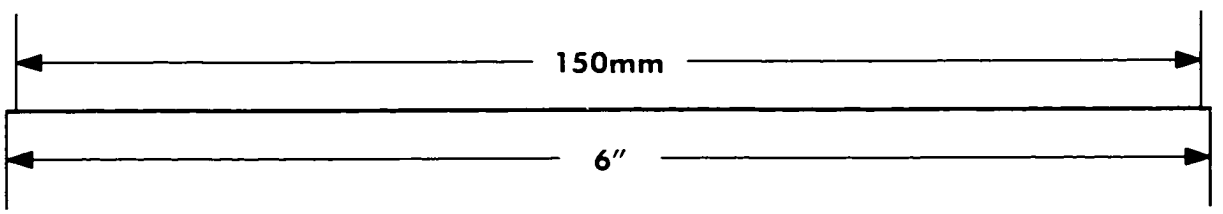

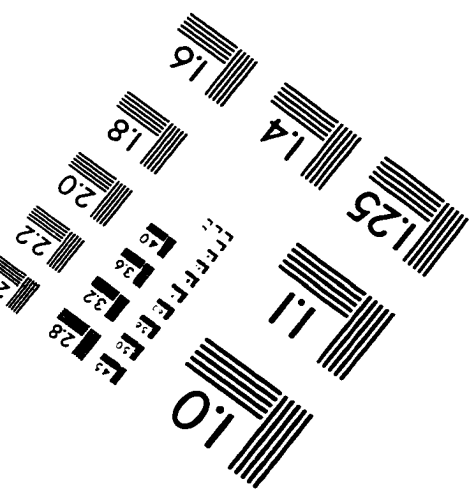

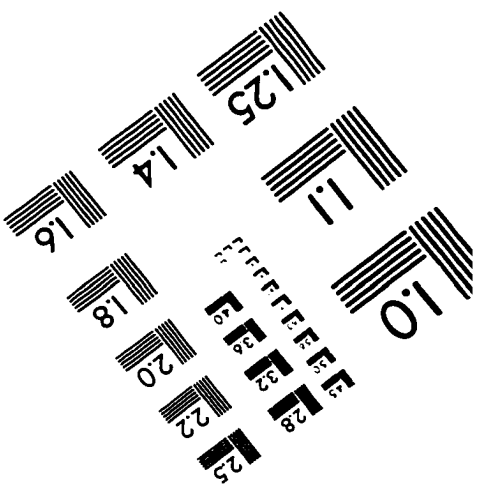

APPLIED IMAGE, Inc
1653 East Main Street
Rochester, NY 14609 USA
Phone: 716/482-0300
Fax: 716/288-5989